FACULTY OF SCIENCE
UNIVERSITY OF COPENHAGEN

Master's Thesis in Physics

Carlos Ortega Taberner

Periodically driven S-QD-S junction

Floquet dynamics of Andreev Bound states.

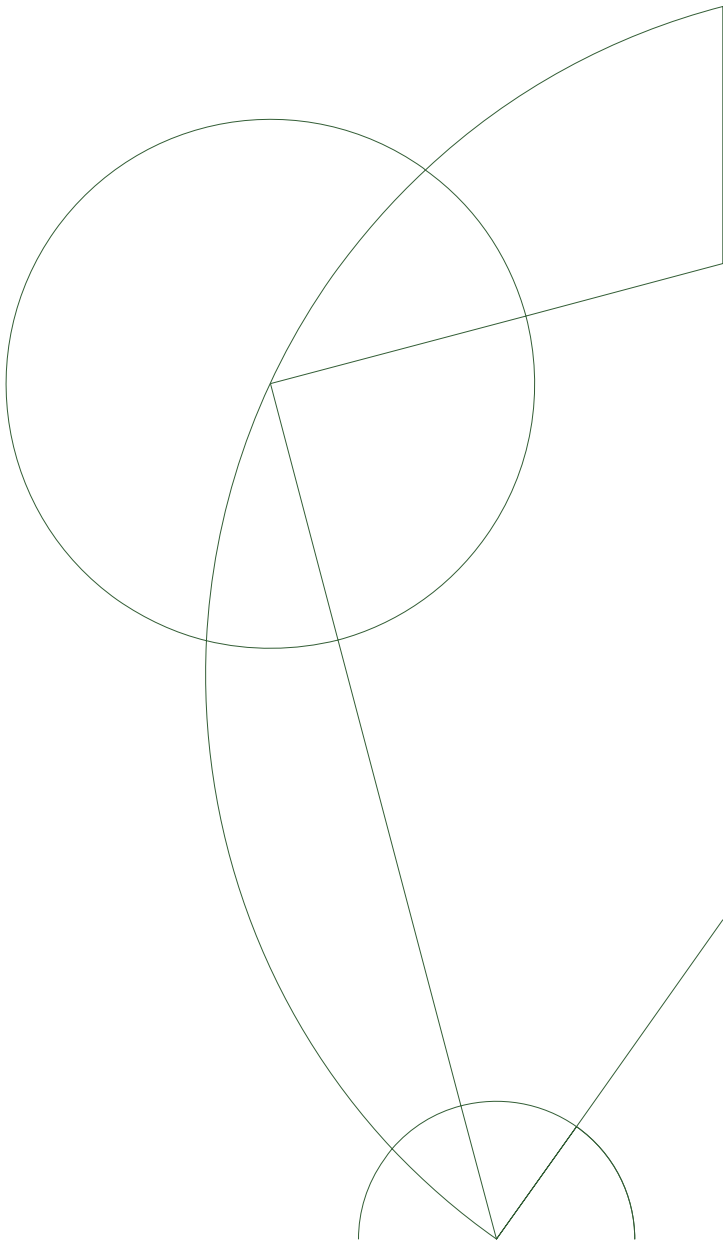

Supervisor: Prof. Jens Paaske.

September 4, 2017

Abstract

In this thesis we study the S-QD-S junction when a harmonic drive is applied on the dot. We are going to perform the numerical calculations using the Floquet-Green's functions technique and interpret the results using the Floquet formalism. We find that the current-phase relation of a junction with an ac magnetic field is proportional to the one at equilibrium, where the propotionality factor can be tuned with the parameters of the drive. The current-magnetic field relation can also be tuned with the parameters of the drive, and in particular we found a $0-\pi$ transition for an applied ac gate voltage and a non-trivial region of vanishing current for an applied ac magnetic field. When we add a harmonic drive to the voltage-biased junction the MAR characteristics of the current-voltage relation are lost and the current gains a complex phase-dependence. For an applied magnetic field we find resonant tunneling and for an ac gate voltage and a phase bias of π we observe suppression of the sub-gap current. In the infinite gap limit we the current vanishes for an applied ac magnetic field due to the transport being non-local in the extended space and for an ac gate voltage, in the high frequency limit the junction behaves effectively as a $\varphi-$junction in equilibrium where the φ phase can be tuned with the phase of the drive.

Contents

Chapter 1

Introduction

The formalism used to study periodically driven systems was formulated a long time ago [1, 2]. The most interesting result about periodically driven systems in d dimensions is that they can be mapped to an extended Hilbert space in $d+1$ dimensions governed by a time-independent Hamiltonian where the interactions on the new dimension are given by the time-dependent part of the Hamiltonian. This equivalence allows one to explore the physics of the system in $d+1$ dimensions with engineered Hamiltonians. And quite interestingly, one can obtain a time-independent effective Hamiltonian for the system in d dimension which governs the long-time dynamics of the system that can also be engineered [3–5].

This last fact has been the reason periodically driven systems have attracted a lot of attention in the last decade. Recent technological advances have opened the door to accurately engineer effective Hamiltonians with all kinds of interesting physics found in equilibrium. Some examples of this are artificial gauge fields [6, 7], topological properties [8, 9] or spin-orbit coupling [10] .

Another reason periodical drives are interesting is because, since one has full control of the drive, it is possible to adiabatically tune parameters of the effective Hamiltonian that are either impossible to modify in equilibrium, because they are intrinsic properties of the system, or very difficult to modify because of experimental limitations. Because of this, periodical drives are a promising technology for control of quantum circuits.

In view of this, in this thesis we are going to focus on the Josephson junction, composed of an insulator sandwiched between two superconductors, which is an essential part of many quantum circuits, like SQUIDS or superconducting qubits [11]. For simplicity we are going to consider the case where instead of an insulator we have a quantum dot, and we are going to study how adding a periodical drive on the dot affects the dynamics of the junction.

The thesis is organized as follows. In chapter 2 we will first describe the formalism of periodically driven systems used to obtain and interpret the numerical results and then, as an example, the periodically driven quantum dot contacted by metallic leads with a voltage bias will be studied. In chapter 3 we will focus on the superconducting junction, where first we will describe the formalism extends to the superconducting junction and the transport through the junction under different circumstances will be analyzed. Finally, in chapter 4 we will summarized the results obtained in this thesis and we will discuss briefly several ways this work could be extended.

Chapter 2

Theoretical formalism

In this chapter we will develop the formalism employed throughout the thesis, and as undergraduate classical mechanics students studying the tilted plane, we are going to illustrate it along the way with the simplest example of driven phenomena, the harmonically driven resonant level.

There are two main techniques used in the literature to solve time-periodic problems. Using the Floquet formalism one can obtain a time-independent Hamiltonian describing the dynamics of the system which can be diagonalized to obtained all the necessary information to solve the system [2–4, 12]. We will start this chapter by describing this formalism, and although we are not going to use it to perform the numerical calculations, it will prove very useful when interpreting the results obtained.

The second technique widely used in the literature is the non-equilibrium Green's functions technique [13, 14], and in particular for time-periodic systems, the Floquet-Green's function technique [15–18], which is the one we will use to perform the numerical calculations. We will describe this technique in the second section of this chapter and explain how it relates to the Floquet formalism.

Finally, in the third section of this chapter we will present results for a harmonically driven resonant level between two metallic leads with a voltage-bias. This system has been studied using the technique described here [15, 16] and it will serve use to understand how the quantum dot responds to the harmonic drive, which we will use next chapter.

2.1 Floquet formalism and the extended space

In the non-relativistic limit the time evolution of any quantum state $|\psi(t)\rangle$ is given by the time-dependent Schrödinger equation

$$i\partial_t |\psi(t)\rangle = H(t) |\psi(t)\rangle . \tag{2.1}$$

Where we have set $\hbar = 1$. The time evolution operator, defined as

$$|\psi(t)\rangle = U(t, t') |\psi(t')\rangle \tag{2.2}$$

also fulfills the time-dependent Schrödinger equation and its formal solution is given by

$$U(t, t') = \mathcal{T} e^{-i \int_{t'}^{t} dt_1 \, H(t_1)}, \tag{2.3}$$

where $\mathcal{T}$ is the time-ordering operator, defined as

$$\mathcal{T}\{A(t)B(t')\} = \theta(t-t')A(t)B(t') \pm \theta(t'-t)B(t')A(t), \tag{2.4}$$

where $\pm$ refers to the bosonic or fermionic nature of the operators. We are going to consider for a moment the case of a time-independent Hamiltonian. The time-evolution operator is then given by

$$U(t,t') = e^{-iH(t-t')}. \tag{2.5}$$

The problem can be solved by diagonalizing the Hamiltonian, and its eigenstates and eigenenergies fulfill the time-independent Schrödinger equation

$$H|\psi_\nu\rangle = E_\nu|\psi_\nu\rangle. \tag{2.6}$$

Since the Hamiltonian and the time-evolution operator trivially commute, the eigenstates of the Hamiltonian are also eigenstates of the time-evolution operator. We can find their time-dependence easily as

$$|\psi_\nu(t)\rangle = U(t,t')|\psi_\nu(t')\rangle = e^{-iE_\nu(t-t')}|\psi_\nu(t')\rangle, \tag{2.7}$$

and the time-evolution operator can be expressed as

$$U(t,t') = \sum_\nu e^{-iE_\nu(t-t')}|\psi_\nu(t')\rangle\langle\psi_\nu(t')|. \tag{2.8}$$

Consider now the case of a time-periodic Hamiltonian with period T defined on a Hilbert space $\mathcal{H}$,

$$H(t+T) = H(t). \tag{2.9}$$

In this case the Hamiltonian doesn't in general commute with the time-evolution operator anymore, but it does so with the time-evolution operator over one period

$$\begin{aligned} U(t+T,t)H(t)U(t+T,t)^\dagger =& H(t+T) \\ =& H(t). \end{aligned} \tag{2.10}$$

As in the time-independent case, the eigenstates of the Hamiltonian will be also eigenstates of the time-evolution operator over one period (see Appendix B), and we can easily calculate their stroboscopic time evolution over any multiple of periods as

$$\begin{aligned} |\psi_\nu(t+nT)\rangle =& U(t+nT,t)|\psi_\nu(t)\rangle \\ =& e^{-i\varepsilon_\nu nT}|\psi_\nu(t)\rangle. \end{aligned} \tag{2.11}$$

The quantity ε_ν dictaminates the stroboscopic time-evolution and as an analogue with the time-independent case (2.7) we are going to call it quasienergy. Using that fact and the fact that the time-evolution operator is itself periodic for translations of T in both time variables

$$\begin{aligned} U(t+T,t'+T) =& \mathcal{T}e^{-i\int_{t'+T}^{t+T}dt_1\,H(t_1)} \\ =& \mathcal{T}e^{-i\int_{t'}^{t}dt_1\,H(t_1-T)} \\ =& \mathcal{T}e^{-i\int_{t'}^{t}dt_1\,H(t_1)} \\ =& U(t,t'), \end{aligned} \tag{2.12}$$

the Floquet theorem (see Appendix B) ensures that the time-dependence of the eigenstates of a time-periodic Hamiltonian takes the form

$$|\psi_\nu(t)\rangle = e^{-i\varepsilon_\nu t}\,|u_\nu(t)\rangle\,, \tag{2.13}$$

where the state $|u_\nu(t)\rangle$ is periodic in time with period T, $|u_\nu(t+T)\rangle = |u_\nu(t)\rangle$. This solution will remind the reader of Bloch's theorem for spatially periodic Hamiltonians. As an analogue, we call these states Floquet state and we will refer to the states $|u(t)\rangle$ as periodic Floquet state. If we substitute this solution into the Schrödinger equation (2.1) we find that the periodic Floquet states fulfill the eigenvalue equation

$$Q(t)\,|u_\nu(t)\rangle = \varepsilon_\nu\,|u_\nu(t)\rangle\,. \tag{2.14}$$

where the quasienergy operator, $Q(t) = H(t) - i\partial_t$, is well defined, periodic in T and Hermitian, since $(\partial_t\,|\psi(t)\rangle)^\dagger = \langle\psi(t)|\left(-\overleftarrow{\partial_t}\right)$. We have found a time-independent Schrödinger equation with the periodic quasienergy operator, and the periodic states defined by the Floquet states (2.13) and the time-independent quasienergy (2.11). Since all time-dependent objects in the eigenvalue equation are periodic in T one would think that Fourier transforming it will help in finding a solution. By Fourier transforming their periodic part, the Floquet states can be decomposed in any basis $\{|\alpha\rangle\}$ of the Hilbert space $\mathcal{H}$ we are working in as

$$|\psi_\nu(t)\rangle = e^{-i\varepsilon_\nu t}\sum_{\alpha,n} u_\nu^n(\alpha)\,|\alpha\rangle\,e^{-in\omega t}, \tag{2.15}$$

where the coefficients are defined as $u_\nu^n(\alpha) = \langle\alpha|u_\nu^n\rangle$ and they are the n'th Fourier component of $u_\nu(\alpha,t) = \langle\alpha|u_\nu(t)\rangle$. If we substitute this expression into the eigenvalue equation for the quasienergy operator (2.14) and project on the left by $\frac{1}{T}\int_{-\infty}^{\infty} dt\,e^{in\omega t}\,\langle\alpha|$ we obtain

$$\begin{aligned}\frac{1}{T}\int_0^T dt\,e^{in\omega t}\,\langle\alpha|\,(H(t)-i\partial_t)\sum_{\beta,m} u_\nu^m(\beta)\,|\beta\rangle\,e^{-im\omega t}\\ = \frac{1}{T}\int_0^T dt\,e^{in\omega t}\,\langle\alpha|\,\varepsilon_\nu\sum_{\beta,m} u_\nu^m(\beta)\,|\beta\rangle\,e^{-im\omega t},\end{aligned} \tag{2.16}$$

which reduces to an eigenvalue equation in matrix form involving the elements of the Quasienergy operator in the basis $|\alpha\rangle$ of the Hilbert space and the Fourier coefficients $u_\nu^n(\alpha)$

$$\sum_{m,\beta} Q_{\alpha,\beta}^{n-m} u_\nu^m(\beta) = \varepsilon_\nu u_\nu^n(\alpha), \tag{2.17}$$

where the elements of the quasienergy operator are

$$Q_{\alpha,\beta}^{n-m} = \langle\alpha|\left(H^{n-m} - n\omega\delta_{nm}\right)|\beta\rangle\,, \tag{2.18}$$

and H^{n-m} is the $n-m$'th Fourier component of the Hamiltonian. The components $u_\nu^n(\alpha)$ resemble a wavefunction with an additional quantum number n obeying a Hamiltonian given by the elements $Q_{\alpha,\beta}^{n-m}$.

This equivalence is properly defined by mapping the problem in d dimensions with a time-periodic Hamiltonian on the Hilbert space $\mathcal{H}$ to a problem with a time-independent unbounded Hamiltonian on the Hilbert space $\mathcal{H}_E = \mathcal{H} \otimes \mathcal{T}_\omega$ of $d+1$ dimensions [2, 3]. The extended space $\mathcal{H}_E$ is spanned by basis states $\{|\alpha, n\rangle\!\rangle = |\alpha\rangle \otimes |n\rangle\}$, where $\{|\alpha\rangle\}$ is any basis of the original Hilbert space $\mathcal{H}$ and the basis of $\mathcal{T}_\omega$ is labeled with the integer n and is orthonormal. We define a mapping between the original space and the extended space $\hat{\eta}(t) : \mathcal{H}_E \to \mathcal{H}$ as

$$\hat{\eta}(t) = \sum_n e^{-in\omega t} \mathbb{1} \otimes \langle n| \,. \tag{2.19}$$

Operators acting on the extended space $\mathcal{H}_E$ will be written with a hat and states in the extended space are noted by a double bracket. Any state in the extended space $|\psi(t)\rangle\!\rangle$ can now be mapped into the original Hilbert space as

$$|\psi(t)\rangle = \hat{\eta}(t)|\psi(t)\rangle\!\rangle. \tag{2.20}$$

Since the map is only defined one way, we have to define the states $|\psi(t)\rangle\!\rangle$ somehow. We do this by assuming that any state in the extended space $|\psi(t)\rangle\!\rangle$ can be obtained by time-evolving the state $|\psi(0)\rangle\!\rangle = |\psi(0)\rangle \otimes |0\rangle$ with a time-independent Hamiltonian following a Schrödinger equation

$$i\partial_t |\psi(t)\rangle\!\rangle = \hat{H}^F |\psi(t)\rangle\!\rangle, \tag{2.21}$$

where $\hat{H}^F$ is the Floquet Hamiltonian, given by

$$\hat{H}^F = \hat{H} - \hat{n}\omega = \sum_{nm} H^{n-m} |n\rangle \langle m| - \hat{n}\omega, \tag{2.22}$$

where $\hat{n} = \sum_n n \, \mathbb{1} \otimes |n\rangle \langle n|$. The elements of the Floquet Hamiltonian are related to those of the quasienergy operator as

$$H^F_{\alpha n, \beta m} = Q^{n-m}_{\alpha,\beta}, \tag{2.23}$$

where $H^F_{\alpha n, \beta m} = \langle\!\langle \alpha n | \hat{H}^F | \beta m \rangle\!\rangle$.

We prove now that the assumption is correct, and the time-evolved state $|\psi(t)\rangle\!\rangle$ obtained by this procedure gives the correct time-evolved state $|\psi(t)\rangle$ with the given map.

$$i\partial_t |\psi(t)\rangle = [i\partial\hat{\eta}(t)]|\psi(t)\rangle\!\rangle + \hat{\eta}(t)\hat{H}^F|\psi(t)\rangle\!\rangle \tag{2.24}$$

By using that the time-derivative of the map is $i\partial_t\hat{\eta}(t) = \hat{\eta}(t)\hat{n}\omega$, we obtain

$$\begin{aligned} i\partial_t |\psi(t)\rangle =& \hat{\eta}(t)[\hat{H}^F + \hat{n}\omega]|\psi(t)\rangle\!\rangle & (2.25)\\ =& \hat{\eta}(t)\hat{H}|\psi(t)\rangle\!\rangle. & (2.26) \end{aligned}$$

We need now the commutator between an operator acting on the extended space and the map,

$$\begin{aligned} \hat{\eta}(t)\hat{H} =& \sum_{nm} H^{n-m} \sum_{n_1} e^{-in_1\omega t} \langle n_1|n\rangle \langle m| \\ =& \sum_{nm} H^{n-m} e^{-i(n-m)\omega t} e^{-im\omega t} \langle m| \\ =& H(t)\hat{\eta}(t). \end{aligned} \tag{2.27}$$

Applying this result to (2.25) we finally obtain that the states mapped back after time-evolving them in the extended space with the Floquet Hamiltonian follow the Schrödinger equation

$$\begin{aligned} i\partial_t |\psi(t)\rangle =& H(t)\hat{\eta}(t)|\psi(t)\rangle\!\rangle \\ =& H(t)\,|\psi(t)\rangle\,. \end{aligned} \tag{2.28}$$

This means that we can map any time-periodic problem into the extended space $\mathcal{H}_E$, where the time-evolution is given by the time independent Hamiltonian as

$$U(t) = e^{-i\hat{H}^F t}, \tag{2.29}$$

and then map back to the original space $\mathcal{H}$ to obtain the time-evolved solution.

The time evolution of the eigenstates of the Floquet Hamiltonian is given by

$$|u_\nu(t)\rangle\!\rangle = e^{-i\varepsilon_\nu(t-t')}|u_\nu(t')\rangle\!\rangle. \tag{2.30}$$

By mapping them to the original space $\mathcal{H}$ one obtains that the resulting states have the same time-evolution as the Floquet states and therefore they must be the same,

$$\begin{aligned} |\psi_\nu(t)\rangle =& \hat{\eta}(t)|u_\nu(t)\rangle\!\rangle \\ =& \sum_n e^{-in\omega t}(\mathbb{1}\otimes\langle n|)|u_\nu(t)\rangle\!\rangle \\ =& \sum_n e^{-i(\varepsilon_\nu+n\omega)t}\,\langle n|\,u_\nu(0)\rangle\!\rangle, \end{aligned} \tag{2.31}$$

where the eigenstates of the Floquet Hamiltonian at zero time can be identified with the Fourier components of the periodic Floquet states,

$$|u_\nu^n\rangle = \langle n|\,u_\nu(0)\rangle\!\rangle. \tag{2.32}$$

There is one last particularity of Floquet systems we haven't discussed yet. Looking at the way we defined the quasienergy (2.11) it becomes clear that this definition is not unique, shifting the quasienergy by $n\omega$ results in a different quasienergy for the same eigenstate. We fix this ambiguity in the definition of the quasienergy by restricting it to the interval $\varepsilon_\nu \in [-\omega/2, \omega/2)$, akin to the first Brillouin zone for Bloch states. Therefore the periodic Floquet state $|u_\nu\rangle\!\rangle$ associated with unbounded quasienergy ε_ν spans the set of periodic Floquet states $|u_{\nu,n}\rangle\!\rangle$ with associated quasienergy $\varepsilon_\nu - n\omega$ where ε_ν lies in the first Brillouin zone. The time-evolved Floquet state can be decomposed as well as

$$|\psi_\nu(t)\rangle = \sum_{\alpha,n} |\alpha\rangle\,\langle\!\langle \alpha n|u_{\nu,m}\rangle\!\rangle e^{-i(\varepsilon_\nu+(n-m)\omega)t}, \tag{2.33}$$

and therefore the periodic Floquet states in different zones are related by

$$\langle\!\langle \alpha n|u_{\nu,m}\rangle\!\rangle = \langle\!\langle \alpha, n-m|u_\nu\rangle\!\rangle. \tag{2.34}$$

Finally we have the eigenvalue equation in the extended space

$$\hat{H}^F|u_{\nu,n}\rangle\!\rangle = (\varepsilon_\nu - n\omega)|u_{\nu,n}\rangle\!\rangle. \tag{2.35}$$

As an example, to develop some intuition about the dynamics in the extended space we can briefly consider a harmonically driven resonant level. The basis of the Hilbert space is given by $\{|\uparrow\rangle, |\downarrow\rangle\}$, and the Hamiltonian by

$$H(t) = \sum_{\sigma=\uparrow,\downarrow} \varepsilon_\sigma(t) |\sigma\rangle \langle\sigma| , \tag{2.36}$$

where the energy of each state is being driven harmonically as $\varepsilon_\sigma(t) = \varepsilon_{\sigma,0} + A_\sigma \cos(\omega t + \phi_\sigma)$. In the extended space, the basis is given by $\{|\uparrow n\rangle\rangle, |\downarrow n\rangle\rangle , \forall n \in \mathcal{Z}\}$. The elements of the Floquet Hamiltonian are

$$\langle\langle \sigma n|\hat{H}^F|\sigma' m\rangle\rangle = \delta_{\sigma\sigma'} \left[(\varepsilon_{\sigma,0} - n\omega)\delta_{nm} + \frac{A_\sigma}{2}(e^{-i\phi_\sigma}\delta_{n-m,1} + e^{i\phi_\sigma}\delta_{n-m,-1}) \right]. \tag{2.37}$$

This Hamiltonian is equivalent to that of a tight-binding model, with the different sites being labeled with the index n at on-site energies $\varepsilon_{\sigma,0} - n\omega$, tunneling between neighboring sites with amplitude $A_\sigma/2$ and an additional phase going to a site with higher on-site energy of ϕ_σ. After we define the Green's function method used for the calculations, we will go back to solve this model and show results that support this interpretation.

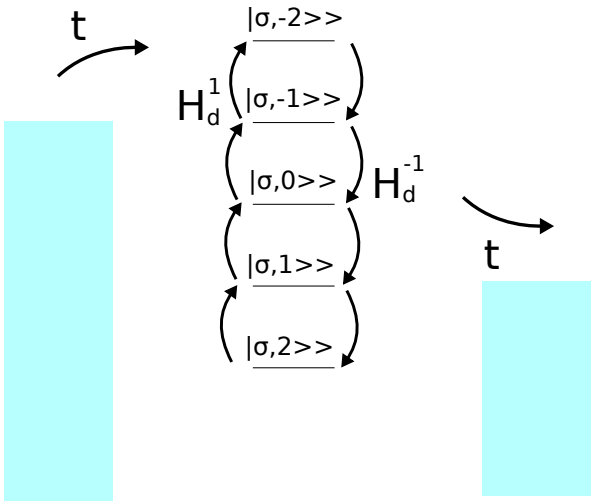

Figure 2.1: Schematic of the transport for a harmonically driven quantum dot between two metallic leads with a voltage bias in the extended space, where it resembles a tight-binding problem with nearest-neighbors hopping.

2.2 Floquet Green's functions technique

The Green's functions are a well known method of solving inhomogeneous differential equations. For a given inhomogeneous differential equation

$$Lu(x) = f(x), \tag{2.38}$$

the Green's function is defined as the function that solves the differential equation

$$LG(x, s) = \delta(x - s), \tag{2.39}$$

from which the solution to the differential equation can be found as

$$u(x) = \int ds\, G(x,s) f(s). \tag{2.40}$$

In quantum mechanics the Green's function is defined as the function that solves

$$(i\partial_t - H)G(x,x') = \delta(x-x'). \tag{2.41}$$

In many-body physics the Green's function can be defined in a different manner, and turns out they are not just a powerful tool to calculate the solutions to the Schrödinger equation, but provide a great knowledge about the correlations in the system by themselves. The contour-ordered Green's function is defined as

$$G^c(t,t') = -i \left\langle \mathcal{T}_C\{d(t)d^\dagger(t')\} \right\rangle, \tag{2.42}$$

where $\mathcal{T}_C$ is the contour-ordered operator which orders operators on the Keldysh contour C [13], shown in Fig. 2.2.

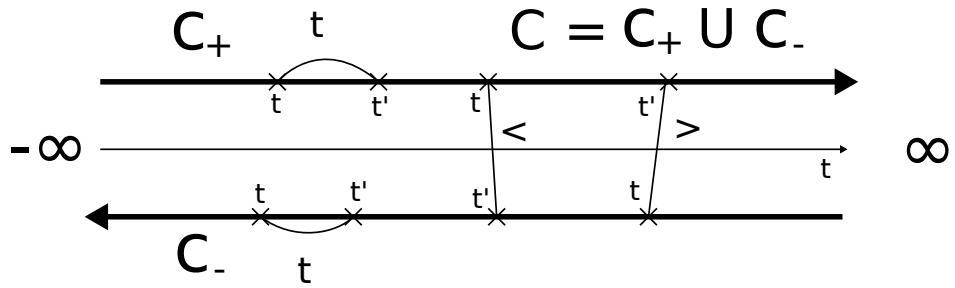

Figure 2.2: Keldysh contour composed of two branches, C_+ going from $-\infty$ to ∞, and C_- going backwards. Depending on where the two times variables t, t' of a function are, the result is the time-ordered function, the lesser or the greater one.

In equilibrium one would make use of the continuous time-translation invariance and find that the Green's function depends only in one time-variable, the time difference. Since now the system is out of equilibrium, the Green's function and related objects depend on the two time variables.

Using the fact that the time-evolution operator is periodic for discrete time-translations in both its variables (2.12) and that

$$U(0,t+T) = U(0,T)U(T,t+T) = U(0,T)U(0,t), \tag{2.43}$$

we show that the Green's function is also periodic for discrete translations of both time variables

$$\begin{aligned} G^c(t+T,t'+T) &= -i \left\langle \mathcal{T}_\mathcal{C}\{d(t+T)d^\dagger(t'+T)\ \} \right\rangle \\ &= -i \left\langle \mathcal{T}_\mathcal{C}\{U(0,t+T)d(0)U(t+T,0)U(0,t'+T)d^\dagger(0)U(t'+T,0)\ \} \right\rangle \\ &= -i \left\langle \mathcal{T}_\mathcal{C}\{U(0,T)U(0,t)d(0)U(t,0)U(0,t')d^\dagger(0)U(t',0)U(T,0)\ \} \right\rangle \\ &= -i \left\langle \mathcal{T}_\mathcal{C}\{U(0,T)d(t)d^\dagger(t')U(T,0)\ \} \right\rangle \\ &= -i \left\langle \mathcal{T}_\mathcal{C}\{d(t)d^\dagger(t')\} \right\rangle = G^c(t,t'), \end{aligned} \tag{2.44}$$

where in the last step we used the fact that we are doing the expectation value over the ground state, which is an eigenstate of the time evolution operator over one period as well (2.11).

We can use the fact that the Green's function is periodic to optimize the numerical calculations by obtaining its Fourier components first and calculating the two-time Green's function after truncating the Fourier sum. The Fourier transform of the two-time objects is not unique, and two different conventions are usually found on the literature. In one, a Wigner transformation is performed, a change of variables to the center of mass time $T = (t + t')/2$ and the time difference $\tau = t - t'$ is made before performing a continuous Fourier transform on τ and a discrete one on T. This is particularly useful for systems which are periodic in a fast timescale with an adiabatic modulation [4]. In our case this is irrelevant because we calculate steady states. And because it makes the connection with the Floquet formalism more clear as we will see later, we choose the other convention where first a continuous Fourier transform is performed integrating t',

$$G(t, \varepsilon) = \int_{-\infty}^{\infty} dt' e^{i\varepsilon(t-t')} G(t, t'), \tag{2.45}$$

after which the transformed object is periodic in its time variable, t, and a discrete Fourier transform can be performed

$$G(t, \varepsilon) = \sum_n G^n(\varepsilon) e^{-in\omega t}. \tag{2.46}$$

Piecing together both Fourier transformations the two-time Green function can be decomposed as

$$G(t, t') = \sum_n \int_{-\infty}^{\infty} d\varepsilon \, e^{-i\varepsilon(t-t')-in\omega t} G^n(\varepsilon) \tag{2.47}$$

To make the connection with the Floquet formalism remember that the Floquet states are defined in the first Brillouin zone. We now decompose the Green function in a way where its energy variable is also defined in a Brillouin zone

$$\begin{aligned} G(t, t') &= \sum_{n,m} \int_{-\omega/2+m\omega}^{\omega/2+m\omega} d\varepsilon \, e^{-i\varepsilon(t-t')-in\omega t} G^n(\varepsilon) \\ &= \sum_{n,m} \int_{-\omega/2}^{\omega/2} d\varepsilon \, e^{-i(\varepsilon+m\omega)(t-t')-in\omega t} G^n(\varepsilon + m\omega), \end{aligned} \tag{2.48}$$

where we restrict ourselves to the first Brillouin zone by introducing a new Fourier index. It seems now natural to define the Floquet Green's function as

$$G_{nm}(\varepsilon) = G^{n-m}(\varepsilon + m\omega). \tag{2.49}$$

Using this representation the two-time Green function and the correspondent Floquet matrix can be found in terms of one another as

$$\begin{aligned} G(t, t') &= \sum_{n,m} \int_{-\omega/2}^{\omega/2} d\varepsilon \, e^{-i(\varepsilon+n\omega)t+i(\varepsilon+m\omega)t'} G_{nm}(\varepsilon) \\ G_{nm}(\varepsilon) &= \int_{-\infty}^{\infty} dt' \, \frac{1}{T} \int_{-T/2}^{T/2} dt \, e^{i(\varepsilon+n\omega)t-i(\varepsilon+m\omega)t'} G(t, t'). \end{aligned} \tag{2.50}$$

This two-index representation of the Green's functions has a very useful property property that simplifies greatly the analytical expressions and optimizes the numerical calculations. Consider a time convolution between any two two-time functions

$$C(t,t') = \int_{-\infty}^{\infty} dt_1\, A(t,t_1)B(t_1,t'). \tag{2.51}$$

By decomposing the functions A and B into their correspondent Floquet matrices we obtain

$$\begin{aligned} C(t,t') &= \int_{-\infty}^{\infty} dt_1\, A(t,t_1)B(t_1,t') \\ &= \left(\prod_{i,j=1,2}\sum_{n_i}\int_{-\omega/2}^{\omega/2} d\varepsilon_j\right) e^{-it(\varepsilon_1+n_1\omega)}e^{it'(\varepsilon_2+m_2\omega)}A_{n_1m_1}(\varepsilon_1)B_{n_2m_2}(\varepsilon_2) \\ &\quad\times \int dt_1\, e^{it_1(\varepsilon_1+m_1\omega-\varepsilon_2-n_2\omega)} \\ &= \left(\prod_{i,j=1,2}\sum_{n_i}\int_{-\omega/2}^{\omega/2} d\varepsilon_j\right) e^{-it(\varepsilon_1-n_1\omega)}e^{it'(\varepsilon_2+m_2)}A_{n_1m_1}(\varepsilon_1)B_{n_2m_2}(\varepsilon_2) \\ &\quad\times \delta(\varepsilon_1-\varepsilon_2+m_1\omega-n_2\omega). \end{aligned} \tag{2.52}$$

Since the energies $\varepsilon' s$ are defined in the first Brillouin Zone, we have $\delta(\varepsilon_1-\varepsilon_2+(m_1-n_2)\omega) = \delta(\varepsilon_1-\varepsilon_2)\delta_{m_1,n_2}$ and the expression reduces to

$$C(t,t') = \sum_{n,m}\int_{-\omega/2}^{\omega/2} d\varepsilon\, e^{-i\varepsilon(t-t')-in\omega t+im\omega t'}\sum_{n_1} A_{nn_1}(\varepsilon)B_{n_1m}(\varepsilon). \tag{2.53}$$

Finally, for the correspondent Floquet matrix of $C(t,t')$, the time-convolution is transformed into simple matrix multiplications

$$C_{nm}(\varepsilon) = \sum_{n_1} A_{nn_1}(\varepsilon)B_{n_1m}(\varepsilon). \tag{2.54}$$

This result can be easily generalized to the time convolution of any number of two-time functions. As it will be needed later, we give the result for the time-averaged any convolution $C(t,t)$,

$$\begin{aligned} \frac{1}{T}\int_0^T C(t,t) &= \sum_{n,m,n_1}\int_{-\omega/2}^{\omega} d\varepsilon\, A_{nn_1}(\varepsilon)B_{n_1,n}(\varepsilon) \\ &= \mathrm{Tr}_F\left[\int_{-\omega/2}^{\omega/2} d\varepsilon\, \boldsymbol{A}(\varepsilon)\boldsymbol{B}(\varepsilon)\right], \end{aligned} \tag{2.55}$$

where Tr_F is the trace over the Floquet indices and $\mathbb{A}$ represents a Floquet matrix.

The other reason for this two-index representation is that the nm component of the Floquet Green's functions between any two states $|\alpha\rangle$ and $|\beta\rangle$ of a basis of $\mathcal{H}$ turns out to be equivalent to the Green's function between the states $|\alpha n\rangle\!\rangle$ and $|\beta m\rangle\!\rangle$ of the basis of the extended space $\mathcal{H}_E$. We prove this equivalence only for the retarded Green's

function, but throughout the thesis we will see results that support this equivalence. Consider the retarded Green's function

$$G^r_{\alpha,\beta}(t,t') = -i\theta(t-t')\,\langle\alpha(t)|\beta(t')\rangle \tag{2.56}$$
$$= -i\theta(t-t')\,\langle\alpha|\,U(t,t')\,|\beta\rangle\,. \tag{2.57}$$

To obtain expressions for the Green's functions we will make use of the equation of motion technique, where we take the derivative of the Green's function with respect to time and then we Fourier transform to obtain a set of coupled differential equations with Green's functions that we can solve. Taking the time derivative of the Green function gives

$$\begin{aligned} i\partial_t G^r_{\alpha,\beta}(t,t') &= \delta(t-t')\delta_{\alpha,\beta} - i\theta(t-t')\,\langle\alpha|\,i\partial_t U(t,t')\,|\beta\rangle \\ &= \delta(t-t')\delta_{\alpha,\beta} - i\theta(t-t')\,\langle\alpha|\,H(t)U(t,t')\,|\beta\rangle \\ &= \delta(t-t')\delta_{\alpha,\beta} - i\theta(t-t')\sum_\gamma H_{\alpha,\gamma}(t)\,\langle\gamma|\,U(t,t')\,|\beta\rangle \\ &= \delta(t-t')\delta_{\alpha,\beta} + \sum_\gamma H_{\alpha,\gamma}(t)G^r_{\gamma,\beta}(t,t'), \end{aligned} \tag{2.58}$$

where $H_{\alpha,\beta}(t) = \langle\alpha|\,H(t)\,|\beta\rangle$. By transforming the two-time Green's function into its Floquet matrix (2.50), we obtain

$$\begin{aligned} &\sum_{nm}\int_{-\omega/2}^{\omega/2} d\varepsilon\,(\varepsilon+n\omega+i0^+)e^{-i(\varepsilon+n\omega)t+i(\varepsilon+m\omega)t'}G^r_{\alpha\beta,nm}(\varepsilon) \\ &= \sum_{nm}\int_{-\omega/2}^{\omega/2} d\varepsilon\, e^{-i(\varepsilon+n\omega)t+i(\varepsilon+n\omega)t')}\delta_{nm}\delta_{\alpha,\beta} \\ &\quad + \sum_{\gamma,k} H^k_{\alpha,\gamma}e^{-ik\omega t}\sum_{nm}\int_{-\omega/2}^{\omega/2} d\varepsilon\, e^{-i(\varepsilon+n\omega)t+i(\varepsilon+m\omega)t'}G^r_{\gamma\beta,nm}(\varepsilon), \end{aligned} \tag{2.59}$$

where we have used that the delta function can be decomposed in Brillouin zones as $\delta(t-t') = \sum_{nm}\int_{-\omega/2}^{\omega/2} e^{-i(\varepsilon+n\omega)t+i(\varepsilon+m\omega)t'}\delta_{nm}$. We can identify term by term in (2.59) and obtain that the retarded Floquet Green's functions fulfill the set of coupled equations

$$(\varepsilon+i0^+ + n\omega)G^r_{\alpha\beta,nm}(\varepsilon) = \delta_{nm}\delta_{\alpha\beta} + \sum_{\gamma k} H^{n-k}_{\alpha,\gamma}G^r_{\gamma\beta,km}(\varepsilon). \tag{2.60}$$

Lets consider now the same system in the extended space. As we mentioned before, in the extended space the dynamics are given by the time independent Floquet Hamiltonian $\hat{H}^F$ (2.22). The retarded Green's function between the states of the basis of $\mathcal{H}_E$, $|\alpha,n\rangle\!\rangle$ and $|\beta,n\rangle\!\rangle$ is

$$\begin{aligned} G^r_{\alpha n,\beta m}(t-t') &= -i\theta(t-t')\langle\!\langle\alpha n(t)|\beta m(t')\rangle\!\rangle \\ &= -i\theta(t-t')\langle\!\langle\alpha n|\hat{U}(t-t')|\beta m\rangle\!\rangle. \end{aligned} \tag{2.61}$$

where the Green's function and the time-evolution operator depend only in the time-difference since the Floquet Hamiltonian is time-independent. By performing the time

derivative of the Green's function one obtains

$$\begin{aligned} i\hat{\partial}_t G^r_{\alpha n,\beta m}(t-t') &= \delta(t-t')\delta_{\alpha n,\beta m} - i\theta(t-t')\left\langle \alpha n\right| i\hat{\partial}_t \hat{U}(t-t')\left|\beta m\right\rangle \\ &= \delta(t-t')\delta_{\alpha n,\beta m} - i\theta(t-t')\left\langle \alpha n\right| \hat{H}^F \hat{U}(t-t')\left|\beta m\right\rangle \\ &= \delta(t-t')\delta_{\alpha n,\beta m} - i\theta(t-t')\sum_{\gamma k} H^F_{\alpha n,\gamma k}\left\langle \gamma k\right| \hat{U}(t-t')\left|\beta m\right\rangle \\ &= \delta(t-t')\delta_{\alpha n,\beta m} + \sum_{\gamma k} H^F_{\alpha n,\gamma k} G^r_{\gamma k,\beta m}(t-t'). \end{aligned} \tag{2.62}$$

And Fourier transforming in the time difference we finally obtain that the time-ordered Green's functions in the extended space fulfill the set of coupled equations

$$(\varepsilon + i0^+)G^r_{\alpha n,\beta m}(\varepsilon) = \delta_{\alpha n,\beta m} + \sum_{\gamma k} H^F_{\alpha n,\gamma k} G^r_{\gamma k,\beta m}(\varepsilon). \tag{2.63}$$

Since $\delta_{\alpha n,\beta m} = \delta_{\alpha,\beta}\delta_{n,m}$ and $H^F_{\alpha n,\gamma k} = H^{n-k}_{\alpha,\gamma} - n\omega\delta_{nk}\delta_{\alpha,\gamma}$ we see that the equations for the Green's functions in the extended space and the Floquet Green's functions in the original space (2.60) are the same, and therefore both objects are equivalent. This equivalence gives a nice interpretation of the Floquet Green's functions that will help later to understand the results obtained.

Now that we know how to work with the Floquet Green's functions and we have some intuition for them we are in a position to calculate expressions for the observables we want to study, the density of states and the current, for any system. The first object one encounters is the Green's function of a quadratic Hamiltonian. As an example, lets consider again the resonant level with a general driving, given by the many-body Hamiltonian

$$H(t) = \sum_{\sigma=\uparrow,\downarrow} d^\dagger_\sigma \varepsilon_\sigma(t) d_\sigma \tag{2.64}$$

The contour-ordered Green's function of the resonant level evaluated in the Keldysh contour is given by

$$g^c_\sigma(t,t') = \left\langle \mathcal{T}_\mathcal{C}\left\{ d_\sigma(t) d^\dagger_\sigma(t')\right\}\right\rangle \tag{2.65}$$

Using the Heisenberg equation, we can obtain the time dependence of the annihilation operator as

$$\begin{aligned} \frac{\partial}{\partial t} d_\sigma(t) &= i[H, d_\sigma](t) \\ &= ie^{i\int_0^t dt_1\, H(t_1)}[\sum_{\sigma'} d^\dagger_{\sigma'}\varepsilon_{\sigma'}(t) d_{\sigma'}, d_\sigma] e^{-i\int_0^t dt_1\, H(t_1)} \\ &= -ie^{i\int_0^t dt_1\, H(t_1)} d_\sigma \varepsilon_\sigma(t) e^{-i\int_0^t dt_1\, H(t_1)} \\ &= -i\varepsilon_\sigma(t) d_\sigma(t). \end{aligned} \tag{2.66}$$

Applying now the equation of motion to the bare Green's function we obtain

$$\begin{aligned} i\partial_t g^c_\sigma(t,t') &= \delta_C(t-t') + \left\langle \mathcal{T}_\mathcal{C}\left\{ i\partial_t d_\sigma(t)^\dagger_\sigma(t')\right\}\right\rangle \\ &= \delta_C(t-t') + \varepsilon_\sigma(t) g^c_\sigma(t,t'), \end{aligned} \tag{2.67}$$

where

$$\delta_C(t-t') = \begin{cases} \delta(t-t') & t,t' \in C_+ \\ -\delta(t-t') & t,t' \in C_- \\ 0 & \text{otherwise} \end{cases}, \tag{2.68}$$

where C_+, C_- are the two branches of the Keldysh contour as shown in fig 2.2. We can rewrite the equation of motion for the Green's function, showing that it is in fact the Green's function for the Schrödinger equation (2.41)

$$(i\partial_t - \varepsilon_\sigma(t))g^c_\sigma(t,t') = \delta_C(t-t'). \tag{2.69}$$

Using the Langreth rules from Appendix B we obtain now the retarded and advanced Green's functions as

$$(i(\partial_t \pm i0^+) + \varepsilon_\sigma(t))g^{r,a}_\sigma(t,t') = \delta(t-t'), \tag{2.70}$$

and we can easily find a solution for the Green's function as one would do with a time-independent Hamiltonian by Fourier transforming the equation, in this case twice

$$\begin{aligned}(i(\partial_t \pm 0^+) - \sum_k e^{-ik\omega t}\varepsilon^k_\sigma) \sum_{nm} \int_{-\omega/2}^{\omega/2} d\varepsilon\, e^{-i(\varepsilon+n\omega)t+i(\varepsilon+m\omega)t'} g^{r,a}_{\sigma,nm}(\varepsilon) \\ = \sum_{nm} \int_{-\omega/2}^{\omega/2} e^{-i(\varepsilon+n\omega)t+i(\varepsilon+m\omega)t'}.\end{aligned} \tag{2.71}$$

We can identify term by term and obtain a result for the elements of the Floquet Green's function as

$$\sum_{n_1} \left[(\varepsilon \pm i0^+ + n\omega)\delta_{nn_1} - \varepsilon^{n-n_1}_\sigma\right] g^{r,a}_{\sigma,n_1m}(\varepsilon) = 1. \tag{2.72}$$

We reach a very important result. We found an analytical expression for the inverse of the retarded and advanced Floquet Green's function of any quadratic time-periodic Hamiltonian as

$$g^{r,a\,-1}_{\sigma,nm}(\varepsilon) = (\varepsilon \pm i0^+ + n\omega)\delta_{nm} - \varepsilon^{n-m}_\sigma, \tag{2.73}$$

We also identify (2.72) as the Schrödinger equation (2.41) of the extended space with the Floquet Hamiltonian. Finding now the Floquet Green's function and with that the two time Green's function sums up to simply inverting a matrix. We can do this by first finding the unitary transformation that diagonalizes the Green's function in Floquet space

$$Q^{r,a\,-1}_{\sigma,nn}(\varepsilon) = \sum_{n_1n_2} \Lambda^\dagger_{\sigma,nn_1}(\varepsilon) g^{r,a\,-1}_{\sigma,n_1m_2}(\varepsilon)\Lambda_{\sigma,n_2m}(\varepsilon). \tag{2.74}$$

Assuming that this is a Green's function in the extended space, diagonalizing the Green's function sums up to writing it in the basis of the eigenstates of the Floquet Hamiltonian, the Floquet states. First note that since the Hamiltonian is quadratic the Floquet states are the time-evolved states $|\sigma(t)\rangle$ with quasienergy ε^0_σ

$$U(t+T,t)\,|\sigma(t)\rangle = e^{-i\int_t^{t+T} dt_1\, \varepsilon_\sigma(t_1)}\,|\sigma(t)\rangle = e^{-i\varepsilon^0_\sigma T}\,|\sigma(t)\rangle\,. \tag{2.75}$$

The equivalent Green's function in the extended space, expanded in the basis of the eigenstates of the Floquet Hamiltonian, is then given by

$$\begin{aligned} g^r_{\sigma n,\sigma m}(t-t') &= -i\theta(t-t')\langle\!\langle \sigma n|\hat{U}(t-t')|\sigma m\rangle\!\rangle \\ &= \sum_{\nu\mu,n_1n_2} \langle\!\langle \sigma n|u^{n_1}_\nu\rangle\!\rangle(-i\theta(t-t')\langle\!\langle u^{n_1}_\nu|\hat{U}(t-t')|u_{\mu,n_2}\rangle\!\rangle)\langle\!\langle u_{\mu,n_2}|\sigma m\rangle\!\rangle \\ &= \sum_{n_1}\langle\!\langle \sigma n|u_{\sigma,n_1}\rangle\!\rangle(-i\theta(t-t')\langle\!\langle u_{\sigma,n_1}|\hat{U}(t-t')|u_{\sigma,n_1}\rangle\!\rangle)\langle\!\langle u_{\sigma,n_1}|\sigma m\rangle\!\rangle, \end{aligned} \tag{2.76}$$

where we can identify the diagonalized Green's function as

$$Q^r_{\sigma n,\sigma n}(t-t') = -i\theta(t-t')\langle\!\langle u_{\sigma,n}|\hat{U}(t-t')|u_{\sigma,n}\rangle\!\rangle, \tag{2.77}$$

and the Λ matrix as

$$\begin{aligned} \Lambda_{\sigma,nm} &= \langle\!\langle \sigma n|u_{\sigma,m}\rangle\!\rangle \\ &= \left\langle \sigma\middle|u^{n-m}_\sigma\right\rangle \\ &= \langle\sigma|\,\frac{1}{T}\int_0^T dt\, e^{i(n-m)\omega t}\,|u_\sigma(t)\rangle \\ &= \langle\sigma|\,\frac{1}{T}\int_0^T dt\, e^{i(n-m)\omega t}e^{i\varepsilon^0_d t}\,|\sigma(t)\rangle \\ &= \frac{1}{T}\int_0^T dt\, e^{i(n-m)\omega t}e^{i\varepsilon^0_d t}e^{-i\int_0^t dt_1\,\varepsilon_d(t_1)} \\ &= \frac{1}{T}\int_0^T dt\, e^{i(n-m)\omega t}e^{-i\int_0^t dt_1\,(\varepsilon_d(t_1)-\varepsilon^0_d)}, \end{aligned} \tag{2.78}$$

where we used the relation for Floquet states in different Brillouin zones (2.34). This same result for the Λ matrix and the decomposition of the Green's function in terms of the diagonalized one can be found in [19] with a much more complicated derivation, which comes to show how powerful the Floquet formalism is. These matrices are in fact unitary

$$\begin{aligned} \sum_{n_1}\Lambda_{\sigma,nn_1}\Lambda^\dagger_{\sigma,n_1m} &= \frac{1}{T}\int_0^T dt_1 e^{-i(n-n_1)\omega t_1}e^{-i\int_0^{t_1}\,dt_2(\varepsilon_\sigma(t_1)-\varepsilon_{\sigma,0})}\frac{1}{T} \\ &\quad\times\int_0^T dt_1 e^{i(n_1-m)\omega t_1}e^{i\int_0^{t_1}\,dt_2(\varepsilon_\sigma(t_1)-\varepsilon_{\sigma,0})} \\ &= \int_{-\pi}^{\pi}\frac{dx}{2\pi}\int_{-\pi}^{\pi}\frac{dy}{2\pi}\sum_{n_1}e^{i(nx-my)-in_1(x-y)}e^{-\frac{i}{\omega}\int_y^x dz\,(\varepsilon_\sigma(t)-\varepsilon_{\sigma,0})} \\ &= \int_{-\pi}^{\pi}\frac{dx}{2\pi}e^{i(n-m)x} = \delta_{n,m}. \end{aligned} \tag{2.79}$$

Applying them to the $n\omega$ term we obtain

$$\begin{aligned}
&\sum_{n_1}\Lambda_{\sigma,nn_1}n_1\omega\Lambda^{\dagger}_{\sigma n_1 m}\\
&=\int_{-\pi}^{\pi}\frac{dx}{2\pi}\int_{-\pi}^{\pi}\frac{dy}{2\pi}\sum_{n_1}e^{i(nx-my)-in_1(x-y)}n_1\omega e^{-\frac{i}{\omega}\int_y^x dz(\varepsilon_\sigma(z/\omega)-\varepsilon_{\sigma,0})}\\
&=\int_{-\pi}^{\pi}\frac{dx}{2\pi}\int_{-\pi}^{\pi}dy\,e^{i(nx-my)}i\omega[\frac{\partial}{\partial x}\delta(x-y)]e^{-\frac{i}{\omega}\int_y^x dz(\varepsilon_\sigma(z/\omega)-\varepsilon_{\sigma,0})}\\
&=i\omega e^{i(n-m)x}|_{-\pi}^{\pi}-\int_{-\pi}^{\pi}\frac{dx}{2\pi}\int_{-\pi}^{\pi}dy\,\delta(x-y)[n\omega-\varepsilon_\sigma(x/\omega)+\varepsilon_{\sigma,0}])\\
&\quad\times e^{i(nx-my)}e^{-\frac{i}{\omega}\int_y^x dz(\varepsilon_\sigma(z/\omega)-\varepsilon_{\sigma,0})}\\
&=[n\omega+\varepsilon_{\sigma,0}]\delta_{n,m}-\varepsilon_{\sigma,n-m}.
\end{aligned}\tag{2.80}$$

And we can find the diagonalized inverse Floquet Green's function as

$$Q^{r,a\,-1}_{\sigma,nn}(\varepsilon)=\varepsilon\pm i0^{+}+n\omega-\varepsilon^{0}_{\sigma},\tag{2.81}$$

which in fact coincides with the inverse Green's function of the state $|u_{\sigma,n}\rangle\!\rangle$ in the extended space.

$$Q^{r,a\,-1}_{u_{\sigma,n},u_{\sigma,n}}=\varepsilon\pm i0^{+}-\langle\!\langle u_{\sigma,n}|\hat{H}^{F}|u_{\sigma,n}\rangle\!\rangle.\tag{2.82}$$

The inverse Floquet Green's function can be written in matrix form in Floquet space as

$$\boldsymbol{g}^{r,a\,-1}_{\sigma}(\varepsilon)=\boldsymbol{\Lambda}_{\sigma}\boldsymbol{Q}^{r,a\,-1}_{\sigma}(\varepsilon)\boldsymbol{\Lambda}^{\dagger}_{\sigma},\tag{2.83}$$

and using the fact that the matrices $\boldsymbol{\Lambda}$ are unitary the Floquet Green's function can be obtained as

$$\begin{aligned}
\boldsymbol{g}^{r,a}_{\sigma}(\varepsilon)=&[\boldsymbol{\Lambda}_{\sigma}\boldsymbol{Q}^{r,a\,-1}_{\sigma}(\varepsilon)\boldsymbol{\Lambda}^{\dagger}_{\sigma}]^{-1}\\
=&\boldsymbol{\Lambda}_{\sigma}\boldsymbol{Q}^{r,a}_{\sigma}(\varepsilon)\boldsymbol{\Lambda}^{\dagger}_{\sigma}.
\end{aligned}\tag{2.84}$$

Lets consider again a harmonic drive for the resonant level given by $\varepsilon_\sigma(t)=\varepsilon^0_\sigma+A_\sigma\cos(\omega t+\phi_\sigma)$. The unitary matrices that diagonalize the Floquet Green's functions in the Floquet space are

$$\begin{aligned}
\Lambda_{\sigma,nm}&=\frac{1}{T}\int_0^T dt\,e^{i(n-m)\omega t}e^{-i\int_0^t dt'\,(\varepsilon_\sigma(t)-\varepsilon^0_\sigma)}\\
&=\frac{1}{T}\int_0^T dt\,e^{i(n-m)\omega t}e^{-i\int_0^t dt'\,A_\sigma\cos(\omega t+\phi_\sigma)}\\
&=\frac{1}{T}\int_0^T dt\,e^{i(n-m)\omega t}e^{-i\frac{A_\sigma}{\omega}\sin(\omega t+\phi_\sigma)}e^{i\frac{A_\sigma}{\omega}\sin(\phi_\sigma)}.
\end{aligned}\tag{2.85}$$

Using the identity $e^{-i\alpha\sin(\omega t+\phi_n)}=\sum_{k=-\infty}^{\infty}e^{-ik\phi_n}e^{-ik\omega t}J_k(\alpha)$, the elements of $\boldsymbol{\Lambda}_\sigma$ reduce to

$$\begin{aligned}
\Lambda_{\sigma,nm}&=e^{i\frac{A_\sigma}{\omega}\sin(\phi_\sigma)}\frac{1}{T}\int_0^T dt\,\sum_{n_1}e^{i(n-m-n_1)\omega t}e^{-in_1\phi_\sigma}J_{n_1}\left(\frac{A_\sigma}{\omega}\right)\\
&=e^{i\frac{A_\sigma}{\omega}\sin(\phi_\sigma)}e^{-i(n-m)\phi_\sigma}J_{n-m}\left(\frac{A_\sigma}{\omega}\right),
\end{aligned}\tag{2.86}$$

and using this result we get a final expression for the Floquet Green's function,

$$g^{r,a}_{\sigma,nm}(\varepsilon) = e^{-i(n-m)\phi_\sigma} \sum_{n_1} \frac{J_{n-n_1}(\frac{A_\sigma}{\omega}) J_{m-n_1}\left(\frac{A_\sigma}{\omega}\right)}{\varepsilon + n_1\omega \pm i0^+ - \varepsilon^0_\sigma}. \tag{2.87}$$

With this result we can already calculate one of the observables we are interested in, the spectral function, for the case of the isolated resonant level, defined as

$$A_\sigma(t,t') = -2\mathrm{Im}\left\{g^r_\sigma(t,t')\right\}. \tag{2.88}$$

For a time-independent Hamiltonian, the Fourier transform of the spectral function on the time difference is interpreted as the spectral weight of electron σ at an energy ε given by the Fourier variable, and tracing over it one obtains the density of states (DOS). To simplify things, throughout the thesis we will only look at the time-averaged spectral function

$$\begin{aligned} A^0_\sigma(\varepsilon) &= \frac{1}{T}\int_0^T dt \int_{-\infty}^{\infty} e^{-i\varepsilon(t-t')} A_\sigma(t,t') \\ &= -2\mathrm{Im}\left\{g^r_{\sigma,00}(\varepsilon)\right\}. \end{aligned} \tag{2.89}$$

Note that the density of states is defined for $\varepsilon \in (-\infty,\infty)$ but our Floquet Green function are only defined on the first Brillouin zone, $\varepsilon \in [-\omega/2, \omega/2)$. In order to calculate the full energy range of the density of states we make use of the relation (2.49), which relates the Floquet Green's functions in different zones as

$$g_{nm}(\varepsilon + n_1\omega) = g_{n+n_1,m+n_1}(\varepsilon), \tag{2.90}$$

and we obtain the time-averaged spectral function by piecing together all diagonal components of the retarded Floquet Green's function

$$A^0_\sigma = -2\mathrm{Im}\left\{\sum_n g^r_{\sigma,nn}(\varepsilon)\right\} = \sum_n A_{\sigma n}(\varepsilon), \tag{2.91}$$

which can be interpreted as the sum of the spectral weights of the states $|\sigma n\rangle\!\rangle$ in the extended space. Substituting the expression we obtained for the time-ordered level Floquet Green's function (2.87) we finally obtain a result for the time-averaged density of states of the driven dot, which is shown in Fig. 2.3,

$$A^0_d(\varepsilon) = \sum_{n,\sigma} J_n\left(\frac{A_\sigma}{\omega}\right)^2 \delta(\varepsilon + n\omega - \varepsilon^0_d), \tag{2.92}$$

which we can understand as one electron being spread into the different Floquet states at energies $\varepsilon^0_d - n\omega$ with spectral weight $J_n(\frac{A_\sigma}{\omega})^2$, as the Bessel functions of the first kind obey the sum rule $\sum_n J_n(x)^2 = 1$.

Since the Floquet Hamiltonian is not bounded one might ask what happens to the occupation of the states $|\sigma, n\rangle\!\rangle$, given by the lesser Green's function $g^<_{\sigma n}(\varepsilon)$. Consider the time periodic Hamiltonian of a metal

$$H(t) = \sum_k \varepsilon_k(t) c^\dagger_k c_k. \tag{2.93}$$

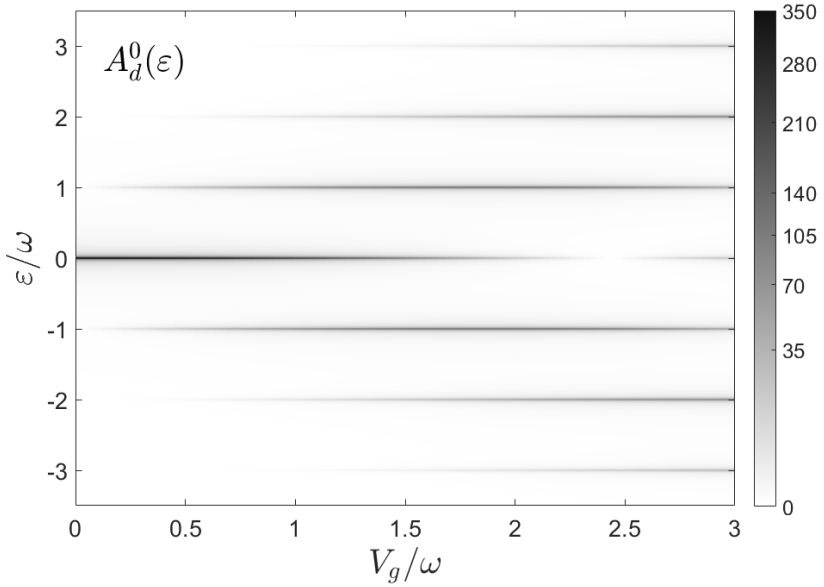

Figure 2.3: Time-averaged density of states of a driven isolated dot with frequency $\omega = 1$, driving amplitude $A_\sigma = V_g$ and time-averaged energy $\varepsilon_d^0 = 0$, with the bound states broaden from the coupling to a metallic lead with $\Gamma_m = 0.2\omega$. There is a bound state at zero energy as in equilibrium and Floquet bands appear at energies $n\omega$.

We consider that the bath was at equilibrium at some point in the past and the driving has been turned on adiabatically. The lesser Green's function is the given by

$$\begin{aligned} g_k^<(t,t') =& i\left\langle c_k^\dagger(t')c_k(t)\right\rangle \\ =& i\left\langle c_k^\dagger(t)c_k(t)\right\rangle e^{-i\int_t^{t'} dt_1\,\varepsilon_k(t_1)} \\ =& i n_F(\varepsilon_k^0) e^{-i\int_t^{t'} dt_1\,\varepsilon_k(t_1)}, \end{aligned} \tag{2.94}$$

where we assumed that the period of the drive is much smaller than the time it takes the bath to equilibrate and therefore it follows the Fermi equilibrium distribution $n_F(\varepsilon)$ [14]. In the specific case of an harmonic drive, after doing the integral and transforming we finally obtain

$$g_{k,nm}^<(\varepsilon) = i\sum_{n_1} J_{n-n_1}\left(\frac{A_k}{\omega}\right) J_{m-n_1}\left(\frac{A_k}{\omega}\right) n_F(\varepsilon_k^0)\delta(\varepsilon + n_1\omega - \varepsilon_k^0), \tag{2.95}$$

Which does not follow a simple Fermi distribution, but rather, each band can be considered to follow a Fermi distribution. That means that the low energy Floquet modes $|kn\rangle\rangle$ of a high energy state $|k\rangle$ are not occupied as long as $A_k << \omega$. Looking at the result we see that it could also obtained as we did for the retarded and advanced functions

$$g_{k,nm}^<(\varepsilon) = [\boldsymbol{\Lambda}_k \boldsymbol{Q}_k^<(\varepsilon)\boldsymbol{\Lambda}_k^\dagger]_{nm}. \tag{2.96}$$

The diagonalized lesser Green's function can then be calculated as

$$\begin{aligned} Q_{k,nn}^<(\varepsilon) &= -n_F(\varepsilon_k^0)(Q_{k,nn}^r(\varepsilon) - Q_{k,nn}^a(\varepsilon)) \\ &= i n_F(\varepsilon_k^0)\delta(\varepsilon + n\omega - \varepsilon_k^0), \end{aligned} \tag{2.97}$$

where we see that it does follow the usual Fermi distribution at equilibrium. The next step in studying our model of the driven resonant level is considering what happens if we add tunneling into the resonant level, i.e. non-quadratic terms to the Hamiltonian. Consider a harmonically driven resonant level contacted by two metallic leads that might also be driven. The Hamiltonian of the system is given by

$$H(t) = H_m(t) + H_d(t) + H_t, \tag{2.98}$$

where $H_m(t)$ describes the metallic leads, $H_d(t)$ the resonant level and H_t the tunneling between them, which we consider time-independent. To simplify the model we are going to consider only the case of symmetric coupling, independent of spin or momentum, and a driving that respects spin symmetry. We will therefore drop the spin indices because the spins will be degenerate. The Hamiltonians for each part of the system are given by

$$\begin{aligned} H_m(t) &= \sum_{\alpha=L,R;k} (\varepsilon_{\alpha k} - \mu_\alpha(t)) c^\dagger_{\alpha k} c_{\alpha k} \\ H_d &= \varepsilon_d(t) d^\dagger d \\ H_t(t) &= \sum_{\alpha=L,R;k,} \left[t c^\dagger_{\alpha k} d + t^* d^\dagger c_{\alpha k} \right], \end{aligned} \tag{2.99}$$

where the drivings are given by $\varepsilon_d(t) = \varepsilon_d^0 + A_d \cos(\omega t)$ and $\mu_\alpha(t) = \mu_\alpha^0 + A_\alpha \cos(\omega t)$. First we want to calculate the full contour-ordered Green's function on the Keldysh contour, defined again as

$$G^c_{d,d}(t,t') = -i \left\langle \mathcal{T}_\mathcal{C} \left\{ d(t) d^\dagger(t') \right\} \right\rangle. \tag{2.100}$$

To do so we will employ again the equation of motion technique. The Heisenberg equation for the annihilation operator is

$$\begin{aligned} \partial_t d(t) &= i[H(t), d](t) \\ &= i[\varepsilon_d(t) d^\dagger d + \sum_{\alpha k} t^* d^\dagger c_{\alpha k}, d](t) \\ &= -i\varepsilon_d(t) d(t) - i \sum_{\alpha k} t^* c_{\alpha k}(t), \end{aligned} \tag{2.101}$$

and with that result we can calculate the derivative of the full time-ordered Green's function of the level as

$$\begin{aligned} i\partial_t G^c_{d,d}(t,t') &= -i\delta(t-t') - i \left\langle \mathcal{T}_\mathcal{C} \left\{ i\partial_t d(t) d^\dagger(t') \right\} \right\rangle \\ &= -i\delta_C(t-t') - i \left\langle \mathcal{T}_\mathcal{C} \left\{ \left(\varepsilon_d(t) d(t) + \sum_{\alpha k} t^* c_{\alpha k}(t) \right) d^\dagger(t') \right\} \right\rangle \\ &= -i\delta_C(t-t') + \varepsilon_d(t) G^c_{d,d}(t,t') + t^* \sum_{\alpha k} G^c_{\alpha k,d}(t,t'), \end{aligned} \tag{2.102}$$

where the mixed Green's function is defined as

$$G^c_{\alpha k,d}(t,t') = -i \left\langle \mathcal{T}_\mathcal{C} \left\{ c_{\alpha k}(t) d^\dagger(t') \right\} \right\rangle. \tag{2.103}$$

By grouping both terms with the level Green's functions in (2.102) we can identify the term in front as the inverse of the bare Green's function (2.69) , multiplying on the left by it we obtain

$$G^c_{d,d}(t,t') = g^c_{d,d}(t,t') + \int_C dt_1 \sum_{\alpha k} g^c_{d,d}(t,t_1)\, t^*\, G^c_{\alpha k,d}(t_1,t'). \tag{2.104}$$

In order to solve for the full level Green's function we need the mixed Green's function. The Heisenberg equation for the annihilation operator of the lead α is

$$\begin{aligned}\partial_t c_{\alpha k}(t) &= i[H(t), d](t) \\ &= i[\sum_{\alpha' k'} (\varepsilon_{\alpha' k'} - \mu_{\alpha'}(t)) c^\dagger_{\alpha' k'} c_{\alpha' k'} + \sum_{\alpha' k'} t c^\dagger_{\alpha' k'} d, c_{\alpha k}](t) \\ &= -i(\varepsilon_{\alpha k} - \mu_\alpha) c_{\alpha k}(t) - itd(t)\end{aligned} \tag{2.105}$$

and we can use to calculate the time derivative of the mixed Green's function

$$\begin{aligned}i\partial_t G^c_{\alpha k,d}(t,t') &= -i \left\langle \mathcal{T}_\mathcal{C} \left\{ i\partial_t c_{\alpha k}(t) d^\dagger(t') \right\} \right\rangle \\ &= -i \left\langle \mathcal{T}_\mathcal{C} \left\{ ((\varepsilon_{\alpha k} - \mu_\alpha) c_{\alpha k}(t) + td(t))\, d^\dagger(t') \right\} \right\rangle \\ &= t G^c_{d,d}(t,t') + \sum_{\alpha k} (\varepsilon_{\alpha k} - \mu_\alpha) G^c_{\alpha k,d}(t,t').\end{aligned} \tag{2.106}$$

By identifying again the bare lead Green's function and multiplying on the left by it we find an expression for the mixed Green's function in terms of the level Green's function

$$G^t_{\alpha k,d}(t,t') = \int_C dt_1\, g^t_{\alpha k,\alpha k}(t,t_1) t G^t_{d,d}(t_1,t'). \tag{2.107}$$

Substituting this expression for the mixed Green's function into the expression for the level Green's function (2.104) we obtain

$$G^c_{d,d}(t,t') = g^c_{d,d}(t,t') + \int_C dt_1 \int_C dt_2 \sum_{\alpha k} g^c_{d,d}(t,t_1) t^* g_c \alpha k, \alpha k(t_1,t_2) t G^c_{d,d}(t_2,t'). \tag{2.108}$$

By defining the contour-ordered self-energy as

$$\Sigma^c_\alpha(t,t') = \sum_k t^* g^c_{\alpha k}(t,t') t, \tag{2.109}$$

the equation for the full level Green's function can be rewritten into

$$G^c_{d,d}(t,t') = g^c_{d,d}(t,t') + \int_C dt_1 \int_C dt_2\, g^c_d(t,t_1) \Sigma^c_{\alpha k}(t_1,t_2) G^c_{d,d}(t_2,t'), \tag{2.110}$$

a self consistent equation for the full contour-ordered level Green's function known as the Dyson equation. Using the Langreth rules we can obtain the Dyson equation for the retarded and advanced Green's functions

$$G^{r,a}_{d,d}(t,t') = g^{r,a}_{d,d}(t,t') + \int_{-\infty}^{\infty} dt_1 \int_{-\infty}^{\infty} dt_2\, g^{r,a}_d(t,t_1) \Sigma^{r,a}_{\alpha k}(t_1,t_2) G^{r,a}_{d,d}(t_2,t'). \tag{2.111}$$

Using the fact that we can transform the time convolutions into matrix products in Floquet space (2.51) the elements of the full retarded and advanced Floquet Green's functions take the form

$$G^{r,a}_{dd,nm}(\varepsilon) = g^{r,a}_{d,nm}(\varepsilon) + \sum_{n_1,n_2} g^{r,a}_{d,n,n_1}(\varepsilon) \sum_{\alpha} \Sigma^{r,a}_{\alpha,n_1 n_2}(\varepsilon) G^{r,a}_{dd,n_2 m}(\varepsilon). \tag{2.112}$$

By grouping the full Floquet Green's function we find the explicit expression

$$\begin{aligned} G^{r,a}_{dd,nm}(\varepsilon) &= \left[\frac{1}{1 - \boldsymbol{g}^{r,a}_d(\varepsilon) \sum_\alpha \boldsymbol{\Sigma}^{r,a}_\alpha(\varepsilon)} \boldsymbol{g}^{r,a}_d(\varepsilon) \right]_{nm} \\ &= \left[\frac{1}{\boldsymbol{g}^{r,a\,-1}_d(\varepsilon) - \sum_\alpha \boldsymbol{\Sigma}^{r,a}_\alpha(\varepsilon)} \right]_{nm} \\ &= \left[\frac{1}{(\varepsilon \pm i0^+)\boldsymbol{I}_F + \boldsymbol{n}\omega - \boldsymbol{\varepsilon}_d - \sum_\alpha \boldsymbol{\Sigma}^{r,a}_\alpha(\varepsilon)} \right]_{nm}, \end{aligned} \tag{2.113}$$

where in the last part we introduced the Floquet matrices $[\boldsymbol{I}_F]_{nm} = \delta_{nm}$, $[\boldsymbol{n}]_{nm} = n\delta_{nm}$ and $[\boldsymbol{\varepsilon}_d]_{nm} = \varepsilon_d^{n-m}$. We see again the power of the Floquet representation, solving the self-consistent time-dependent Dyson equation turns again into a simple matrix inversion. Since the Hamiltonian of the leads is quadratic we can use the expressions obtained for the level Green's function of the isolated resonant level (2.87), resulting in

$$g^{r,a}_{\alpha k,nm}(\varepsilon) = \sum_{n_1} \frac{J_{n-n_1}\left(\frac{A_\alpha}{\omega}\right) J_{m-n_1}\left(\frac{A_\alpha}{\omega}\right)}{(\varepsilon \pm i0^+) + n_1\omega - (\varepsilon_{\alpha k} - \mu^0_\alpha)}. \tag{2.114}$$

Substituting this result into the expression for the self-energy (2.109) we can calculate the retarded and advanced self-energies

$$\begin{aligned} \Sigma^{r,a}_{\alpha,nm}(\varepsilon) =& \sum_k |t|^2 g^{r,a}_{\alpha k,nm}(\varepsilon) \\ =& |t|^2 \sum_{n_1} J_{n-n_1}\left(\frac{A_\alpha}{\omega}\right) J_{m-n_1}\left(\frac{A_\alpha}{\omega}\right) \\ & \times \int_{-\infty}^{\infty} d\xi_{\alpha k} \frac{\rho_{\alpha k}}{(\varepsilon \pm i0^+) + k_1\omega - \xi_{\alpha k} \pm i\eta} \\ =& \pm i\pi\rho_\alpha |t|^2 \sum_{n_1} J_{n-n_1}\left(\frac{A_\alpha}{\omega}\right) J_{m-n_1}\left(\frac{A_\alpha}{\omega}\right) \\ =& \pm i\frac{\Gamma_\alpha}{2}\delta_{nm}, \end{aligned} \tag{2.115}$$

where $\rho_{\alpha k}$ is the density of states of the metal, and we have defined the coupling constant $\Gamma_\alpha = 2\pi\rho_\alpha |t|^2$ and in the last step we used the completeness property of Bessel functions. To perform the integral we take the wide band limit where we assume that the density of states is constant through the band, which is infinitely wide. Note that with this approximation the retarded and advanced self-energies are diagonal in Floquet space, and therefore the information about the driving of the leads is lost in

the full level Floquet Green's function. As we will need it later, we calculate as well the lesser self energy of the lead

$$\begin{aligned}\Sigma^{<}_{\alpha,nm}(\varepsilon) =& \sum_k |t|^2 g^{<}_{\alpha k,nm}(\varepsilon) \\ =& i|t|^2 \sum_{n_1} J_{n-n_1}\left(\frac{A_\alpha}{\omega}\right) J_{m-n_1}\left(\frac{A_\alpha}{\omega}\right) \\ & \times \int_{-\infty}^{\infty} d\xi_{\alpha k}\, \rho_{\alpha k} n_F(\varepsilon + n_1\omega)\delta(\varepsilon + n_1\omega - \xi_{\alpha,0}) \\ =& i\rho_{\alpha k}|t|^2 \sum_{n_1} J_{n-n_1}\left(\frac{A_\alpha}{\omega}\right) J_{m-n_1}\left(\frac{A_\alpha}{\omega}\right) n_F(\varepsilon + n_1\omega) \\ =& i\frac{\Gamma_\alpha}{2\pi} \sum_{n_1} J_{n-n_1}\left(\frac{A_\alpha}{\omega}\right) J_{m-n_1}\left(\frac{A_\alpha}{\omega}\right) n_F(\varepsilon + n_1\omega). \end{aligned} \tag{2.116}$$

Using the expression for the self-energy the retarded and advanced full level Floquet Green's functions are given by

$$G^{r,a}_{dd,nm}(\varepsilon) = \left[\frac{1}{(\varepsilon \pm i0^+)\boldsymbol{I}_F + \boldsymbol{n}\omega - \boldsymbol{\varepsilon}_d \mp i\sum_\alpha \Gamma_\alpha/2 \boldsymbol{I}_F}\right]_{nm}. \tag{2.117}$$

We can group both terms that are diagonal in Floquet space and identify the solution as the bare level Floquet Green's function with the Fourier variable ε shifted by the self-energy. The expression for the retarded and advanced level Floquet Green's functions then reduces to

$$\begin{aligned} G^{r,a}_{dd,nm}(\varepsilon) =& g^{r,a}_{dd,nm}(\varepsilon \mp i\sum_\alpha \Gamma_\alpha/2) \\ =& \sum_{n_1} \frac{J_{n-n_1}(\frac{A_d}{\omega}) J_{m-n_1}(\frac{A_d}{\omega})}{\varepsilon + n_1\omega - \varepsilon_d^0 \mp i\sum_\alpha \Gamma_\alpha/2}. \end{aligned} \tag{2.118}$$

With this result we can calculate the density of states for the whole system, which will be the same as for the isolated dot (2.92) with the peaks at the quasienergies being broaden by the self-energy, just as it happens in the equilibrium case.

The next observable we are interested in is the current that goes through the resonant level when contacted by two metallic leads with a finite voltage bias. We obtain the time-dependent current going out of a lead by calculating the expectation value of the time derivative of the number operator of the lead

$$\begin{aligned} J_\alpha(t) =& -2\left\langle \dot{N}_\alpha(t)\right\rangle \\ =& -2\left\langle [\mathcal{H}(t), N_\alpha(t)]\right\rangle, \end{aligned} \tag{2.119}$$

where the number operator of lead α is $N_\alpha = \sum_k c^\dagger_{\alpha k} c_{\alpha k}$, the factor 2 accounts for the spin and we have set $e = 1$. Since N_α commutes with H_m and H_d we find

$$J_\alpha(t) = 2i\sum_k \left[t\left\langle c^\dagger_{\alpha k}(t) d(t)\right\rangle - t^*\left\langle d^\dagger(t) c_{\alpha k}(t)\right\rangle\right]. \tag{2.120}$$

The expectation values are the lesser mixed Green's functions and its hermitian conjugate, so we can rewrite the current function as

$$J_\alpha(t) = 4\,\mathrm{Re}\left\{ t \sum_k G^<_{d,\alpha k}(t,t) \right\}. \tag{2.121}$$

We already calculated the full time-ordered mixed Green's function (2.107), to calculate the lesser we perform the analytical continuation prescribed by the Keldysh formalism discussed in Appendix B [13]. Applying the Langreth rules to the time-ordered mixed Green's function we obtain

$$G^<_{d,\alpha k}(t,t') = \int dt_1 \left[G^r_{dd}(t,t_1) t^* g^<_{\alpha k}(t_1,t') + G^<_{dd}(t,t_1) t^* g^a_{k\alpha}(t_1,t') \right]. \tag{2.122}$$

The lesser full level Green's functions can be obtained by applying the Langreth rules to the Dyson equation

$$\begin{aligned} G^<_{dd}(t,t') =& g^<_d(t,t') + \int_{-\infty}^{\infty} dt_1 \int_{-\infty}^{\infty} dt_2\, g^r_d(t,t_1)\Sigma^r_d(t_1,t_2)G^<_{dd}(t_2,t') \\ &+ \int_{-\infty}^{\infty} dt_1 \int_{-\infty}^{\infty} dt_2\, g^r_d(t,t_1)\Sigma^<_d(t_1,t_2)G^a_{dd}(t_2,t') \\ &+ \int_{-\infty}^{\infty} dt_1 \int_{-\infty}^{\infty} dt_2\, g^<_d(t,t_1)\Sigma^a_d(t_1,t_2)G^a_{dd}(t_2,t'), \end{aligned} \tag{2.123}$$

which in the case of steady state systems switched on adiabatically reduces to

$$G^<_{dd}(t,t') = \int_{-\infty}^{\infty} dt_1 \int_{-\infty}^{\infty} dt_2\, G^r_{dd}(t,t_1)\Sigma^<_d(t_1,t_2)G^a_{dd}(t_2,t'). \tag{2.124}$$

With this result we can calculate the Floquet lesser Green's function as

$$G^<_{dd,nm}(\varepsilon) = \sum_{n_1,n_2} G^r_{dd,nn_1}(\varepsilon)\Sigma^<_{d,n_1n_2}(\varepsilon)G^a_{dd,n_2m}(\varepsilon), \tag{2.125}$$

for which a very complicated analytical expression can be found that is not worth showing here. Using the result for the lesser mixed Green's function (2.123) on the expression for the current (2.121) we arrive at the Landauer formula

$$J_\alpha(t) = 4\mathrm{Re}\left\{ \int dt_1 \, \left[G^r_{dd}(t,t_1)\Sigma^<_\alpha(t_1,t) + G^<_{dd}(t,t_1)\Sigma^a_\alpha(t_1,t) \right] \right\}. \tag{2.126}$$

Transforming the Green's functions and self-energies into their corresponding Floquet matrices and Fourier transforming the current we obtain

$$J_\alpha(t) = 4\,\mathrm{Re}\left\{ \sum_{n,m,n_1} e^{-im\omega t} \int_{-\omega/2}^{\omega/2} \frac{d\varepsilon}{2\pi} \left[G^r_{d,nn_1}(\varepsilon)\Sigma^<_{\alpha,n_1n-m}(\varepsilon) + G^<_{d,nn_1}(\varepsilon)\Sigma^a_{\alpha,n_1n-m}(\varepsilon) \right] \right\}. \tag{2.127}$$

In general, the time dependent current and even its Fourier components give a very complicated result we will not be able to understand, but the expression for the time-averaged current,

$$J^0_\alpha = 4\,\mathrm{Re}\left\{\sum_{n,n_1}\int_{-\omega/2}^{\omega/2}\frac{d\varepsilon}{2\pi}\left[G^r_{d,nn_1}(\varepsilon)\Sigma^<_{\alpha,n_1n}(\varepsilon)+G^<_{d,nn_1}(\varepsilon)\Sigma^a_{\alpha,n_1n}(\varepsilon)\right]\right\}$$
$$= 4\,\mathrm{Tr}_F\left[\mathrm{Re}\left\{\int_{-\omega/2}^{\omega/2}\frac{d\varepsilon}{2\pi}\left[\boldsymbol{G}^r_d(\varepsilon)\boldsymbol{\Sigma}^<_\alpha(\varepsilon)+\boldsymbol{G}^<_d(\varepsilon)\boldsymbol{\Sigma}^a_\alpha(\varepsilon)\right]\right\}\right], \tag{2.128}$$

is equivalent to the current of a tight-binding model with the Floquet indices labeling the sites. Therefore, the results we obtain for the time-averaged current can be also interpreted very easily in terms of the Floquet Hamiltonian in the extended space.

Before we go to the numerical calculation for the harmonically driven resonant level contacted by metallic leads we can do a little summary of what we have learned so far. First of all, a time-periodic system in d dimensions is equivalent to a system in $d+1$ dimensions governed by a time-independent Hamiltonian called the Floquet Hamiltonian. In particular for the case of a driven resonant level we have found that it is equivalent to a 1 dimensional system labeled by the Floquet indices, and the expressions both the time-averaged density of states and the time-averaged current are then equivalent to those of a tight-binding model. We have also learned how to easily calculate the Floquet Green's function of any quadratic Hamiltonian and given a self-energy, we have obtained an expression for the full Floquet Green's function of any Hamiltonian with one-body interactions.

2.3 Numerical calculation with the Floquet Green's function technique

Now that we have explicit expressions to numerically calculate the Green's functions, the density of states and the current, we are in a good position to study more in detail the model for the driven resonant level contacted by metallic leads. Seeing the numerical results for this model will confirm that we have a good intuition for the time-averaged dynamics of the system but at the same time it will illustrate that even for the simplest model of driven phenomena, the time-dependent dynamics are highly non-trivial.

The results from this section are obtained by utilizing the expression for the inverse bare level Floquet Green's function (2.73) and the Floquet Self-energies (2.115) to calculate the inverse of the full level retarded and advanced Floquet Green's function (2.117), which are built truncating the high n Floquet states, $|\varepsilon_\nu - n\omega| >> \Gamma, A_\nu$. The full retarded and advanced Green's function is then build by numerically inverting the matrix in Floquet space. Using that result, the lesser Floquet Green's function is obtained and finally the time-averaged current can be calculated.

For the sake of simplicity and for computational reasons we are going to study the dynamics of few Floquet states, so that the matrix obtained after truncating the high n states is small. The Floquet state $|\psi_{\sigma,n}\rangle\!\rangle$ is at an energy $|\varepsilon^0_\sigma - n\omega| < |(n+1)\omega|$, and the maximum number of relevant Floquet states can be guessed as a rule of thumb by

$n = (A+\Gamma)/\omega$, where A is the amplitude of the drive and Γ the coupling constant, since it wouldn't make physical sense for the system to have states in the extended space at energies the state in $\mathcal{H}$ does not reach at any time. Because of computational limitations the calculations shown throughout the thesis are done by truncating the Green's function in Floquet space to be larger than n but of the same order of magnitude. The accuracy of the results might be improved, but we made sure that all the relevant features arising from the driving that we discuss in this thesis are qualitatively correct, and they are sill present when we include more Floquet modes in the truncation.

There is another issue point regarding the truncation. The models we discuss can be also solved by diagonalizing the Floquet Hamiltonian and obtaining the quasienergies and Floquet states, as we discussed before. But, if we consider that we have to perform a truncation of the Hamiltonian before numerically diagonalizing it, the truncation will result in the energy of the different Floquet bands no longer being separated by ω. This is a problem that does not appear in the Floquet Green's function technique, as this relation between the energies of the different Floquet bands is built in on each Floquet element (2.117). One would think that this feature is preserved at the expense of a less accurate quasienergy ε_ν or amplitude of the Floquet modes, given by the Λ matrices, but it is more desirable because it makes more clear what Floquet bands are related to the same Floquet state, and this fact will make more clear the results of the next chapter.

We proceed to discuss the results obtained numerically. For simplicity we consider only a constant voltage-bias. First, lets take a look at the time-averaged spectral density in Fig.2.4. As we argued before, it consists of a series of delta peaks broaden by the metallic leads, at energies $\varepsilon_d^0 + n\omega$. Also note that these peaks have different weights. The time-dependent spectral function is not an observable, a discussion on

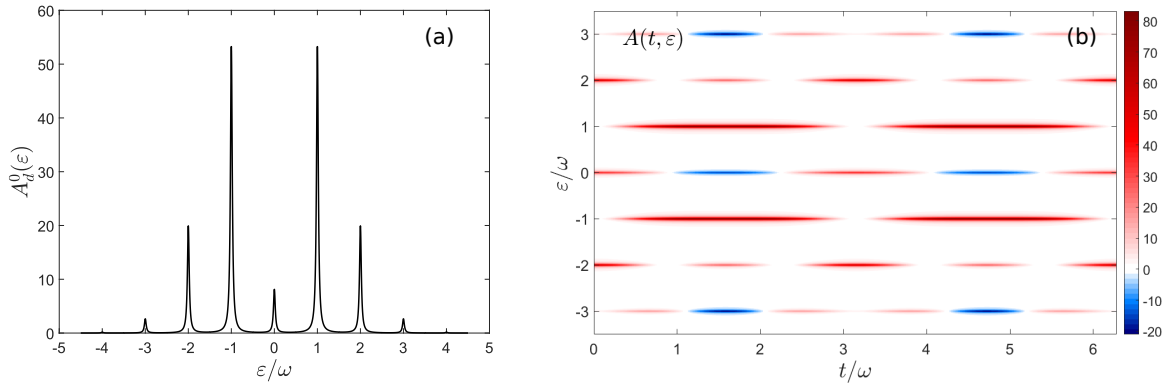

Figure 2.4: Density of states of a dot harmonically driven with $\omega = 1, A_\sigma = 2\omega$ contacted by metallic leads with $\Gamma_m = 0.2\omega$. Note that, as discussed, the density of states is independent of the voltage-bias. (a) Time-averaged density of states of the dot showing the bound states and the Floquet bands. (b) Time-dependent density of states of the dot showing pockets with negative values indicating that it cannot be interpreted as a probability, but rather as a quasiprobability distribution.

this issue can be found in [20]. The result for the time-dependent spectral function in Fig. 2.4 in fact shows pockets with negative weight, meaning that it can no longer be interpreted as a probability.

This might remind the reader of the Wigner function and its interpretation as a quasiprobability distribution. In spatially periodic systems a quasiprobability distribution can be obtained in terms of position and momentum variables as

$$W(x,p) = \int_{-\infty}^{\infty} \frac{dy}{2\pi} dy\, e^{-iky} \psi(x+y/2)\psi^*(x-y/2), \tag{2.129}$$

where the Wigner function is periodic on x. The interpretation of probability is regained again by taking into account the uncertainty principle

$$\sigma_x \sigma_k \geq \frac{1}{2}, \tag{2.130}$$

where $\sigma_{x,k}$ are the standard deviations in position and momentum, and defining a transformed Wigner function which is defined positive,

$$\hat{W}(x,k) = \int_{-\infty}^{\infty}\int_{-\infty}^{\infty} dx_1 dk_1\, W(x_1,k_1) \frac{1}{2\pi\sigma_x\sigma_k} e^{-\frac{x^2}{2\sigma_x^2} - \frac{k^2}{2\sigma_k}} \geq 0. \tag{2.131}$$

We see that in fact our time-dependent spectral function is an analogue of the Wigner function for the time and space variables, and we can use this fact to obtain a new time-dependent DOS as

$$\tilde{A}(t,\sigma_t,\varepsilon,\sigma_\varepsilon) = \int_{-\infty}^{\infty} d\varepsilon_1 \int_{-\infty}^{\infty} dt_1 A(t_1,\varepsilon_1) \frac{1}{2\pi\sigma_\varepsilon\sigma_t} e^{-\frac{(\varepsilon-\varepsilon_1)^2}{2\sigma_\varepsilon^2} - \frac{(t-t_1)^2}{2\sigma_t^2}}, \tag{2.132}$$

which is positive defined as long as the uncertainty principle between time and energy,

$$\sigma_t \sigma_\varepsilon \geq \frac{1}{2}, \tag{2.133}$$

is met. When measuring the time-dependent DOS in an experimental setup, the object we should compare the results with is the transformed time-dependent DOS, where σ_t and σ_ε will depend on the specifics of the measurement. In Fig. 2.5 we show the transformed time-dependent spectral function in two limiting cases. We see that in fact the negative pockets disappeared in both cases. In the case of a good energy resolution, $\sigma_t > \sigma_\varepsilon$ we observe very little time-dependence and we observe the Floquet peaks. In the opposite case, with a good time resolution the time periodicity is recovered, but one cannot make out the Floquet features. For any case in between there is a mixture of time-dependent and Floquet features.

Note that the time-averaged DOS is equal to the transformed DOS with $\sigma_\varepsilon \to \infty$, which ensures that the time-averaged DOS can be interpret as a probability distribution.

Now that we understand our results for the density of states we show the results for the time-averaged current and conductance at different voltages and their time-dependence in Fig.2.6. As we argued when we calculated the expression for the time-averaged current (2.128), it can be understood as the current through a tight-binding model with the Floquet states $|\psi_{\sigma,n}\rangle\rangle$ representing the states at site n with energy $\varepsilon_\sigma^0 + n\omega$. As expected, the time-averaged current is a step-wise function that has a jump when the voltage reaches the energy of each Floquet state. The time-dependent

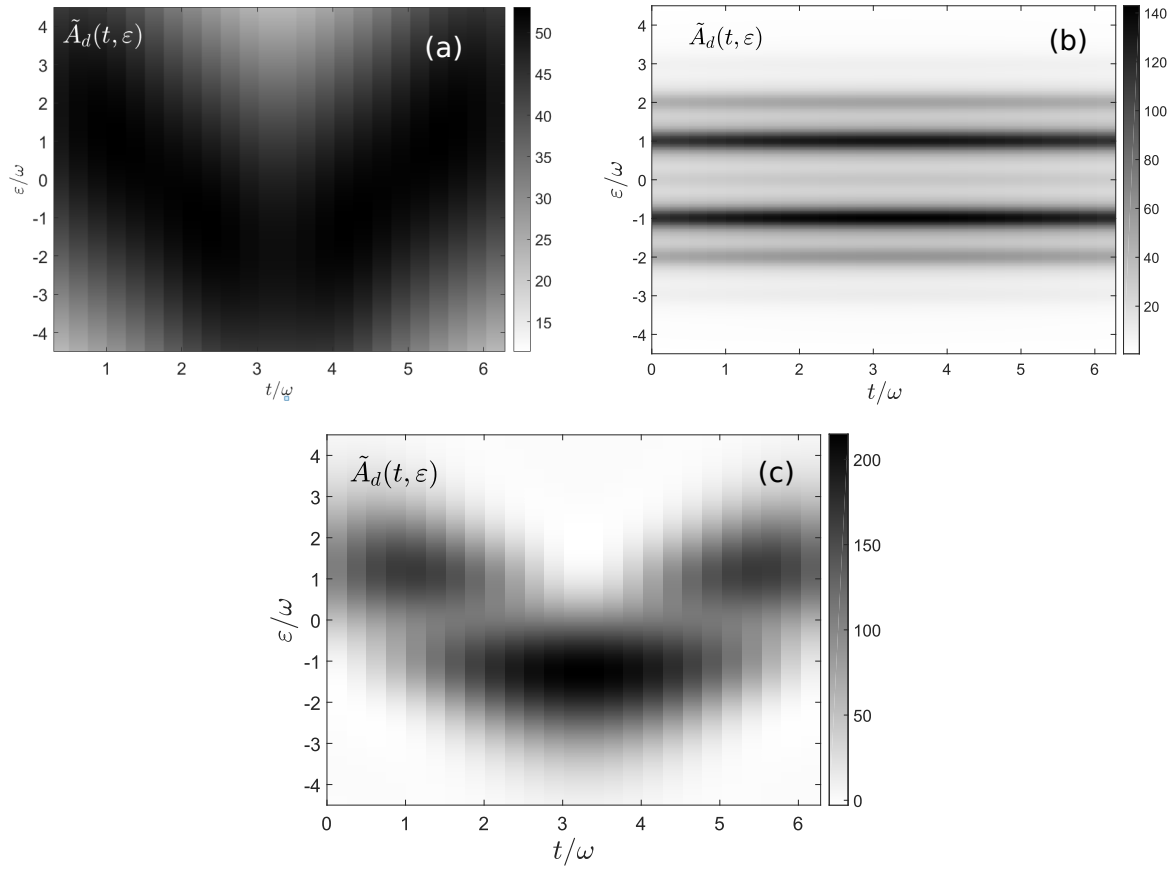

Figure 2.5: Transformed time-dependent dot density of states incorporating the uncertainty principle which can be interpreted as a probability for a driven dot with $\omega = 1, V_g = 2\omega$ coupled to metallic leads with $\Gamma = 0.2\omega$. (a) Case with a good time resolution, $\sigma_t = 0.1, \sigma_\varepsilon = 5$ where we can see the dot oscillating in energy. (b) Case with a good energy resolution $\sigma_t = 5, \sigma_\varepsilon = 0.1$ where we can observe the Floquet features. (c) Case in between, with $\sigma_t = \sigma_\varepsilon = 1/\sqrt{2}$, where we still see the oscillation in energy and Floquet features start to appear.

current and conductance allow us to see both the Floquet and periodicity features. We see that for higher voltages more Fourier components are relevant, since more Floquet modes are involved, but besides that the results are highly non-trivial. To illustrate this, we observe an interesting feature in the time-dependent conductance. If we look at the point where the leads reach the first Floquet mode, we observe that at the times where the energy oscillation of the resonant level reaches the minimum and maximum the conductance is zero. This feature appears in systems symmetric with a low coupling with the metallic leads compared with the amplitude of the drive, which results in sharp peaks in the density of states. The same feature appears in the current in one specific case shown in Fig.2.7. Since the current is given by the integral of the conductance over the voltage, if we take the case where the amplitude of the zeroth Floquet mode vanishes, i.e. when $J_0(\frac{A_d}{\omega}) = 0$, the first contribution to the current will be from the first Floquet mode, and therefore, the zeros of the conductance at this point will appear as zeros in the current as well. This means that for this set of parameters, when the oscillation of the energy of the resonant level reaches its maximum or minimum the

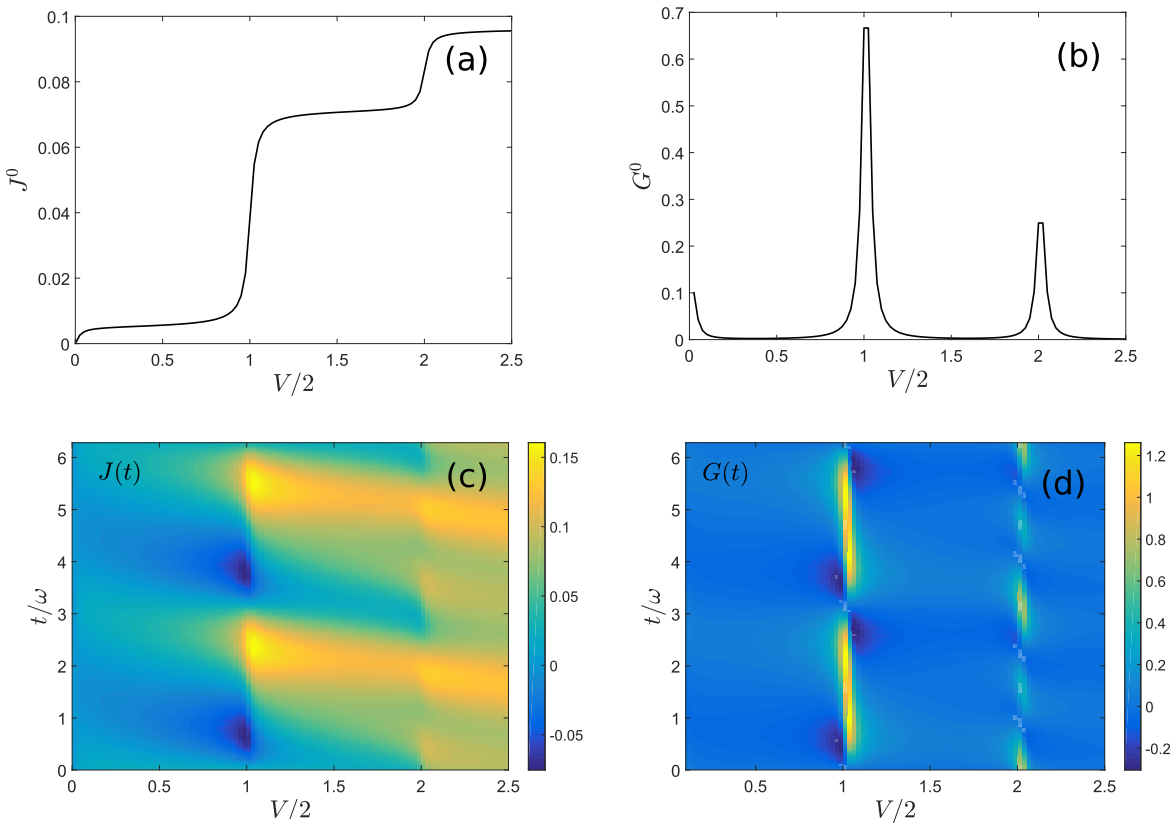

Figure 2.6: Current and conductance for the harmonically driven dot with $A_\sigma = 2\omega, \omega = 1$ contacted by metallic leads with a coupling constant $\Gamma = 0.2\omega$ and a voltage bias V across the junction. (a) Voltage-bias dependence of the time-averaged current showing the step-like response one expects from a multidot system. (b) Voltage-bias dependence of the time-averaged conductance which reproduces the time-averaged density of states of the dot. (c) time and voltage-bias dependence of the current showing that for higher voltages more Floquet bands are involved and the time-dependence of the current becomes more complex. (d) Time and voltage-bias dependence of the conductance. The conductance at the voltage bias when the leads reach the first Floquet band at the time where the dot is at maximum or minimum energy vanishes.

current for a voltage bias just above the resonance or just below the resonance is in both cases zero, which is a highly non trivial behavior.

2.4 Discussion

In this chapter we have described the Floquet formalism in which a periodically driven system in d dimensions can be mapped into a system in an extended space, $\mathcal{H}_E$, with $d+1$ dimensions with the dynamics given by a time-independent Hamiltonian. In particular, for the system studied here, a periodically driven quantum dot can be mapped into a tight-binding model with on-site energy equispaced by ω and hoping between the sites given by the Fourier components of the Hamiltonian.

We have also described the non-equilibrium Green's function technique, and in particular the Floquet-Green's functions technique used in the literature to solve peri-

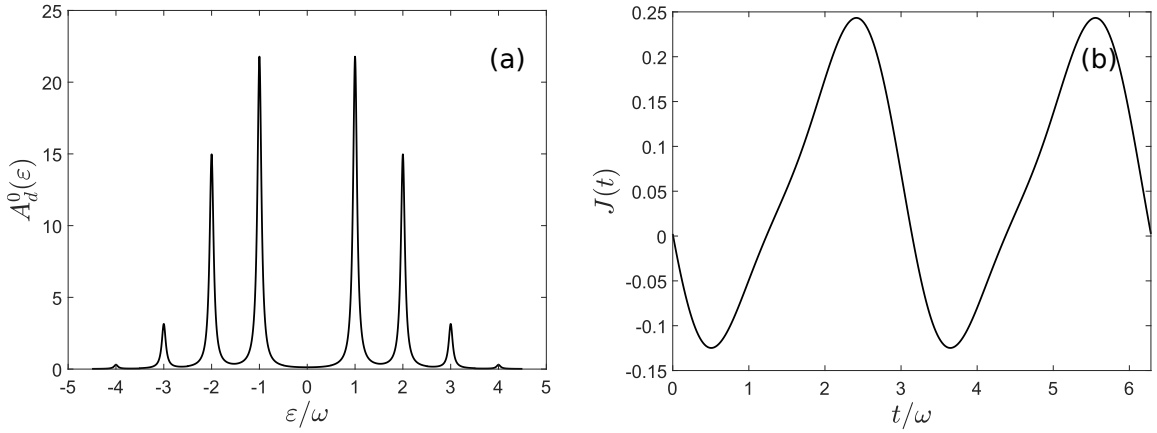

Figure 2.7: Time-averaged density of states and time-dependent current for a harmonically driven dot with $\omega = 1, A_\sigma = 2.405\omega$, so that the amplitude of the zeroth Floquet band vanishes, $J_0(V/\omega) = 0$, coupled to metallic leads with coupling constant $\Gamma_m = 0.2\omega$ and a voltage-bias across the junction of $V = 2\omega$. (a) Time-averaged density of states showing that the zeroth Floquet band indeed vanishes. (b) As a consequence the current where the dot is at maximum or minimum energy at $t/\omega = 0, \pi, 2\pi$ vanishes.

odically driven systems. We have showed that there is a clear connection between the Floquet-Green's functions and the Green's functions in the extended space. Finally, we have solved the problem of a non-interacting quantum dot being driven harmonically contacted by normal leads with a voltage-bias, for which we have found that, in fact, the time-averaged density of states and current resemble those of a tight-binding model and can be easily explained in terms of the Floquet formalism.

Chapter 3

Driven S-QD-S junction

In this chapter we will discuss the non-equilibrium dynamics of the S-QD-S junction, a quantum dot contacted by two superconducting leads. We are going to start by describing the Nambu Green's functions technique used to obtain the numerical results. Then we will derive the observables we are interested in for the most general case and finally we will analyze the results for the junction with different setups.

We are going to start by studying the system at equilibrium, with only a phase bias between the superconducting leads. This system has been studied extensively and it is known to host Andreev Bound States which can carry a supercurrent when a phase gradient is present across the junction [21, 22]. Once we understand the behavior of the junction at equilibrium we are going to drive the system out of equilibrium with two different methods.

First we will study the junction when we drive the dot harmonically like in last chapter. This system is similar to the junction under microwave radiation, which has been studied using the Floquet-Green's function, where some interesting features were found on the current-phase relation [17, 23, 24]. In this section we will give a more detailed and systematic description of the behavior of the junction under the driving using the Floquet formalism.

Then we will consider a voltage-biased junction, which has also been studied extensively [17, 18, 21, 25, 26]. We will describe the well known behavior of the system but also provide an interpretation using the Floquet formalism which will be useful for the last section.

Finally we will consider the case with both drives. The voltage-biased junction has also been studied under the influence of microwave radiation [27], but here we will present a more extensive study of the driven junction which will provide some new and interesting results.

3.1 Nambu-Green's function technique

Consider a non-interacting quantum dot with only one orbital, represented as a resonant level, coupled to two superconducting leads. In this section we will solve the model for the most general case, with a phase and constant voltage bias between the superconductors and a harmonically driven level. In later sections we will discuss each

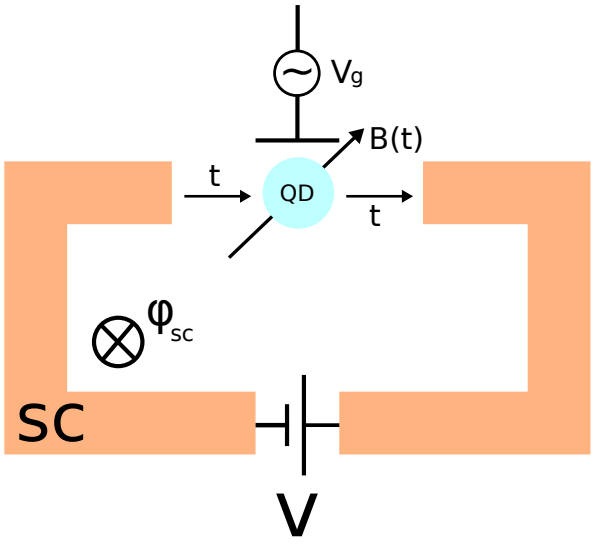

Figure 3.1: Schematic of the S-QD-S junction in the most general case, with a phase bias, ϕ_{sc}, and a voltage bias, V, across the junction, with the dot being driven either with an ac gate voltage $V_g(t)$ or an ac magnetic field $B(t)$.

driving case. The most general Hamiltonian of the system reads

$$H(t) = \sum_{\alpha=L,R} (H_\alpha - \mu_\alpha(t) N_\alpha) + H_d(t) + H_t \tag{3.1}$$

where H_α is the mean-field BCS Hamiltonian of the superconducting leads, μ_α is the chemical potential of the leads, $H_d(t)$ the Hamiltonian for the driven quantum dot and H_t the time-independent tunneling Hamiltonian between leads and dot. Each Hamiltonian is given by

$$H_L + H_R = \sum_{\alpha k\sigma} \varepsilon_{\alpha k} c^\dagger_{\alpha k\sigma} c_{\alpha k\sigma} + \sum_{\alpha k} (\Delta^*_\alpha c_{\alpha k\uparrow} c_{\alpha -k\downarrow} + \Delta_\alpha c^\dagger_{\alpha -k\downarrow} c^\dagger_{\alpha k\uparrow}) \tag{3.2}$$

$$H_d = \sum_\sigma \varepsilon_{d,\sigma}(t) d^\dagger_\sigma d_\sigma \tag{3.3}$$

$$H_t(t) = \sum_{\alpha,k,\sigma} \left(t c^\dagger_{\alpha k\sigma} d_\sigma + t d^\dagger_\sigma c_{\alpha k\sigma} \right), \tag{3.4}$$

where $\Delta_\alpha = \Delta e^{i\phi_\alpha}$ is the superconducting parameter, which absolute value we consider the same for both leads and independent of momentum, and the superconducting phase $\phi_{sc} = \phi_L - \phi_R$ is originated by applying a flux between the superconductors. The tunneling constant t is also considered lead, spin and momentum independent as well as real. As for the time-dependent dot on-site energy, to keep it simple we are going to consider a dot at zero energy, with an applied ac gate voltage as well as a dc and ac magnetic field, $\varepsilon_{d,\sigma}(t) = V_g \cos(\omega t + \phi_d) + \sigma(B_0/2 + B\cos(\omega t + \phi_d))$, where $\sigma = 1, -1$ for $\uparrow$ and $\downarrow$ respectively. As it will become obvious later, to describe the voltage-biased junction with the Floquet formalism it is necessary to symmetrize the chemical potentials, $\mu_\alpha = \mu + V_\alpha$, $V_{L,R} = \pm V/2$. To simplify the calculations a bit we can get rid of the voltage bias in the lead Hamiltonian so we can calculate the bare

lead Green's functions in equilibrium. We do this by time-evolving the Hamiltonian with the chemical potential term

$$U(t,0) = e^{i(N_L V/2 - N_R V/2)t}, \tag{3.5}$$

Note that the mean field superconducting Hamiltonian doesn't conserve particle number and therefore it doesn't commute with the chemical potential term. This is an artificial result that we avoid by simply imposing this commutation. After time-evolving the Hamiltonian with (3.5) the chemical potential appears as a time-dependent phase on the tunneling constant t. We can also make a gauge transformation

$$c_{\alpha k\sigma} \to c_{\alpha k\sigma} e^{i\phi_\alpha/2}, \tag{3.6}$$

which moves the superconducting phase dependence from the superconducting parameter into the tunneling constant. Finally, the transformed Hamiltonian takes the form

$$H(t) = H_L - \mu N_L + H_R - \mu N_R + H_D(t) + H_T(t), \tag{3.7}$$

where each term is given by

$$H_L + H_R = \sum_{\alpha k\sigma} \varepsilon_{\alpha k} c^\dagger_{\alpha k\sigma} c_{\alpha k\sigma} + \sum_{\alpha k} (\Delta c_{\alpha k\uparrow} c_{\alpha -k\downarrow} + \Delta c^\dagger_{\alpha -k\downarrow} c^\dagger_{\alpha k\uparrow}) \tag{3.8}$$

$$H_d = \sum_\sigma \varepsilon_{d,\sigma}(t) d^\dagger_\sigma d_\sigma \tag{3.9}$$

$$H_t(t) = \sum_{\alpha,k,\sigma} \left(t_\alpha(t) c^\dagger_{\alpha k\sigma} d_\sigma + t^*_\alpha(t) d^\dagger_\sigma c_{\alpha k\sigma} \right) \tag{3.10}$$

where the tunneling constant is now $t_\alpha(t) = te^{i\phi_\alpha(t)}$, with the time-dependent phase $\phi_{L,R}(t) = (\phi_{L,R} \pm Vt)/2$. In order to simplify the equations when working with superconductors it is usual to work with Nambu spinors instead of the electron operators. Different conventions can be found in the literature, the one we are going to use in this thesis is defined by the Nambu 4-spinors

$$\psi^\dagger_{\alpha k} = \begin{pmatrix} c^\dagger_{\alpha k\uparrow}, & c^\dagger_{\alpha k\downarrow}, & c_{\alpha -k\downarrow}, & -c_{\alpha -k\uparrow} \end{pmatrix}, \quad \psi_{\alpha k} = \begin{pmatrix} c_{\alpha k\uparrow} \\ c_{\alpha k\downarrow} \\ c^\dagger_{\alpha -k\downarrow} \\ -c^\dagger_{\alpha -k\uparrow} \end{pmatrix} \tag{3.11}$$

and

$$\phi^\dagger = \begin{pmatrix} d^\dagger_\uparrow, & d^\dagger_\downarrow, & d_\downarrow, & -d_\uparrow \end{pmatrix}, \quad \phi = \begin{pmatrix} d_\uparrow \\ d_\downarrow \\ d^\dagger_\downarrow \\ -d^\dagger_\uparrow \end{pmatrix}. \tag{3.12}$$

In order to write the equations in a compact form we will also use the matrices

$$m^0 = \sigma^0 \otimes \tau^0 = \begin{pmatrix} 1 & 0 & 0 & 0 \\ 0 & 1 & 0 & 0 \\ 0 & 0 & 1 & 0 \\ 0 & 0 & 0 & 1 \end{pmatrix}, \quad m^2 = \sigma^2 \otimes \tau^0 = \begin{pmatrix} 0 & 0 & -i & 0 \\ 0 & 0 & 0 & -i \\ i & 0 & 0 & 0 \\ 0 & i & 0 & 0 \end{pmatrix},$$
$$m^1 = \sigma^1 \otimes \tau^0 = \begin{pmatrix} 0 & 0 & 1 & 0 \\ 0 & 0 & 0 & 1 \\ 1 & 0 & 0 & 0 \\ 0 & 1 & 0 & 0 \end{pmatrix}, \quad m^3 = \sigma^3 \otimes \tau^0 = \begin{pmatrix} 1 & 0 & 0 & 0 \\ 0 & 1 & 0 & 0 \\ 0 & 0 & -1 & 0 \\ 0 & 0 & 0 & -1 \end{pmatrix},$$
$$m^4 = \sigma^2 \otimes \tau^2 = \begin{pmatrix} 0 & 0 & 0 & -1 \\ 0 & 0 & 1 & 0 \\ 0 & 1 & 0 & 0 \\ -1 & 0 & 0 & 0 \end{pmatrix}, \tag{3.13}$$

and

$$m^x = \sigma^0 \otimes \sigma^1 = \begin{pmatrix} 0 & 1 & 0 & 0 \\ 1 & 0 & 0 & 0 \\ 0 & 0 & 0 & 1 \\ 0 & 0 & 1 & 0 \end{pmatrix}, \quad m^y = \sigma^0 \otimes \sigma^2 = \begin{pmatrix} 0 & -i & 0 & 0 \\ i & 0 & 0 & 0 \\ 0 & 0 & 0 & -i \\ 0 & 0 & i & 0 \end{pmatrix},$$
$$m^z = \sigma^0 \otimes \sigma^3 = \begin{pmatrix} 1 & 0 & 0 & 0 \\ 0 & -1 & 0 & 0 \\ 0 & 0 & 1 & 0 \\ 0 & 0 & 0 & -1 \end{pmatrix}, \tag{3.14}$$

defined in terms of the Pauli-matrices $\{\sigma^0, \sigma^1, \sigma^2, \sigma^3\} = \{\boldsymbol{I}_2, \sigma_x, \sigma_y, \sigma_z\}$. Note that with this definition the matrices $\{m^0, m^1, m^2, m^3\}$ have the same properties as the Pauli matrices. These Nambu spinors satisfy the anticommutation relations

$$\{\psi_{\alpha k\eta}, \psi^\dagger_{\alpha' k'\eta'}\} = \delta_{\alpha\alpha'}\delta_{kk'}m^0_{\eta\eta'}, \qquad \{\psi^{(\dagger)}_{\alpha k\eta}, \psi^{(\dagger)}_{\alpha' k'\eta'}\} = \delta_{\alpha\alpha'}\delta_{-kk'}m^4_{\eta\eta'}$$
$$\{\phi_\eta, \phi^\dagger_{\eta'}\} = m^0_{\eta\eta'}, \qquad \{\phi^{(\dagger)}_\eta, \phi^{(\dagger)}_{\eta'}\} = m^4_{\eta\eta'} \tag{3.15}$$

where the $m^4_{\eta\eta'}$ in the last anticommutator reflects the redundancy in the spinor notation. To differentiate them with labels of states and Floquet indeces we will always label the Nambu components of an object with η. Using the Nambu spinor notation the Hamiltonian (3.8) reduces to

$$H_L - \mu N_L + H_R - \mu N_R = \frac{1}{2}\sum_{\alpha k,\eta\eta'} \Psi^\dagger_{\alpha k\eta} M^{sc}_{\alpha k,\eta\eta'} \Psi_{\alpha k\eta'} \tag{3.16}$$

$$H_d(t) = \frac{1}{2}\sum_{\eta,\eta\eta'} \phi^\dagger_\eta M^d(t)_{\eta\eta'}\phi_{\eta'} \tag{3.17}$$

$$H_t(t) = \sum_{\alpha k,\eta\eta'} \psi^\dagger_{\alpha k\eta} M^t_{\alpha,\mu\mu'}(t)\phi_{\eta'}, \tag{3.18}$$

where we have introduced the matrices

$$M^{sc}_{\alpha k} = \xi_{\alpha k} m^3 - \Delta m^1 \tag{3.19}$$

$$M^{d}_{\eta\eta'}(t) = V_g \cos(\omega t + \phi_d) m^3 + (B_0/2 + B\cos(\omega t + \phi_d))\, m^z \tag{3.20}$$

$$M^{t}_{\alpha}(t) = \frac{1}{2}\left[t_\alpha(t)(m^0 + m^3) + t^*_\alpha(t)(m^0 - m^3)\right] \tag{3.21}$$

$$= t m^3 e^{i m^3 \phi_\alpha(t)}, \tag{3.22}$$

where $\xi_{\alpha k} = \varepsilon_{\alpha k} - \mu$. Note that although it might not seem like it at first glance due to the redundancy of the Nambu spinors, the tunneling Hamiltonian (3.16) is hermitian.

We are going to use Nambu Green's functions which are defined as usual for the Nambu spinors, for which we will use the notation

$$G^{c}_{d\eta,\alpha' k'\eta'}(t,t') = -i\left\langle \mathcal{T}_{\mathcal{C}}\left\{\phi_\eta(t)\psi^\dagger_{\alpha' k'\eta'}(t')\right\}\right\rangle. \tag{3.23}$$

The first step is to calculate the bare Green's functions for the dot and the leads. The contour-ordered Green's function for the dot in Nambu basis is

$$g^{c}_{d,\eta\eta'}(t,t') = -i\left\langle \mathcal{T}_{\mathcal{C}}\left\{\phi_\eta(t)\phi^\dagger_{\eta'}(t')\right\}\right\rangle_{H_d(t)}, \tag{3.24}$$

where the expectation value is performed over the dot Hamiltonian. Using the expression derived last chapter for the inverse of Green's function of a quadratic Hamiltonian (2.73) we obtain for the inverse of the retarded and advanced bare dot Floquet Green's functions in Nambu basis

$$\begin{aligned} g^{r,a\,-1}_{d,\eta\eta,nm}(\varepsilon) &= \left[(\varepsilon + n\omega + \pm i0^+)m^0\delta_{nm} - M^{d\,n-m}_{\eta\eta'}\right] \\ &= \big[((\varepsilon + n\omega + \pm i0^+)m^0 - B_0 m^z)\delta_{nm} \\ &\quad - V_g e^{-i(n-m)\phi_d}(\delta_{n-m,1} + \delta_{n-m,-1})m^3 \\ &\quad - B e^{-i(n-m)\phi_d}(\delta_{n-m,1} + \delta_{n-m,-1})m^z\big]_{\eta\eta} \end{aligned} \tag{3.25}$$

Using the fact that we can calculate the bare Green's function of the lead in equilibrium the retarded and advanced bare lead Nambu Green's function are

$$\begin{aligned} g^{r,a}_{\alpha k,\eta\eta'}(t-t') &= \mp i\theta(\pm t \mp t')\left\langle\left\{\psi_{\alpha k\eta}(t), \psi^\dagger_{\alpha k\eta'}(t')\right\}\right\rangle \\ &= \mp i\theta(\pm t \mp t')\sum_{\eta_1}[e^{-iM^{SC}_{\alpha k}(t-t')}]_{\eta_1\eta'}\left\langle\left\{\psi_{\alpha k\eta}(t), \psi^\dagger_{\alpha k\eta_1}(t)\right\}\right\rangle \\ &= \mp i\theta(\pm t \mp t')\sum_{\eta_1}[e^{-iM^{SC}_{\alpha k}(t-t')}]_{\eta_1\eta'} m^0_{\eta,\eta_1} \\ &= \mp i\theta(\pm t \mp t')[e^{-iM^{SC}_{\alpha k}(t-t')}]_{\eta\eta'}. \end{aligned} \tag{3.26}$$

Since the bare lead Green's function only depends on the time difference we can simply Fourier transform and obtain

$$g^{r,a}_{\alpha k,\eta\eta}(\varepsilon) = [(\varepsilon \pm i0^+)m^0 - M^{SC}_{\alpha k}]^{-1}_{\eta\eta} \tag{3.27}$$

We can find the inverse of a vector of Identity and Pauli matrices as

$$\begin{aligned} m^0 &= (a_0 m^0 + \vec{a}\cdot\vec{m})\cdot(b_0 m^0 + \vec{b}\cdot\vec{m}) = a_0 b_0 m^0 + a_0\vec{b}\cdot\vec{m} + b_0\vec{a}\cdot\vec{m} + (\vec{a}\cdot\vec{m})\cdot(\vec{b}\cdot\vec{m}) \\ &= a_0 b_0 m^0 + a_0\vec{b}\cdot\vec{m} + b_0\vec{a}\cdot\vec{m} + (\vec{a}\cdot\vec{b})m^0 + i(\vec{a}\times\vec{b})\cdot\vec{m} \\ &= (a_0 b_0 + (\vec{a}\cdot\vec{b}))m^0 + (a_0\vec{b} + b_0\vec{a} + i(\vec{a}\times\vec{b}))\cdot\vec{m}. \end{aligned} \tag{3.28}$$

Noting that the identity and the Pauli matrices are linearly independent we can solve and find

$$[b_0 m^0 + \vec{b}\cdot\vec{m}]^{-1} = \frac{b_0 m^0 - \vec{b}\cdot\vec{m}}{b_0^2 - \left|\vec{b}\right|^2}, \tag{3.29}$$

which applied to the inverse Green's function (3.27) gives

$$g^{r,a}_{\alpha k}(\varepsilon) = \frac{(\varepsilon \pm i0^+)m^0 + M^{SC}_{\alpha k}}{(\varepsilon \pm i0^+)^2 + \det(M^{SC}_{\alpha k})} = \frac{(\varepsilon \pm i0^+)m^0 + \xi_{\alpha k} m^3 - \Delta m^1}{(\varepsilon \pm i0^+)^2 - E^2_{\alpha k}}, \tag{3.30}$$

where in the last step we used $\det\left(M^{SC}_{\alpha k}\right) = -E^2_{\alpha k} = -(\xi^2_{\alpha k} + \Delta^2_{\alpha k})$, where $E_{\alpha k}$ are the eigenenergies of the superconducting Hamiltonian, which can be obtained by diagonalizing it with the Bogoliubov transformation. We also need to calculate the lesser lead Green's functions for which the fluctuation-dissipation theorem can be used. We can rewrite the retarded and advanced Green's functions as

$$\begin{aligned} g^{r,a}_{\alpha k}(\varepsilon) &= \left(\frac{1}{\varepsilon - E_{\alpha k} \pm i0^+} + \frac{1}{\varepsilon + E_{\alpha k} + i0^+}\right)\frac{1}{2}m^0 \\ &+ \left(\frac{1}{\varepsilon - E_{\alpha k} \pm i0^+} - \frac{1}{\varepsilon + E_{\alpha k} \pm i0^+}\right)\frac{1}{2E_{\alpha k}}M^{SC}_{\alpha k} \\ &= \int \frac{d\varepsilon_1}{2\pi}\frac{a_{\alpha k}(\varepsilon_1)}{\varepsilon - \varepsilon_1 \pm i0^+}, \end{aligned} \tag{3.31}$$

where we can identify the spectral function of the lead Hamiltonian as

$$\begin{aligned} a_{\alpha k}(\varepsilon) =& 2\pi[\delta(\varepsilon - E_{\alpha k}) + \delta(\varepsilon + E_{\alpha k})]\frac{1}{2}m^0 \\ &+ 2\pi[\delta(\varepsilon - E_{\alpha k}) - \delta(\varepsilon + E_{\alpha k})]\frac{1}{2E_{\alpha k}}M^{SC}_{\alpha k}, \end{aligned} \tag{3.32}$$

and with that result we can calculate the lesser lead Green's function as

$$\begin{aligned} g^{<}_{\alpha k}(\varepsilon) &= i a_{\alpha k}(\varepsilon) n_F(\varepsilon) \\ &= 2i\pi n_F(\varepsilon)\left[(\delta(\varepsilon - E_{\alpha k}) + \delta(\varepsilon + E_{\alpha k}))\frac{1}{2}m^0\right. \\ &\left.+(\delta(\varepsilon - E_{\alpha k}) - \delta(\varepsilon + E_{\alpha k}))\frac{1}{2E_{\alpha k}}M^{SC}_{\alpha k}\right]. \end{aligned} \tag{3.33}$$

Note that we calculated the Fourier transform of both lead bare Green's functions which are defined on the real axis $\varepsilon \in (-\infty, \infty)$. To incorporate them later on the

calculations we need the equivalent Floquet matrix of a Fourier function. Any function of the time difference can be decomposed as

$$\begin{aligned} g(t-t') &= \int_{-\infty}^{\infty} d\varepsilon\, e^{-i\varepsilon(t-t')} g(\varepsilon) \\ &= \sum_n \int_{-\omega/2+n\omega}^{\omega/2+n\omega} d\varepsilon\, e^{-i\varepsilon(t-t')} g(\varepsilon) \\ &= \sum_n \int_{-\omega/2}^{\omega/2} d\varepsilon\, e^{-i(\varepsilon+n\omega)(t-t')} g(\varepsilon+n\omega) \\ &= \sum_n \int_{-\omega/2}^{\omega/2} d\varepsilon\, e^{-i(\varepsilon+n\omega)t+i(\varepsilon+m\omega)t'} g(\varepsilon+n\omega)\delta_{nm}, \end{aligned} \tag{3.34}$$

where the correspondent Floquet matrix, defined in the first Brillouin zone is

$$g_{nm}(\varepsilon) = g(\varepsilon+n\omega)\delta_{nm}. \tag{3.35}$$

The lead Floquet Green's functions are therefore

$$g^{r,a}_{\alpha k,nm}(\varepsilon) = \frac{(\varepsilon+n\omega\pm i0^+)m^0 + \xi_{\alpha k}m^3 - \Delta m^1}{(\varepsilon+n\omega\pm i0^+)^2 - E^2_{\alpha k}}\delta_{nm} \tag{3.36}$$

$$\begin{aligned} g^{<}_{\alpha k,nm}(\varepsilon) = 2i\pi n_F(\varepsilon) \Bigg[&(\delta(\varepsilon+n\omega-E_{\alpha k}) + \delta(\varepsilon+n\omega+E_{\alpha k}))\frac{1}{2}m^0 \\ &+(\delta(\varepsilon+n\omega-E_{\alpha k}) - \delta(\varepsilon+n\omega+E_{\alpha k}))\frac{1}{2E_{\alpha k}}M^{SC}_{\alpha k}\Bigg]\delta_{nm}. \end{aligned} \tag{3.37}$$

With that result we can now calculate the full lead retarded and advanced Green's functions. The derivation might seem more complicated than the one from last chapter because of the Nambu structure, but it is structurally the same. We start by calculating the time-evolution of the creation and annihilation operators

$$\begin{aligned} \partial_t \psi_{\alpha k\eta}(t) &= i\left[H, \psi_{\alpha k\eta}\right](t) \\ &= -i\sum_{\eta_1} M^{sc}_{\alpha k,\eta\eta_1}\psi_{\alpha k\eta_1}(t) - iM^{t\,*}_{\alpha,\eta\eta}(t)\phi_\eta(t) \end{aligned} \tag{3.38}$$

and

$$\begin{aligned} \partial_{t'}\psi^\dagger_{\alpha' k'\eta'}(t') &= i\left[H, \psi^\dagger_{\alpha' k'\eta'}\right] \\ &= i\sum_{\eta_1}\psi^\dagger_{\alpha' k'\eta_1}(t')M^{sc}_{\alpha k,\eta_1\eta'} + i\phi^\dagger_{\eta'}(t')M^{t}_{\alpha,\eta'\eta'}(t'), \end{aligned} \tag{3.39}$$

then, with that result, we can obtain the time derivative of the contour-ordered lead

Green's function

$$\begin{aligned} i\partial_t G^c_{\alpha k\eta,\alpha' k'\eta'}(t,t') =& \delta_C(t-t')\left\langle\{\psi_{\alpha k\eta}(t),\psi^\dagger_{\alpha' k'\eta'}(t)\}\right\rangle - i\left\langle\mathcal{T}_\mathcal{C}\left\{i\partial_t\psi_{\alpha k\eta}(t)\psi^\dagger_{\alpha' k'\eta'}(t')\right\}\right\rangle \\ =& \delta_C(t-t')\delta_{\alpha\alpha'}\delta_{kk'}m^0_{\eta\eta'} \\ & - i\left\langle\mathcal{T}_\mathcal{C}\left\{\left[\sum_{\eta_1} M^{sc}_{\alpha k,\eta\eta_1}\psi_{\alpha k\eta_1}(t) + M^t_{\alpha,\eta\eta}(t)\phi_\eta(t)\right]\psi^\dagger_{\alpha' k'\eta'}(t')\right\}\right\rangle \\ =& \delta_C(t-t')\delta_{\alpha\alpha'}\delta_{kk'}m^0_{\eta\eta'} \\ & + \sum_{\eta_1} M^{sc}_{\alpha k,\eta\eta_1}G^c_{\alpha k\eta_1,\alpha' k'\eta'}(t,t') + M^t_{\alpha,\eta\eta}(t)G^c_{d\eta,\alpha' k'\eta'}(t,t'). \end{aligned} \tag{3.40}$$

We can again group the full lead Green's functions

$$\begin{aligned} \sum_{\eta_1}\left[i\partial_t m^0_{\eta\eta_1} - M^{sc}_{\alpha k,\eta\eta_1}\right]G^c_{\alpha k\eta_1,\alpha' k'\eta'}(t,t') = \\ \delta_C(t-t')\delta_{\alpha\alpha'}\delta_{kk'}m^0_{\eta\eta'} + M^t_{\alpha,\eta\eta}(t)G^c_{d\eta,\alpha' k'\eta'}(t,t'), \end{aligned} \tag{3.41}$$

where we identify the term in front of the full lead Green's function as the inverse of the bare lead Green's function

$$\sum_{\eta_1}[i\partial_t m^0_{\eta\eta_1} - M^s c_{\alpha k,\eta\eta_1}]g_{\alpha k,\eta_1\eta'}(t,t') = \delta_C(t-t')m^0_{\eta\eta'}. \tag{3.42}$$

Multiplying on the left by it one obtains the Dyson equation for the contour-ordered full lead Green's function

$$\begin{aligned} G^c_{\alpha k\eta,\alpha' k'\eta'}(t,t') =& g^c_{\alpha k,\eta\eta'}(t,t')\delta_{\alpha\alpha'}\delta_{kk'} \\ & + \sum_{\eta_1,\eta_2}\int_C dt_1\, g^c_{\alpha k,\eta\eta_1}(t,t_1)M^t_{\alpha k,\eta_1\eta_1}(t_1)G^c_{d\eta_1,\alpha' k'\eta'}(t_1,t'). \end{aligned} \tag{3.43}$$

We then need the mixed contour-ordered Green's function

$$\begin{aligned} i\partial_{t'}G^c_{d\eta,\alpha' k'\eta'}(t,t') =& -i\left\langle\mathcal{T}_\mathcal{C}\left\{\phi_\eta(t),\partial_{t'}\psi^\dagger_{\alpha' k'\eta'}(t')\right\}\right\rangle \\ =& \sum_{\eta_1} G^c_{d\eta,\alpha' k'\eta_1}(t,t')M^{sc}_{\alpha k,\eta_1\eta'} + G^c_{d\eta,d\eta'}(t,t')M^{t\,*}_{\alpha',\eta'\eta'}(t'), \end{aligned} \tag{3.44}$$

which can be rewritten, grouping the two terms with the mixed Green's function as

$$\sum_{\eta_1} G^c_{d\eta,\alpha' k'\eta_1}(t,t')\left[i\overleftarrow{\partial_{t'}}m^0_{\eta_1\eta} - M^{sc}_{\alpha' k',\eta_1\eta'}\right] = G^c_{d\eta,d\eta'}(t,t')M^{t\,*}_{\alpha',\eta'\eta'}(t'). \tag{3.45}$$

The term on the right of the mixed Green's function can again be identify as the bare lead Green's function and by multiplying by it on the right the expression for the contour-ordered mixed Green's function reduces to

$$G^c_{d\eta,\alpha k\eta'}(t,t') = \sum_{\eta_1}\int_C dt_1\, G^c_{d\eta,d\eta_1}(t,t_1)M^{t\,*}_{\alpha,\eta_1\eta_1}(t_1)g^c_{\alpha k,\eta_1\eta'}(t_1,t'). \tag{3.46}$$

We can now calculate the last contour-ordered full Green's function we need, the one of the dot, defined as

$$G^c_{d\eta,d\eta'}(t,t') = -i\left\langle \mathcal{T}_\mathcal{C}\left\{\phi_\eta(t)\phi^\dagger_{\eta'}(t)\right\}\right\rangle. \tag{3.47}$$

First we obtain the time-evolution of the creation operator

$$\begin{aligned} i\partial_{t'}\phi^\dagger_{\eta'}(t') &= -[H,\phi^\dagger_{\eta'}](t') \\ &= -\sum_{\eta_1}\phi^\dagger_{\eta_1}(t)M^d_{\eta_1\eta'}(t) - \sum_{\alpha k,\eta_1}\psi^\dagger_{\alpha k,\eta_1}M^t_{\alpha,\eta_1\eta'}(t), \end{aligned} \tag{3.48}$$

and with that we can calculate the time-derivative of the contour-ordered full dot Green's function

$$\begin{aligned} i\partial_{t'}G^c_{d\eta,d\eta'}(t,t') =& -\delta_C(t-t')m^0_{\eta\eta'} - i\left\langle \mathcal{T}_\mathcal{C}\left\{\phi_\eta(t)i\partial_{t'}\phi^\dagger_{\eta'}(t')\right\}\right\rangle \\ =& -\delta_C(t-t')m^0_{\eta\eta'} \\ &+ -i\left\langle \mathcal{T}_\mathcal{C}\left\{\phi_\eta(t)\left[-\sum_{\eta_1}\phi^\dagger_{\eta_1}(t)M^d_{\eta_1\eta'}(t) - \sum_{\alpha k,\eta_1}\psi^\dagger_{\alpha k,\eta_1}M^t_{\alpha,\eta_1\eta'}(t)\right]\right\}\right\rangle \\ =& -\delta_C(t-t')m^0_{\eta\eta'} \\ &- \sum_{\eta_1}G^t_{d\eta,d\eta_1}(t,t')M^d_{\eta_1\eta'}(t') - \sum_{\alpha k,\eta_1}G^c_{d\eta,\alpha k\eta_1}(t,t')M^t_{\alpha,\eta_1\eta'}(t') \end{aligned} \tag{3.49}$$

We can again group the full dot Green's functions, identify the term in front of it as the inverse of the bare dot Green's function, and by multiplying by it on the right we obtain

$$G^c_{d\eta,d\eta'}(t,t') = g^c_{d,\eta\eta'}(t,t') + \sum_{\alpha k,\eta_1\eta_2}\int_C dt_1\, G^c_{d\eta,\alpha k\eta_1}(t,t_1)M^t_{\alpha k,\eta_1\eta_2}(t_1)g^c_{d,\eta_2\eta'}(t_1,t'). \tag{3.50}$$

Using the expression for the mixed Green's function (3.46) in last equation we obtain we obtain

$$\begin{aligned} &G^c_{d\eta,d\eta'}(t,t') = g^c_{d,\eta\eta'}(t,t') \\ &+ \sum_{\alpha k,\eta_1}\int_C dt_1\,[\sum_{\eta_2}\int_C dt_2\, G^c_{d\eta,d\eta_2}(t,t_2)M^{t*}_{\alpha,\eta_2\eta_2}(t_2)g^c_{\alpha k,\eta_2\eta_1}(t_2,t_1)]M^t_{\alpha k,\eta_1\eta_1}(t_1)g^c_{d,\eta_1\eta'}(t_1,t'). \end{aligned} \tag{3.51}$$

By defining the contour-ordered self-energy as

$$\Sigma^c_{\alpha,\eta\eta'}(t,t') = \sum_k M^{t*}_{\alpha,\eta\eta}(t)g^c_{\alpha k,\eta\eta'}(t,t')M^t_{\alpha,\eta'\eta'}(t'), \tag{3.52}$$

we finally find the Dyson equation for the contour-ordered full dot Green's function

$$\begin{aligned} &G^c_{d\eta,d\eta'}(t,t') = g^c_{d,\eta\eta'}(t,t') \\ &+ \sum_{\eta_1\eta_2}\int_C dt_1\int_C dt_2\, G^c_{d\eta,d\eta_1}(t,t_1)\sum_\alpha \Sigma^c_{\alpha,\eta_1\eta_2}(t_1,t_2)g^c_{d,\eta_2\eta'}(t_2,t'). \end{aligned} \tag{3.53}$$

Seeing as the expression for the two-time full contour-ordered dot Green's function has the same form as the one obtained last chapter (2.110), we can obtain the retarded and advanced Floquet matrix the same way, by applying the property of time-convolutions and isolating the Floquet Green's function, which takes the form

$$G^{r,a}_{d\eta,d\eta',nm}(\varepsilon) = \left[\frac{1}{\boldsymbol{g}^{r,a\,-1}(\varepsilon) - \sum_\alpha \boldsymbol{\Sigma}^{r,a}_\alpha(\varepsilon)}\right]_{\eta\eta',nm}, \tag{3.54}$$

where $\boldsymbol{g}^{r,a\,-1}(\varepsilon)$ and $\boldsymbol{\Sigma}^{r,a}_\alpha$ are matrices in Floquet and Nambu space. The two-time self-energies can be decomposed as

$$\begin{aligned}
\Sigma^\nu_{\alpha,\eta\eta'}(t,t') =& \sum_n M^{t\,*}_{\alpha,\eta\eta,n} e^{in\omega t} \sum_k \int_{-\infty}^{\infty} d\varepsilon\, g^\nu_{\alpha k,\eta\eta'}(\varepsilon) e^{-i\varepsilon(t-t')} \sum_m M^t_{\alpha,\eta'\eta',m} e^{-im\omega t'} \\
=& \sum_n M^{t\,*}_{\alpha,\eta\eta,n} e^{in\omega t} \\
& \times \sum_{k,n_1} \int_{-\omega/2}^{\omega/2} d\varepsilon\, g^\nu_{\alpha k,\eta\eta'}(\varepsilon + n_1\omega) e^{-i(\varepsilon+n_1\omega)(t-t')} \sum_m M^t_{\alpha,\eta'\eta',m} e^{-im\omega t'} \\
=& \sum_{nm} \int_{-\omega/2}^{\omega/2} d\varepsilon \sum_{n_1} e^{-i(\varepsilon+n_1\omega-n\omega)t} e^{i(\varepsilon+n_1\omega-m\omega)t'} \\
& \times M^{t\,*}_{\alpha,\eta\eta,n} \sum_k g^\nu_{\alpha k,\eta\eta'}(\varepsilon + n_1\omega) M^t_{\alpha,\eta'\eta',m} \\
=& \sum_{nm} \int_{-\omega/2}^{\omega/2} d\varepsilon\, e^{-i(\varepsilon+n\omega)t + i(\varepsilon+m\omega)t'} \\
& \times \sum_{n_1,k} M^{t\,*}_{\alpha,\eta\eta,n_1-n} g^\nu_{\alpha k,\eta\eta',n_1n_1}(\varepsilon) M^t_{\alpha,\eta'\eta',n_1-m},
\end{aligned} \tag{3.55}$$

where we can identify the Floquet matrix for the $\nu = r, a, <$ self-energy as

$$\Sigma^\nu_{\alpha,\eta\eta',nm}(\varepsilon) = \sum_{n_1} M^{t\,*}_{\alpha,\eta\eta,n_1-n} \sum_k g^\nu_{\alpha k,\eta\eta',n_1n_1}(\varepsilon) M^t_{\alpha,\eta'\eta',n_1-m}. \tag{3.56}$$

Performing the momentum sum of the Floquet Nambu Green's functions (3.36) gives

$$\begin{aligned}
g^{r,a}_{\alpha,\eta\eta',nm}(\varepsilon) =& \sum_k g^{r,a}_{\alpha k,\eta\eta',nm}(\varepsilon) \\
=& \int_{-\infty}^{\infty} d\xi_{\alpha k}\, \rho_\alpha \frac{(\varepsilon + n\omega \pm i0^+) m^0_{\eta\eta'} + \xi_{\alpha k} m^3_{\eta\eta'} - \Delta m^1_{\eta\eta'}}{(\varepsilon + n\omega \pm i0^+)^2 - \xi^2_{\alpha k} - \Delta^2} \delta_{nm} \\
=& 2\rho_\alpha [(\varepsilon + n\omega \pm i0^+) m^0 - \Delta m^1]_{\eta\eta'} \delta_{nm} \\
& \times \int_0^{\infty} d\xi_{\alpha k} \frac{1}{[(\varepsilon + n\omega \pm i0^+)^2 - \Delta^2] - \xi^2_{\alpha k}} \\
=& -\pi\rho_\alpha \frac{(\varepsilon + n\omega \pm i0^+) m^0_{\eta\eta'} - \Delta m^1_{\eta\eta'}}{\sqrt{|(\varepsilon + n\omega)^2 - \Delta^2|}} \\
& \times [\theta(\Delta - |\varepsilon + n\omega|) \mp i\,\mathrm{sign}(\varepsilon + n\omega)\theta(|\varepsilon + n\omega| - \Delta)] \delta_{nm},
\end{aligned} \tag{3.57}$$

and

$$\begin{aligned}
g^{<}_{\alpha,\eta\eta',nm}(\varepsilon) =& \sum_k g^{<}_{\alpha k,\eta\eta',nm}(\varepsilon) \\
=& 2i\pi n_F(\varepsilon+n\omega)\delta_{nm} \\
&\times \int_\infty^\infty \frac{d\xi_{\alpha k}}{2E_{\alpha k}}\rho_\alpha \left[(\delta(\varepsilon+n\omega-E_{\alpha k})+\delta(\varepsilon+n\omega+E_{\alpha k}))E_{\alpha k}m^0_{\eta\eta'}\right. \\
&\left.+(\delta(\varepsilon+n\omega-E_{\alpha k})-\delta(\varepsilon+n\omega+E_{\alpha k}))(\xi_{\alpha k}m^3_{\eta\eta'}-\Delta m^1_{\eta\eta'})\right] \\
=& 2i\pi n_F(\varepsilon+n\omega)\delta_{nm}\rho_\alpha \int_\Delta^\infty \frac{dE_{\alpha k}}{\sqrt{E^2_{\alpha k}-\Delta^2}}\left[\delta(\varepsilon+n\omega-E_{\alpha k})(E_{\alpha k}m^0_{\eta\eta'}-\Delta_{\alpha k}m^1_{\eta\eta'})\right. \\
&\left.+\delta(\varepsilon+n\omega+E_{\alpha k})(E_{\alpha k}m^0_{\eta\eta'}+\Delta m^1_{\eta\eta'})\right] \\
=& 2i\pi n_F(\varepsilon+n\omega)\delta_{nm}\rho_\alpha\theta(|\varepsilon+n\omega|-\Delta) \\
&\times \mathrm{sign}(\varepsilon+n\omega)\frac{(\varepsilon+n\omega)m^0_{\eta\eta'}-\Delta m^1_{\eta\eta'}}{\sqrt{(\varepsilon+n\omega)^2-\Delta^2_{\alpha k}}}.
\end{aligned} \tag{3.58}$$

We need to calculate also the Fourier components of the tunneling matrix

$$\begin{aligned}
M^T_{\alpha,n} =& tm^3 e^{im^3\phi_\alpha/2}\frac{1}{T}\int_{-T/2}^{T/2} dt\, e^{i(m^3V_\alpha+n\omega)t} \\
=& tm^3 e^{im^3\phi_\alpha/2}\delta_{n,V_\alpha/\omega}.
\end{aligned} \tag{3.59}$$

We can use those results in the expression of the Floquet self-energy and we obtain for its matrix in Nambu space

$$\begin{aligned}
\Sigma^\nu_{\alpha,nm}(\varepsilon) =& t^2m^3e^{-im^3\phi_\alpha/2}\sum_{n_1}[\delta_{n_1,n-V_\alpha/\omega}\frac{m^0+m^3}{2}+\delta_{n_1,n+V_\alpha/\omega}\frac{m^0-m^3}{2}] \\
&\times g^\nu_{\alpha,n_1n_1}(\varepsilon)m^3e^{im^3\phi_\alpha/2}[\delta_{n_1,m-V_\alpha/\omega}\frac{m^0+m^3}{2}+\delta_{n_1,m+V_\alpha/\omega}\frac{m^0-m^3}{2}] \\
=& t^2m^3e^{-im^3\phi_\alpha/2}\left[\frac{m^0+m^3}{2}g^\nu_{\alpha,n-V_\alpha/\omega,n-V_\alpha/\omega}(\varepsilon)\delta_{n,m}\frac{m^0+m^3}{2}+\right. \\
&+\frac{m^0+m^3}{2}g^\nu_{\alpha,n-V_\alpha/\omega,n-V_\alpha/\omega}(\varepsilon)\delta_{n-m,2V_\alpha/\omega}\frac{m^0-m^3}{2} \\
&+\frac{m^0-m^3}{2}g^\nu_{\alpha,n+V_\alpha/\omega,n+V_\alpha/\omega}(\varepsilon)\delta_{n-m,-2V_\alpha/\omega}\frac{m^0+m^3}{2} \\
&\left.+\frac{m^0-m^3}{2}g^\nu_{\alpha,n+V_\alpha/\omega,n+V_\alpha/\omega}(\varepsilon)\delta_{n,m}\frac{m^0-m^3}{2}\right]m^3e^{im^3\phi_\alpha/2}
\end{aligned} \tag{3.60}$$

By decomposing the momentum summed Green's functions as $g = \sum_i g_{m^i}m^i$ the Nambu matrix of the Floquet self-energy can be written as

$$\begin{aligned}
&\Sigma^\nu_{\alpha,nm}(\varepsilon) = \\
&= \frac{\Gamma_\alpha}{2\pi}\begin{pmatrix} g^\nu_{\alpha,m^0,n-\frac{V_\alpha}{\omega},n-\frac{V_\alpha}{\omega}}(\varepsilon)\delta_{n,m} & -g^\nu_{\alpha,m^1,n-\frac{V_\alpha}{\omega},n-\frac{V_\alpha}{\omega}}(\varepsilon)e^{i\phi_\alpha}\delta_{n-m,2\frac{V_\alpha}{\omega}} \\ -g^\nu_{\alpha,m^1,n+\frac{V_\alpha}{\omega},n+\frac{V_\alpha}{\omega}}(\varepsilon)e^{-i\phi_\alpha}\delta_{n-m,-2\frac{V_\alpha}{\omega}} & g^\nu_{\alpha,m^0,n+\frac{V_\alpha}{\omega},n+\frac{V_\alpha}{\omega}}(\varepsilon)\delta_{nm}\end{pmatrix}\otimes\sigma_0.
\end{aligned} \tag{3.61}$$

With that result we have all the components we need to calculate the retarded and advanced full Green's functions of the dot (3.54). The lesser one follows from applying the Langreth rules on the Dyson equation (3.53) and transforming the time-convolution into a matrix product in Floquet space, resulting in

$$G^{<}_{dd,\eta\eta',nm}(\varepsilon) = \sum_{\eta_1\eta_2,n_1n_2} G^{r}_{dd,\eta\eta_1,nn_1}(\varepsilon) \sum_{\alpha} \Sigma^{<}_{\alpha,\eta_1\eta_2,n_1n_2}(\varepsilon) G^{a}_{dd,\eta_2\eta',n_2m}. \tag{3.62}$$

Now that we have explicit expressions to calculate numerically all the Green's functions we need, we proceed to calculate the current, given by

$$J_\alpha(t) = -i \left\langle [H(t), N_\alpha(t)] \right\rangle . \tag{3.63}$$

First note that we encounter the same issue we had when we transforming our Hamiltonian with (3.5), the number operator does not commute with the mean field superconducting Hamiltonian, but we set again this commutator to zero, so that

$$\begin{aligned} J_\alpha(t) &= -i \left\langle [H_t(t), N_\alpha(t)] \right\rangle = -i \sum_{k,\eta} m^3_{\eta\eta} \left\langle [H_t, \psi^\dagger_{\alpha k\eta}\psi_{\alpha k\eta}](t) \right\rangle \\ &= -i \sum_{k,\eta} m^3_{\eta\eta} \left\langle \psi^\dagger_{\alpha k\eta}(t)[H_t, \psi_{\alpha k\eta}](t) + [H_t, \psi^\dagger_{\alpha k\eta}](t)\psi_{\alpha k\eta}(t) \right\rangle \\ &= i \sum_{k,\eta} m^3_{\eta\eta} M^t_{\alpha,\eta\eta}(t) \left\langle \psi^\dagger_{\alpha k\eta}(t)\phi_\eta(t) \right\rangle - i \sum_{k,\eta} m^3_{\eta\eta} M^{t\,*}_{\alpha,\eta\eta}(t) \left\langle \phi^\dagger_\eta(t)\psi'_{Lk\eta}(t) \right\rangle \\ &= 2\,\mathrm{Re}\left\{ \sum_{k,\eta} m^3_{\eta\eta} M^t_{\alpha,\eta\eta}(t) G^{<}_{d\eta,\alpha k\eta}(t,t) \right\}. \end{aligned} \tag{3.64}$$

Using the expression we have for the lesser mixed Green's function (3.46) and the self-energies (3.61) the expression for the current reduces to

$$J_\alpha(t) = 2\,\mathrm{Re}\left\{ \sum_{k,\eta,\eta'} m^3_{\eta\eta} \int dt_1 \left[G^{r}_{d\eta,d\eta'}(t,t_1)\Sigma^{<}_{\alpha,\eta'\eta}(t_1,t) + G^{<}_{d\eta,d\eta'}(t,t_1)\Sigma^{a}_{\alpha,\eta'\eta}(t_1,t) \right] \right\} \tag{3.65}$$

which is equivalent to that obtained last chapter (2.127). The current can be Fourier transformed and expressed in terms of the Floquet matrices as

$$\begin{aligned} J_\alpha(t) =& 2\mathrm{Re}\left\{ \sum_{n,m} e^{-im\omega t} \sum_{k,\eta,\eta'} m^3_{\eta\eta} \int d\varepsilon \left[G^{r}_{d\eta,d\eta',nn_1}(\varepsilon)\Sigma^{<}_{\alpha,\eta'\eta,n_1,n-m}(\varepsilon) \right.\right. \\ &\left.\left. + G^{<}_{d\eta,d\eta',nn_1}(\varepsilon)\Sigma^{a}_{\alpha,\eta'\eta,n_1,n-m}(\varepsilon) \right] \right\}, \end{aligned} \tag{3.66}$$

and the time-averaged current can be written as a product of matrices

$$J^0_\alpha = 2\,\mathrm{Re}\left\{ \mathrm{Tr}\left[m^3 \int d\varepsilon \left[\boldsymbol{G}^{r}_{dd}(\varepsilon)\boldsymbol{\Sigma}^{<}_{\alpha}(\varepsilon) + \boldsymbol{G}^{<}_{dd}(\varepsilon)\boldsymbol{\Sigma}^{a}_{\alpha,}(\varepsilon) \right] \right] \right\}, \tag{3.67}$$

where $\boldsymbol{G}^{\nu}_{dd}(\varepsilon)$ and $\boldsymbol{\Sigma}^{\nu}_{\alpha}$ are the dot Green's function and lead self energy matrices in Floquet and Nambu space and where the trace now is performed over the Floquet and Nambu spaces.

Now that we have expressions to calculate everything in the most general case, we can study one by one the different setups mentioned at the beginning of the chapter. All the numerical calculations in the next sections are performed in the same way as discussed in section 2.3, with only one peculiarity. As we will see later, when we calculate the time-averaged density of states, bound states will appear inside the gap. This states would be broaden, as in the case of the metallic leads, by the imaginary part of the diagonal of the self-energy. As we can see in (3.61), for a junction without a voltage bias, inside the gap the self-energy is real and therefore the bound states will appear as delta peaks. When performing numerical calculations this is an issue because the resolution we use in energy is finite and we have to artificially broaden the bound states in order to perform the numerical calculations. We do this by introducing a metallic lead with a low coupling constant Γ_m. There is going to be a compromise between the resolution we have to use on the energy variable, or the computational power needed, and the strength of the coupling to the metallic lead, which introduces artificial results we are not interested in.

3.2 Phase biased junction at equilibrium

We are going to start by studying the behavior of the junction at equilibrium. Since the system is at equilibrium, we can forget about the Floquet formalism and work as usual by Fourier transforming. We can obtain the Fourier functions from a Floquet matrix by dropping the Floquet indeces, since they are diagonal in Floquet space, and considering them defined in the real axis, $\varepsilon \in (-\infty, \infty)$. The lead Green's functions (3.36) are obtained as

$$g^{r,a}_{\alpha,\eta\eta'}(\varepsilon) = -\pi\rho_\alpha \frac{(\varepsilon \pm i0^+)m^0_{\eta\eta'} - \Delta m^1_{\eta\eta'}}{\sqrt{|\varepsilon^2 - \Delta^2|}} [\theta(\Delta - |\varepsilon|) \mp i\text{sign}(\varepsilon)\theta(|\varepsilon| - \Delta)] \tag{3.68}$$

$$g^{<}_{\alpha,\eta\eta',nm}(\varepsilon) = 2i\pi n_F(\varepsilon)\rho_\alpha \theta(|\varepsilon| - \Delta)\text{sign}(\varepsilon) \frac{\varepsilon m^0_{\eta\eta'} - \Delta m^1_{\eta\eta'}}{\sqrt{\varepsilon^2 - \Delta^2}}, \tag{3.69}$$

and the self-energy reduces to

$$\Sigma^\nu_\alpha(\varepsilon) = \frac{\Gamma_\alpha}{2\pi} \begin{pmatrix} g^\nu_{\alpha,m^0}(\varepsilon) & -g^\nu_{\alpha,m^1}(\varepsilon)e^{i\phi_\alpha} \\ -g^\nu_{\alpha,m^1}(\varepsilon)e^{-i\phi_\alpha} & g^\nu_{\alpha,m^0}(\varepsilon) \end{pmatrix} \otimes \sigma_0. \tag{3.70}$$

The spectral function of the lead is obtained as

$$\begin{aligned} A_{\alpha,\eta\eta'}(\varepsilon) =& \text{Im}\left\{g^r_{\alpha,\eta\eta'}(\varepsilon)\right\} \\ =& -\pi\rho_\alpha \frac{\varepsilon m^0_{\eta\eta'} - \Delta m^1_{\eta\eta'}}{\sqrt{|\varepsilon^2 - \Delta^2|}} i\text{sign}(\varepsilon)\theta(|\varepsilon| - \Delta). \end{aligned} \tag{3.71}$$

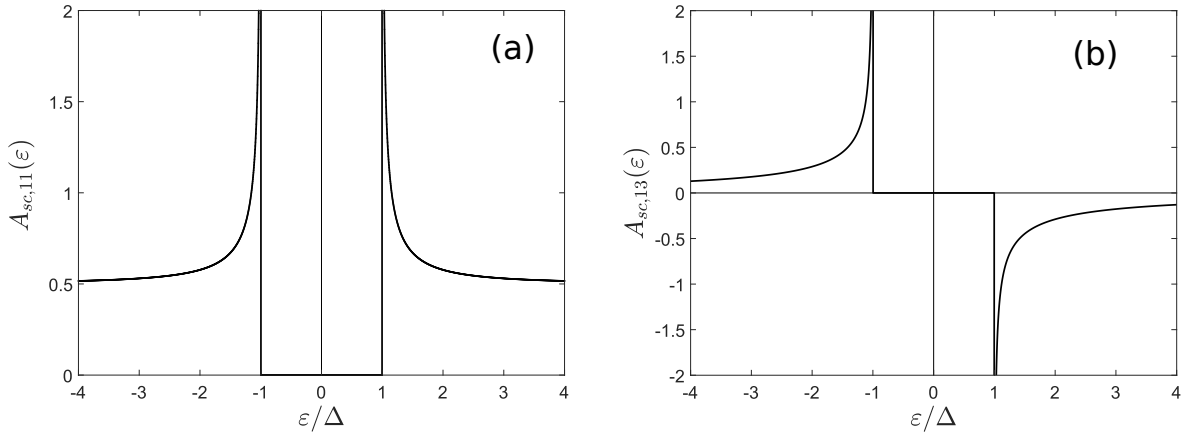

Figure 3.2: Momentum summed spectral function of an isolated superconductor described with the mean-field BCS Hamiltonian with the normal-state density of states $\rho = 1/2\Delta$, a phase bias $\phi_{sc} = \pi/2$ and superconducting parameter $\Delta = 1$. (a) Diagonal component, proportional to the density of states, showing the characteristic gap equal to Δ in the DOS and a peak just outside the gap.(b) Off-diagonal Nambu component with negative contributions at positive energy, implying that it cannot be interpreted as a probability distribution.

The diagonal and off-diagonal Nambu components of the momentum summed spectral function can be seen in Fig. 3.2. The diagonal components are all equal and therefore proportional to the density of states, which presents a gap equal to the superconducting parameter Δ and a peak just outside the gap, as it is well known for superconductors. The off-diagonal components can be negative and therefore they are not to be interpreted as a probability distribution.

The inverse of the retarded and advanced dot Green's functions reduces to

$$g^{r,a\,-1}_{d,\eta\eta}(\varepsilon) = (\varepsilon \pm i0^+)m^0_{\eta\eta} - B_0/2m^z_{\eta\eta}. \tag{3.72}$$

Using those results, the retarded and advanced full dot Green's functions can be obtained as

$$G^{r,a}_{d\eta,d\eta'} = [\boldsymbol{g}^{r,a\,-1}_d - \sum_\alpha \boldsymbol{\Sigma}^{r,a}_\alpha]^{-1}_{\eta\eta'}. \tag{3.73}$$

We will later calculate the Green's function numerically by obtaining the inverse Green's function first and then inverting the matrix numerically, but we can show here that in fact, the proximized dot has a pair of bound states, known as Andreev Bound States (ABS) at energies inside the gap. For simplicity lets consider the case without a magnetic field, $B_0 = 0$. The determinant of the inverse of the Green's function is given by

$$\begin{aligned}\mathrm{Det}[G^{r\,-1}_d(\varepsilon)] = &\left(\varepsilon + \frac{\Gamma\varepsilon}{2\sqrt{\Delta^2 - (\varepsilon + i0^+)^2}}\right)^2 \\ &- \frac{\Gamma^2\Delta^2}{2\sqrt{\Delta^2 - (\varepsilon + i0^+)^2}}(1 + \cos(\phi_r - \phi_l)).\end{aligned} \tag{3.74}$$

By setting the determinant to zero we can obtain the energies of the bound states,

$$\varepsilon^2_{ABS} = \Delta^2 \frac{\Gamma^2}{(\sqrt{\Delta^2 - \varepsilon^2_{ABS}} + \Gamma)^2}(1 - \sin^2(\frac{\phi_L - \phi_R}{2})), \tag{3.75}$$

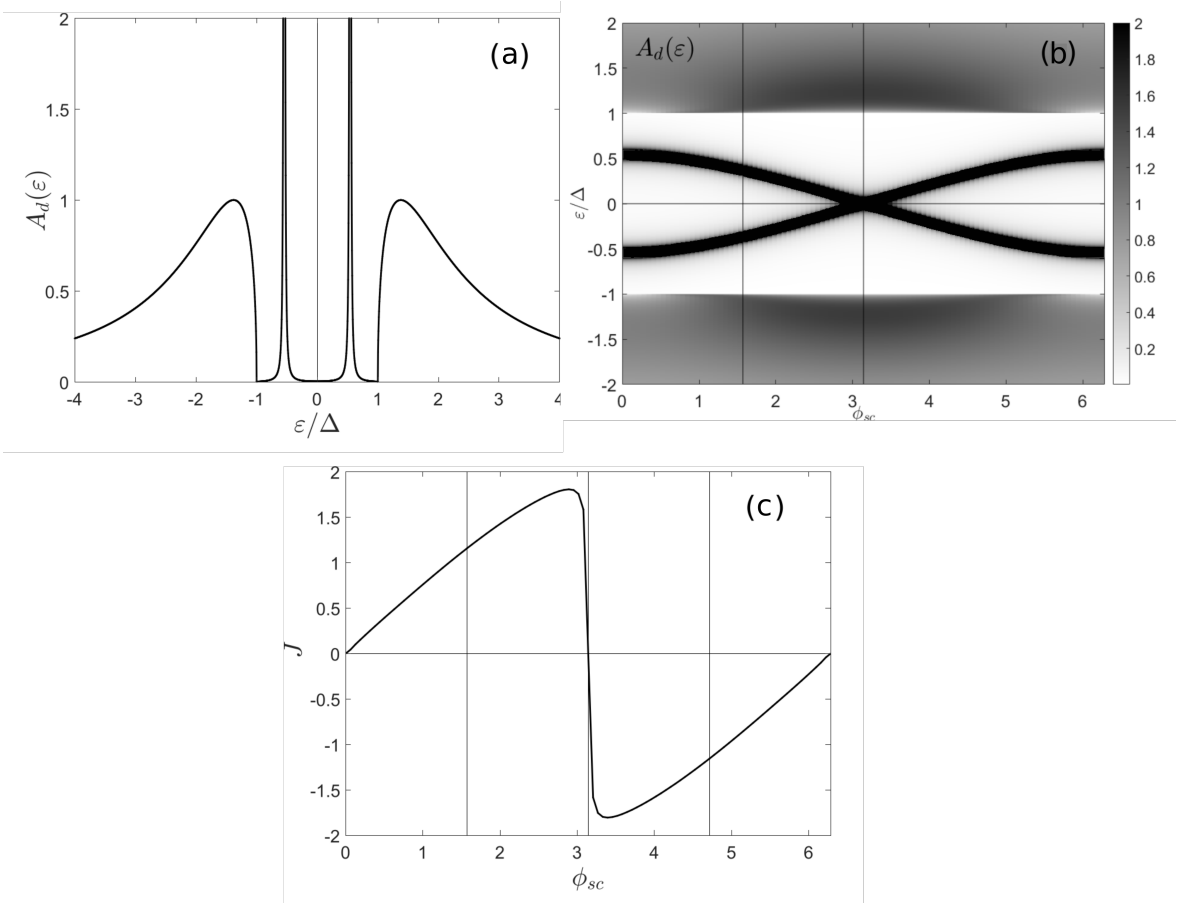

Figure 3.3: Dot density of states and current-phase relation for a S-QD-S junction with a phase bias ϕ_{sc}, coupling constant $\Gamma = \Delta$ and a superconducting parameter $\Delta = 1$. The dot is coupled to a metallic lead with coupling constant Γ_m to broaden the bound states. (a) Dot density of states calculated with $\phi_{sc} = \pi/2, \Gamma_m = 0.02\Delta$. As in the SC DOS it presents a gap of Δ above which there are continuum states. The peak in the DOS from the SC has become smoother and two Andreev Bound States appear inside the gap. (b) Phase dependence of the dot DOS obtained with $\Gamma_m = 0.2\Delta$ in order to see better the bound states. The range of the plot has been cut to show the phase-dependence of the continuum. The position of the gap is phase-independent but the height of the DOS peak in the continuum oscillates with the phase. The energies of the bound states oscillate with the phase but their amplitude remains constant. (c) Current-phase relation of the junction showing a sinusoidal dependence with the phase bias and a sign change at $\phi_{sc} = \pi$.

where we see that in order for the energies of the bound states to be real, they have to be inside the gap $|\varepsilon_{ABS}| < \Delta$. In the infinite gap the energies of the bound states are

$$\varepsilon_{ABS} = \pm\Gamma \cos\left(\frac{\phi_L - \phi_R}{2}\right), \tag{3.76}$$

which shows that the system has a pair of bound states at mirrored energies that oscillate with the phase difference between the superconductors.

The breaking of gauge-symmetry on the superconductor generates a correspondent supercurrent

$$J_{SC} = -2\partial_{\phi_{sc}} F, \tag{3.77}$$

where F is the Free energy, defined as

$$F = -T\ln \sum_{\nu} e^{-E_\nu/T} \tag{3.78}$$

where E_i are the eigenenergies of the system. At zero temperature only the many-body ground state contributes and the current reduces to

$$J_{SC} = 2\phi E_0. \tag{3.79}$$

Since we saw that the energy of the ABS depend on the phase-bias of the superconductor, they will contribute to the supercurrent, together with the continuum. We will always calculate the current using the Green's function technique unless stated otherwise, but we are going to use this expression in order to interpret the results. The density of states of the dot and the current-phase relation showing this features are shown in Fig. 3.3.

Most of the properties we are going to study in this thesis arise from the dynamics of the ABS due to the driving. For the sake of simplicity, for most of this chapter we are going to consider the infinite gap limit, where the continuum is not present and all properties of the junction arise from the ABS. By integrating out the leads degrees of freedom [28] an effective Hamiltonian for the dot can be found as

$$H_{d,\text{eff}} = H_d - \sum_{\alpha,\eta\eta'} \phi^\dagger_\eta \Sigma^r_{\alpha,\eta\eta'} \phi_{\eta'}, \tag{3.80}$$

so that the bare dot Green's function calculated with this Hamiltonian is equal to the full dot Green's function calculated with the original Hamiltonian in the infinite gap limit. In this limit the Nambu matrix of the self-energy reduces to

$$\Sigma_\alpha = \begin{pmatrix} 0 & -\Gamma e^{i\phi_\alpha} \\ -\Gamma e^{-i\phi_\alpha} & 0 \end{pmatrix} \otimes \sigma_0, \tag{3.81}$$

and by symmetrizing the phases $\phi_L = -\phi_R = \phi_{sc}/2$, the effective dot Hamiltonian takes the form

$$H_{d,\text{eff}} = \sum_{\eta\eta'} \phi^\dagger_\eta \left[B_0/2m^z - \Gamma\cos(\phi_{sc}/2)m^1\right]_{\eta\eta'} \phi_{\eta'}, \tag{3.82}$$

which comparing with (3.16) can be identified as a superconducting Hamiltonian with the superconducting parameter being $\Gamma\cos(\phi_{sc}/2)$. The energy of the bound states can be obtained now by diagonalizing the Hamiltonian with the Bogoliubov transformation defined by the unitary Nambu matrix

$$U_{\eta\eta'} = \frac{1}{\sqrt{2}}(m^0 + im^2)_{\eta\eta'}, \tag{3.83}$$

which results in

$$H_{d,\text{eff}} = \sum_{\eta\eta'} \gamma^\dagger_\eta (B_0/2m^z + \Gamma\cos(\phi_{sc}/2)m^3)_{\eta\eta'} \gamma_{\eta'} \tag{3.84}$$

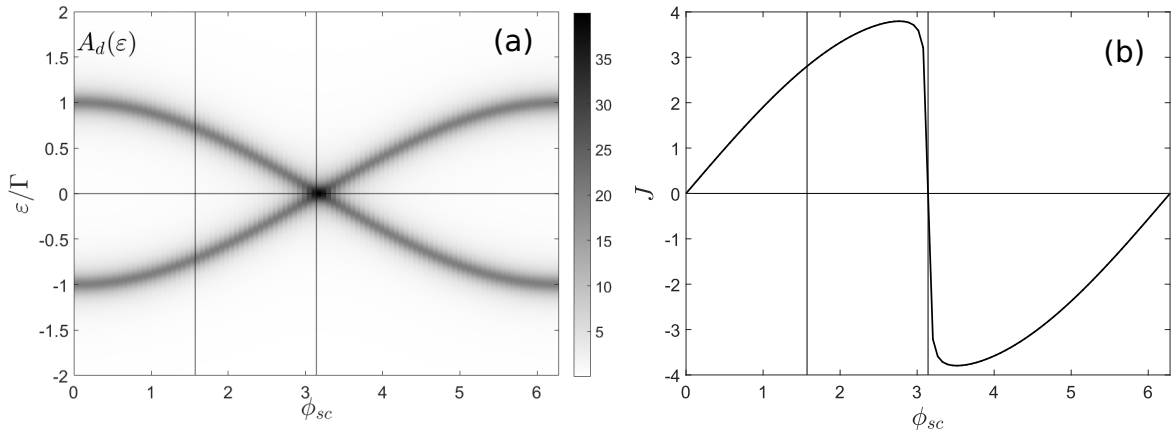

Figure 3.4: phase dependence of the dot DOS an current-phase relation for a S-QD-S junction in the infinite gap limit, $\Delta \to \infty$ with $\Gamma = 1$ contacted with a metallic lead with coupling constant Γ_m in order to broaden the bound states. (a) Phase dependence of the dot density of states calculated with a coupling to a metallic lead with coupling $\Gamma_m = 0.2\Gamma$ in order to show better the bound state. The energies of the bound states depend on the phase-bias as a cosine. The bound states cross at $\phi = \pi$. (b) Current-phase relation calculated with $\Gamma_m = 0.02\Gamma$ for better accuracy. The current follows the same relation as in the gapped case, but the amplitude is doubled, meaning that the contribution from the continuum has to be lower than the one from the bound states.

where $\gamma_\eta = \sum_{\eta_1} U^\dagger_{\eta\eta_1}\phi_{\eta_1}$ is the annihilation operator that destruct quasiparticles in the ABS $|\pm,\sigma\rangle$ with eigenenergies

$$\varepsilon_{\pm,\sigma} = \sigma B_0/2 \pm \Gamma\cos(\phi_{sc}/2)). \tag{3.85}$$

In the infinite gap limit the only state contributing to the current is the one at negative energy because it is the only one occupied. At zero magnetic field the two spins of the ABS are degenerate and the current can then be obtained as

$$\begin{aligned} J_{SC} &= -2\partial_{\phi_{sc}}(\varepsilon_+\theta(-\varepsilon_+) + \varepsilon_-\theta(-\varepsilon_-)) && (3.86)\\ &= 2\Gamma\sin(\phi_{sc}/2)(\theta(\pi-\phi_{sc}) - \theta(\phi_{sc}-\pi)). && (3.87)\end{aligned}$$

The current can also be obtained with the density of states as

$$J = \frac{1}{2\pi}\int_{-\infty}^{0} d\varepsilon\, J(\varepsilon), \tag{3.88}$$

where $J(\varepsilon) = \int_{-\varepsilon}^{0} d\varepsilon_1\, \partial_{\phi_{sc}} A_d(\varepsilon_1)$ is the current density. We show the current-phase relation and the dot density of states in the infinite gap limit at zero magnetic field in Fig. 3.4. Since only one bound state carries current the current-phase relation is sinusoidal, with a change of sign in $\phi_{sc} = \pi$ due to the fact that the two bound states cross zero energy and the positive ABS, which carries negative current, is now the only one occupied. The width of the jump is proportional to the artificial broadening of the bound states.

The magnetic field dependence of the current density and the total current at $\phi_{sc} = \pi/2$ is shown in Fig.3.5. The only effect the magnetic field has on the ABS is to

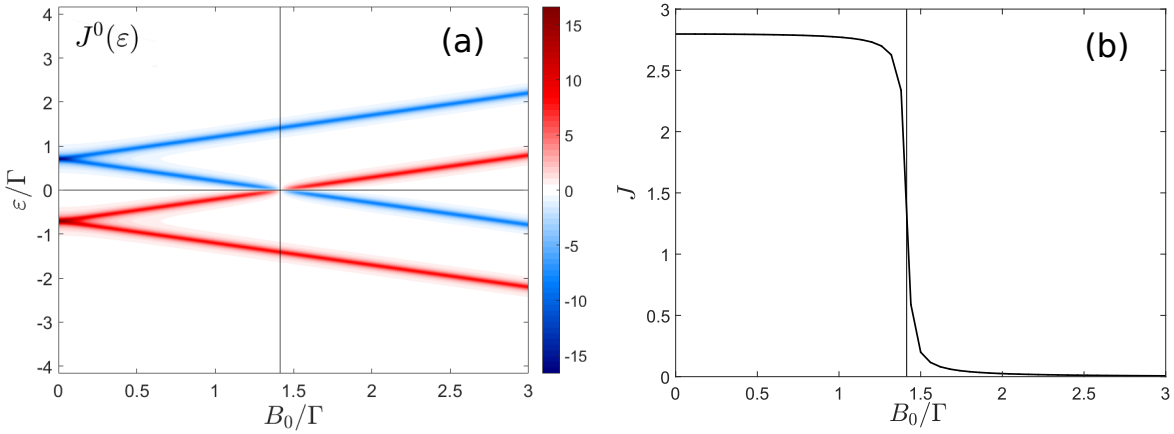

Figure 3.5: Dependence on magnetic field of the current density and total current for a phase-biased S-QD-S junction with $\phi_{sc} = \pi/2$ and coupling constant $\Gamma = 1$. A vertical line has been added at the critical magnetic field $B_c = \sqrt{2}$ for clarity. (a) Current density showing the current carried by each bound state. Calculated for a junction with the dot coupled to a metallic lead with coupling constant $\Gamma_m = 0.2\Gamma$ needed to broaden the bound states. The magnetic field splits the energy of the ABS. (b) Current-magnetic field relation calculated with $\Gamma_m = 0.02\Gamma$ for more accuracy with two clearly distinct regions with constant positive and vanishing current separated by the critical magnetic field $B_c = 2\Gamma\cos(\phi_{sc})$ characterized by a change in the occupation of the ABS.

split the energy of the two spin components of the ABS with a linear dependence on the magnetic field. The dependence on the phase-bias, and therefore the current these states carry is the same.

We plotted the current density in order to see clearly which bound state carries which sign of current. We had trouble calculating the current density numerically because small numerical errors in the density of states are enhanced by the phase derivative and posterior integral, specially in the points were bound states cross, making the current density not vanish outside the bound states. We avoided this problem by calculating the current density for each bound state at zero magnetic field and then, using that it is the same for any magnetic field and that the dependence of the energy is linear, we extrapolated for finite magnetic field. All the plots of current density in this thesis were obtained this way.

In the current-magnetic field plot we see two different regions. The first region is characterized by an occupation of the states $|-,\uparrow\rangle$ and $|-,\downarrow\rangle$, which carry the same current, resulting in a positive and constant current throughout the region. At a critical point given by $B_c = 2\Gamma\cos(\phi_{sc}/2)$ the states $|-,\uparrow\rangle$ and $|+,\downarrow\rangle$ cross at zero energy, and for any magnetic field above this point the occupied bound states contributing to the total current are $|-,\downarrow\rangle$ and $|+,\downarrow\rangle$, which carry opposite current and therefore the total current vanishes.

3.3 Phase biased junction with a driven dot

The same kind of response to a magnetic field is found in multidot junctions, but with a much richer dependence [28]. One would think that if the time-average dynamics of a harmonically driven resonant level are similar to those of a multilevel system as the Floquet formalism says, we will find a richer magnetic field dependence of the current when we turn on the drive on our dot as well. This is the main focus of this section. We will work again in the infinite gap limit $\Delta \to \infty$ with the effective Hamiltonian of the proximitized dot.

We will consider again the cases of an applied ac gate voltage and dc and ac magnetic fields. The on-site energy of the dot is therefore

$$\varepsilon_{d,\sigma}(t) = V_g \cos(\omega t) + \sigma(B_0/2 + B\cos(\omega t)), \tag{3.89}$$

where we drop the phase of the drive because it is irrelevant for this section, since it equates to a shift in the time variable and we are only interested in time-averaged observables. The effective Hamiltonian can then be written as

$$H_{d,\text{eff}}(t) = \sum_{\eta\eta'} \phi_\eta^\dagger \left[V_g \cos(\omega t) m^3 + (B_0/2 + B\cos(\omega t)) m^z - \Gamma \cos(\phi_{sc}/2) m^1\right]_{\eta\eta'} \phi_{\eta'}. \tag{3.90}$$

In order to explain the results we are going to make use of the Floquet formalism. The Floquet Hamiltonian (2.22) is given by the elements

$$\begin{aligned} H^F_{d,\text{eff},nm} = &\sum_{\eta\eta'} \phi_\eta^\dagger \left[V_g/2(\delta_{n-m,1} + \delta_{n-m,-1}) m^3 \right. \\ &\left. + (B_0/2\delta_{nm} + B/2(\delta_{n-m,1} + \delta_{n-m,-1})) m^z - \Gamma \cos(\phi_{sc}/2)\delta_{nm} m^1\right]_{\eta\eta'} \phi_{\eta'} + n\omega\delta_{nm}. \end{aligned} \tag{3.91}$$

As we learned in the last chapter, as a result from the periodic drive, the ABS will span two sets of bound states. The Floquet states $|u_{\nu,n}\rangle\!\rangle$ at energies $\varepsilon_\nu - n\omega$ and different spectral weights $A_{\nu,n}$. In order to simplify the interpretation of the results we will use the following nomenclature and notation. The Floquet state $|u_{\pm\sigma,n}\rangle\!\rangle$ adiabatically connected to the state $|\pm\sigma\rangle$ when we turn down the drive will be referred to as the zeroth Floquet band of the Floquet Andreev Bound State (FABS) $|\pm\sigma\rangle\!\rangle$ with energy $\varepsilon_{\pm\sigma}$ and will be denoted by $|\pm\sigma, 0\rangle\!\rangle$, i.e. $\lim_{A\to 0} \varepsilon_{\pm\sigma}(A) = \varepsilon_{ABS,\pm\sigma}$, where A is the amplitude of the drive. The rest of the states at energies $\varepsilon_{\pm\sigma} - n\omega$ will be referred as the n'th Floquet band of the FABS $|\pm\sigma\rangle\!\rangle$ and will be denoted by $|\pm\sigma, n\rangle\!\rangle \neq |\pm\sigma\rangle \otimes |n\rangle$, not to confuse the label n with the basis of the Hilbert space $\mathcal{T}_\omega$. In Fig. 3.8 we labeled some of the bound states in order to illustrate the notation we are going to use.

Last section we found that in the infinite gap limit and zero temperature the current going trough the junction can be obtained as

$$J = \sum_{\varepsilon_\nu < 0} \partial_{\phi_{sc}} \varepsilon_\nu. \tag{3.92}$$

Since we found last chapter that the time-averaged dynamics of the periodically driven dot are similar to those of a multidot system, we are going to make the assumption here that the time-averaged current takes the form

$$J^0 = \sum_{\varepsilon_\nu - n\omega < 0} A_{\nu,n} \partial_{\phi_{sc}} (\varepsilon_\nu - n\omega). \tag{3.93}$$

Electron-hole symmetry ensures that $\partial_{\phi_{sc}}(\varepsilon_{+\sigma} - n\omega) = -\partial_{\phi_{sc}}(\varepsilon_{-\sigma} - m\omega) = -j$ and therefore the expression for the time-averaged current becomes

$$\begin{aligned} J^0 &= -j \sum_{\varepsilon_\nu - n\omega < 0} A_{\nu,n} \operatorname{sign}(\varepsilon_\nu) \\ &= \int_{-\infty}^{0} d\varepsilon \, \left(-jA^0(\varepsilon)\operatorname{sign}(\varepsilon)\right) \\ &= \int_{-\infty}^{0} d\varepsilon \, J^0(\varepsilon), \end{aligned} \tag{3.94}$$

where $J^0(\varepsilon)$ is the time-averaged current density. Note that in order to use this expression one has to obtain the spectral weight of the Floquet bands of the FABS and their energies separately in order to do the phase derivative. We had trouble doing this numerically when different bound states overlapped because of numerical errors. There is one case where one does not need to calculate them separately, when the spectral weight of the Floquet bands does not depend on the phase. In that case the current density can be obtained as in equilibrium,

$$J(\varepsilon) = \int_{-\varepsilon}^{0} d\varepsilon_1 \partial_{\phi_{sc}} A^0(\varepsilon_1). \tag{3.95}$$

There is no formal proof this expression for the time-averaged current is correct, but throughout this chapter we are going to see results that can be explained with this expressions, supporting that it is correct, and later we will see one case where we could calculate the time-averaged current with this expression and we obtained the same result as the one obtained via the Green's functions technique.

Lets look first at the case with only a magnetic field, $V_g = 0$. The elements of the Floquet effective dot Hamiltonian are given by

$$\begin{aligned} H^F_{d,\text{eff},nm} = &\sum_{\eta\eta'} \phi^\dagger_\eta \left[(B_0/2\delta_{nm} + B/2(\delta_{n-m,1} + \delta_{n-m,-1}))m^z \right. \\ &\left. -\Gamma\cos(\phi_{sc}/2)\delta_{nm}m^1\right]_{\eta\eta'} \phi_{\eta'} + n\omega\delta_{nm}. \end{aligned} \tag{3.96}$$

We can use the Bogoliubov transformation (3.83) to obtain the Hamiltonian in terms of the creation and annihilation operators of ABS,

$$\begin{aligned} H^F_{d,\text{eff},nm} = &\sum_{\eta} \gamma^\dagger_\eta \left[(B_0/2\delta_{nm} + B/2(\delta_{n-m,1} + \delta_{n-m,-1}))m^z \right. \qquad (3.97) \\ &\left. +\Gamma\cos(\phi_{sc}/2)\delta_{nm}m^3\right]_{\eta\eta'} \gamma_{\eta'} + n\omega\delta_{nm}. \qquad (3.98) \end{aligned}$$

Since the Hamiltonian is diagonal now in Nambu space, the two types of ABS, $|\pm\sigma\rangle$, do not interact with each other. And the Floquet structure is the same one we had for an isolated level being driven with an ac magnetic field and on-site energy $\pm\Gamma\cos(\phi_{sc}/2)$.

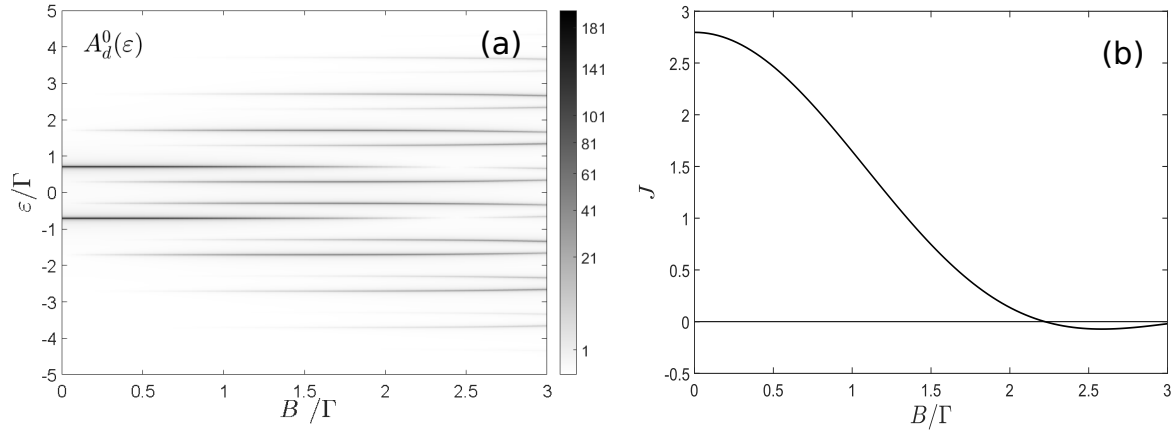

Figure 3.7: Dependence of the time-averaged density of states and current with the amplitude of an ac magnetic field, $V_g = 0$, for a phase-biased S-QD-S junction in the infinite gap limit, $\Delta \to \infty$, with parameters $\omega = \Gamma, \phi_{sc} = \pi/2$ and a coupling to a metallic lead to broaden the bound states with coupling constant $\Gamma_m = 0.02\Gamma$. (a) Time-averaged density of states of the dot. The two ABS do not interact through the drive, resulting in a DOS composed of two copies of the DOS of an isolated level. (d) Amplitude dependence of the time-averaged current. Apart from a small numerical error the current is proportional to the Bessel function $|J_0(B/\omega)|^2$ because only the zeroth Floquet band contributes.

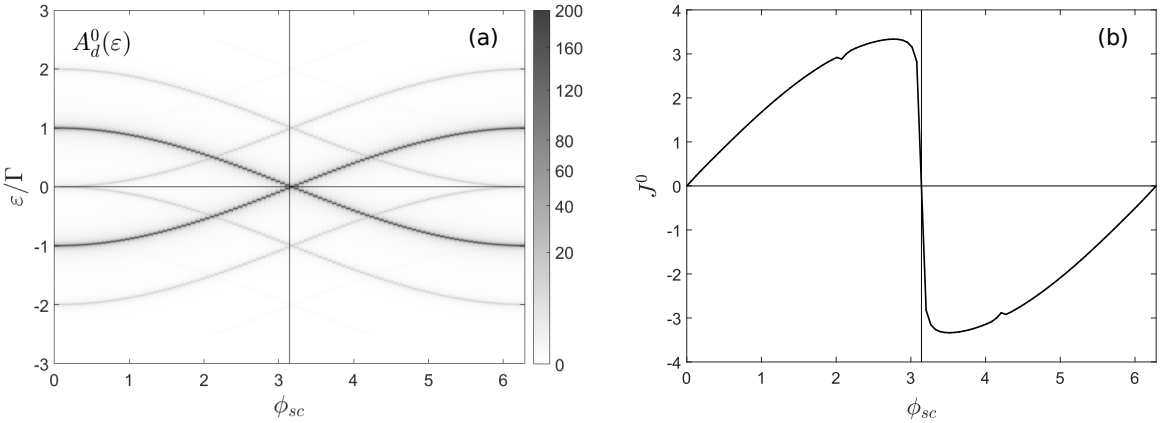

Figure 3.6: Phase dependence of the time-averaged density of states and current for a phase-biased S-QD-S junction in the infinite gap limit, $\Delta \to \infty$, being driven with an ac magnetic field $B = \Gamma/2, \omega = \Gamma, \Gamma = 1$ and coupled to a metallic lead to broaden the bound states with a coupling constant $\Gamma_m = 0.02\Gamma$. (a) The Floquet bands of the ABS do not interact with each other through the drive and the time-averaged density of states is that of equilibrium for each Floquet band. (b) Time-averaged current. Only the zeroth Floquet band $|\pm\sigma, 0\rangle\rangle$ contributes to the current and hence it is equal to the equilibrium relation weighted by $|J_0(B/\omega)|^2$. The two small bumps at $\phi_{sc} \simeq 2, 4$ are due to numerical errors coming from the crossing of different Floquet bands seen in the plot of the density of states.

From last chapter we now that the resulting eigenstates $|\pm\sigma, n\rangle\rangle$ have energies $\varepsilon_{\pm\sigma} - n\omega$ where $\varepsilon_{\pm\sigma}$ is the energy of the ABS in equilibrium, and spectral weight $|J_n(B/\omega)|^2$.

As we can see in Fig. 3.7, the dependence of the time-averaged density of states with the amplitude of the drive B is in fact the result for two driven levels. Since the

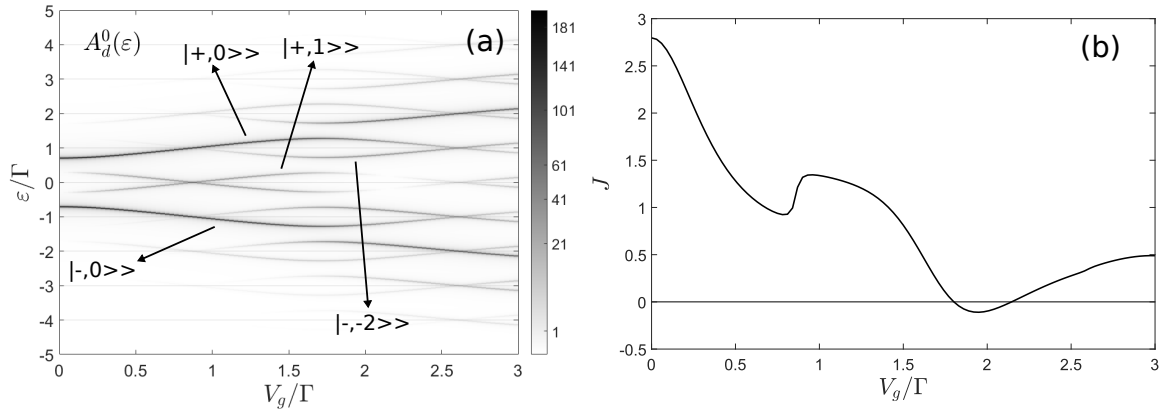

Figure 3.8: Dependence of the time-averaged density of states and current with the amplitude of ac gate voltage for a phase-biased S-QD-S junction in the infinite gap limit, $\Delta \to \infty$, with parameters $\omega = \Gamma, \phi_{sc} = \pi/2$ and a coupling to a metallic lead to broaden the bound states with coupling constant $\Gamma_m = 0.02\Gamma$. (a) Time-averaged density of states of the dot. The drive induces interactions between neighboring Floquet bands of the different ABS $|\pm\rangle$ and results in avoided crossings. (b) The time-averaged current decreases because the transport through the Floquet bands is off resonance. Apart from a numerical error the current vanishes at the point of the avoided crossing.

energy of the FABS is the same as in equilibrium, the phase dependence of the density of states, shown in Fig.3.6, results also in the solution at equilibrium for each Floquet bands. For the parameters used in Fig. 3.6 the first Floquet band of the two FABS have negative energies and the total current carried by these states cancels. Only the zeroth Floquet band contributes to the current. As a result, the current-phase relation is the same as in equilibrium, with an overall proportionality factor given by the spectral weight of the zeroth band (2.92), $|J_0(B/\omega)|^2$.

Lets take now the case of an ac gate voltage, $B = 0$. The elements of the Floquet effective dot Hamiltonian are

$$H^F_{d,\text{eff},nm} = \sum_{\eta\eta'} \phi^\dagger_\eta \left[V_g/2(\delta_{n-m,1} + \delta_{n-m,-1})m^3 + B_0/2\delta_{nm}m^z - \Gamma\cos(\phi_{sc}/2)\delta_{nm}m^1 \right]_{\eta\eta'} \phi_{\eta'} + n\omega\delta_{nm}. \tag{3.99}$$

Applying again the Bogoliubov transformation we can express the effective Hamiltonian in the basis of the equilibrium ABS as

$$H^F_{d,\text{eff},nm} = \sum_{\eta\eta'} \gamma^\dagger_\eta \left[B_0\delta_{nm}m^z + \Gamma\cos(\phi_{sc}/2)\delta_{nm}m^3 \right. \tag{3.100}$$

$$\left. + V_g/2(\delta_{n-m,1} + \delta_{n-m,-1})m^1 \right]_{\eta\eta'} \gamma_{\eta'} + n\omega\delta_{nm}. \tag{3.101}$$

In contrast to the ac magnetic field, the ac gate voltage appears as an off-diagonal term coupling neighboring Floquet bands of the two different ABS. As a result we observe in Fig. 3.8 that the dependence of the time-averaged density of states with the amplitude of the drive, V_g is more complex than in the case with the ac magnetic field. At low drive amplitude the zeroth Floquet band of the negative ABS starts interacting with

the first Floquet band of the positive ABS. As the amplitude of the drives increases the avoided crossing between these two states makes the resulting FABS separate from each other. When the amplitude is high enough the zeroth Floquet band of the negative ABS will start interacting with the second Floquet band of the positive ABS and as a result the zeroth Floquet band of the negative FABS will increase in energy. The same thing will happen to the first Floquet band of the negative ABS for higher amplitudes and as a result we observe an oscillatory behavior of the energies of the FABS.

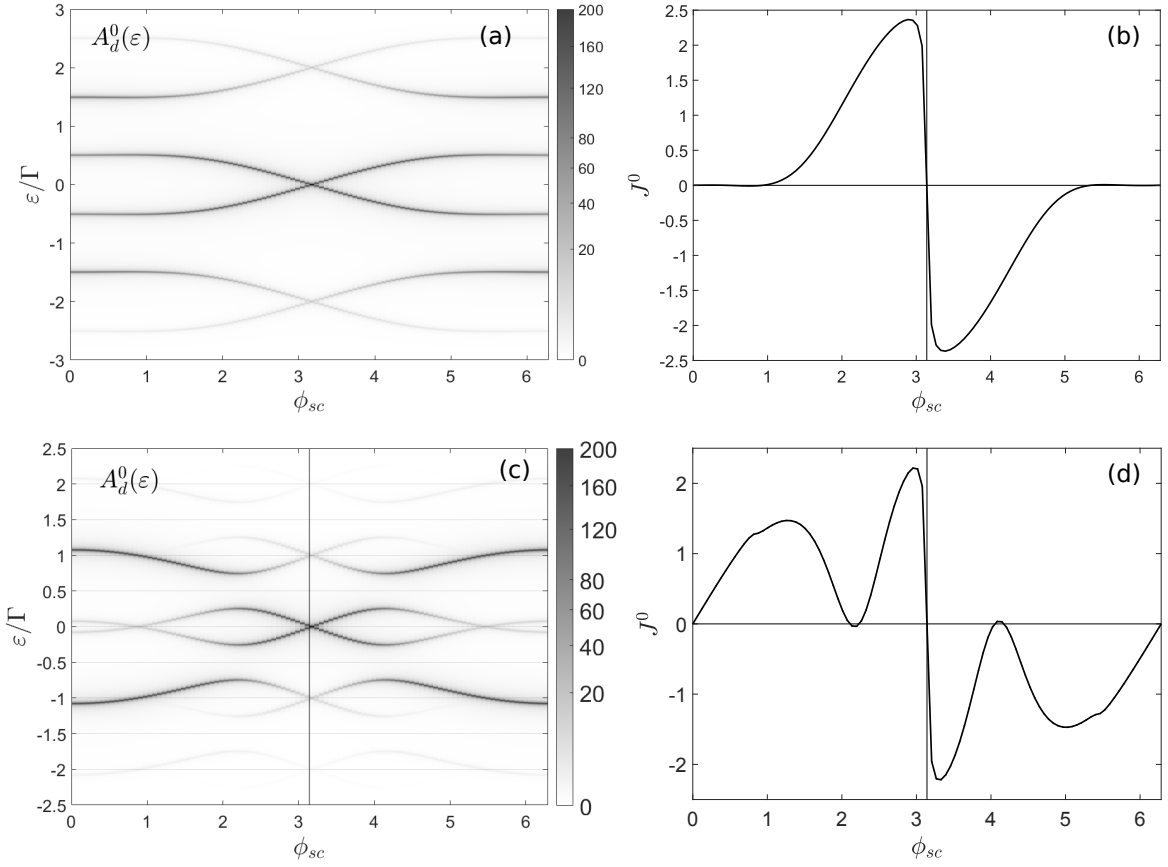

Figure 3.9: Phase dependence of the time-averaged density of states and current for a phase-biased S-QD-S junction in the infinite gap limit, $\Delta \to \infty$, driven with an ac gate-voltage, $B = 0$, and coupled to a metallic lead with coupling constant $\Gamma_m = 0.02\Gamma$. (a) Time-averaged density of states for the junction driven with $V_g = \Gamma, \omega = 2\Gamma$. The interaction between the two ABS in different Floquet bands makes the energies of the FABS constant for small phase-bias. (b) Time-averaged current for the junction with driving parameters $V_g = \Gamma, \omega = 2\Gamma$. The constant energy of the bound states at small phase-bias is reflected in a vanishing current for small phase bias. (c) Time-averaged density of states for the junction with being driven with $V_g = \Gamma/2, \omega = \Gamma$. The avoided crossings here make the energies of the FABS oscillate around $n\omega$. (d) Time-averaged current of the junction with parameters $V_g = \Gamma/2, \omega = \Gamma$. The avoided crossings make the current vanish again, but here in a unique point around $\phi_{sc} \simeq 2$. The bumps around $\phi_{sc} \simeq 1$ are again due to the fact that the fist Floquet band of the positive FABS crosses zero energy.

The phase dependence of the time-averaged density of states, shown in 3.9, can be understood in the same manner in terms of avoided crossings. In the current-phase

relation we observe a novel feature arising from the driving that is similar to what was found on [24], at the point of the avoided crossing the derivative of the energies of the FABS with respect to the phase is necessarily zero and therefore the current vanishes at that point.

This result also supports that the assumed expression for the current is correct. Another expression for the time-averaged current that we thought might be correct is

$$J^0 = \partial_\phi \sum_{\varepsilon_\nu - n\omega < 0} A_{\nu,n}(\varepsilon_\nu - n\omega). \tag{3.102}$$

At the point of the avoided crossing one would have

$$J^0 = \partial_\phi (A_{-,0}\varepsilon_- + A_{+,1}(\varepsilon_+ - \omega)). \tag{3.103}$$

Since we have $A_{-,0} = A_{+,1}$,$\partial_\phi A_{-,0} = -\partial_\phi A_{+,1}$ and $\partial_{\phi_{sc}}\varepsilon_- = -\partial_{\phi_{sc}}(\varepsilon_+ - \omega)$, the current can be obtained as

$$\begin{aligned} J^0 &= \varepsilon_-\partial_\phi A_{-,0} + A_{-,0}\partial_\phi\varepsilon_- + A_{+,1}\partial_\phi(\varepsilon_+ - \omega) + (\varepsilon_+ - \omega)\partial_\phi A_{+,1} \\ &= \varepsilon_-\partial_\phi A_{-,0} + A_{-,0}\partial_\phi\varepsilon_- - A_{-,0}\partial_\phi\varepsilon_- - (\varepsilon_+ - \omega)\partial_\phi A_{-,0} \\ &= (\varepsilon_- - \varepsilon_+ + \omega)\partial_{-,0} \\ &= (2\varepsilon_- + \omega)\partial_\phi A_{-,0}, \end{aligned} \tag{3.104}$$

and the current would not vanish at the point of the avoided crossing, which disagrees with the result obtained using the Green's function technique, and therefore it is not correct.

Now that we understand how the driving affects the bound states we can go on to study the effect on an applied dc magnetic field. The dc magnetic field appears as a diagonal term in both Floquet and Nambu spaces. As in equilibrium, the only effect of an applied constant magnetic field on the dot is to split the bound states, $\varepsilon_{\pm,\sigma,n} = \sigma B_0/2 + \varepsilon_{\pm,n}$, and therefore we expect to see a behavior similar to the one discussed in the last section for the junction in equilibrium.

Since the magnetic field only splits the FABS. All the Floquet bands of the positive (negative) FABS carry negative (positive) current, weighted by their spectral weight. With the results at equilibrium in mind we can expect to have the same amount of transitions between different regions of constant current with the dc magnetic field as Floquet bands with significative spectral weight we have.

Very different current-magnetic field relations can be obtained depending on the order in energy of the different Floquet bands of the FABS and their spectral weight. To simplify the results we consider only the case with 3 significative Floquet bands and we discuss the most interesting case, when $\omega \simeq \Gamma$ and the first Floquet band of the positive FABS, $|+\sigma, 1\rangle\!\rangle$ crosses in energy the zeroth Floquet band of the negative FABS, $|-\sigma, 0\rangle\!\rangle$. Since the magnetic field does not add interactions between the bound states the total current-magnetic field relation is the sum of the current-magnetic field relation for each bound state, which follows the equilibrium one.

Take the case of an applied ac gate voltage, shown in Fig. 3.10, the current in the first region is given by the sum of the current carried by the states $|+, 1\rangle\!\rangle$,$|-, 0\rangle\!\rangle$ and $|-, 1\rangle\!\rangle$. Since the spectral weight of the state $|-, 0\rangle\!\rangle$ is higher than the one from $|+, 1\rangle\!\rangle$,

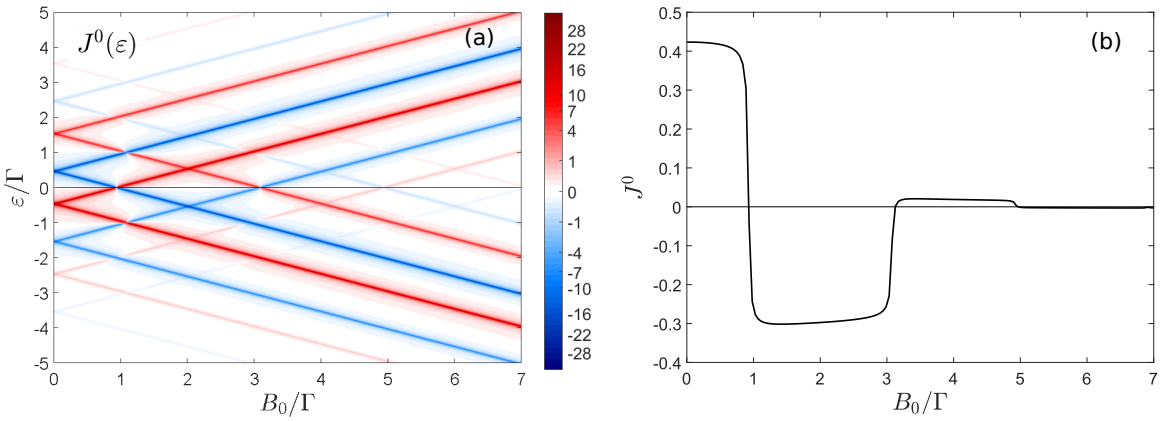

Figure 3.10: Magnetic dependence of the time-averaged current density and total current for a phase-biased junction with $\phi_{sc} = \pi/2, \Gamma = 1$ with the dot being driven with an ac gate-voltage with parameters $V_g = \Gamma, \omega = 2\Gamma$, contacted with a metallic lead with coupling constant $\Gamma_m = 0.02\Gamma$ in order to broaden the bound states. (a) Time-averaged current density showing that all Floquet bands of a state carry current with the same sign. (b) Time-averaged total current. Different regions are obtained with positive, negative and vanishing current depending on which Floquet bands of the FABS are occupied. The negative current region is obtained because in this region the current is dominated by the contribution of the first Floquet band of the positive FABS.

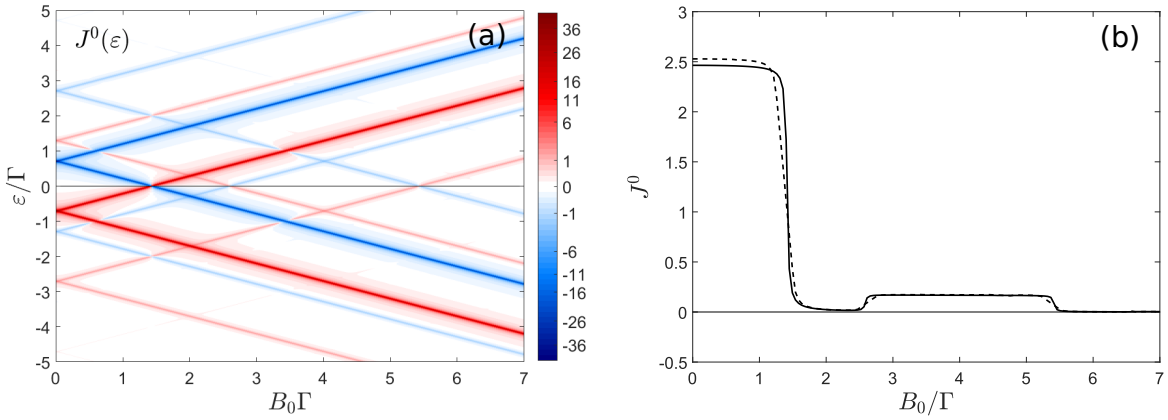

Figure 3.11: Dependence of the time-averaged current density and total current with a dc magnetic field applied on the dot for a phase-biased junction with $\phi_{sc} = \pi/2, \Gamma = 1$ and a dot being driven with an ac gate-voltage $B = \Gamma, \omega = 2\Gamma$ and contacted by a metallic lead to broaden the bound states with coupling constant $\Gamma_m = 0.02\Gamma$. (a) Time-averaged current density. The constant magnetic field splits the bound states and their Floquet bands. (b) Time-averaged current. Different regions are obtained with positive and vanishing current depending on the bound states occupied. The vanishing current in the second region appears because the first Floquet band has crossed the opposite bound state and in the second region both occupied states carry opposite current. The continuous line is calculated with the Green's function technique while the dotted line is the result obtained integrating the current density.

it results in a positive current. In the second region the current carried by the state $|-,0\rangle\rangle$ vanishes, and since the amplitude of $|+,1\rangle\rangle$ is higher than the amplitude from

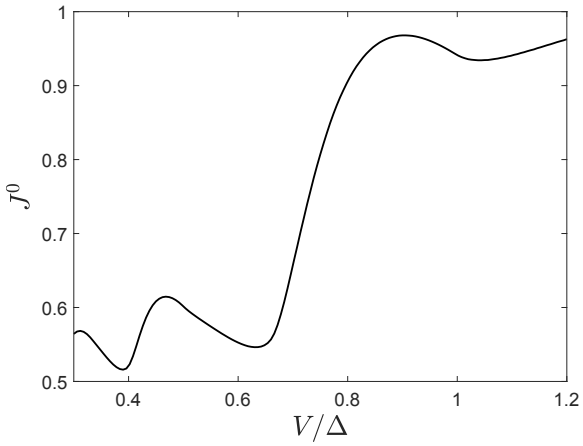

Figure 3.12: Time-averaged current for a S-QD-S junction with a voltage-bias V, coupling constant $\Gamma = \Delta$ and superconducting parameter $\Delta = 1$. For voltage-bias lower than the gap the current is characterized by peaks in the conductance at voltages $V_n = 2\Delta/n$ with odd n arising from Multiple Andreev Reflection (MAR) processes.

$|-,1\rangle\rangle$, the current becomes negative. We have therefore a $0-\pi$ transition with the applied dc magnetic field. In the third region we only have the current carried by the state $|-,1\rangle\rangle$, which is positive, and finally the current vanishes in the fourth region because all the FABS with significative spectral weight have crossed zero energy.

The case of an ac magnetic field with the same parameters, shown in Fig. 3.11, follows the same logic. But as we saw in Fig. 3.7, in this case the Floquet states $|\nu,n\rangle\rangle$ and $|\nu,-n\rangle\rangle$ have the same spectral weight and therefore in the second region the current vanishes. In this case, since the spectral weight of the Floquet bands does not depend on the phase-bias we can calculate the current with (3.95), which is also shown in Fig.3.11 in a dotted line. We see that it gives the same result as the one obtained with the Green's function method.

3.4 Voltage-biased junction

In this section we are going to study the voltage-biased junction with a non-driven dot. The voltage-biased superconducting junction has been studied extensively, both as a tunneling junction, in the quantum point contact limit, [17] and contacted by a quantum dot [18, 25], using the Floquet Green's function method described in this thesis. Here we will explain how this system behaves and more importantly, give a microscopic picture of how voltage-bias affects the tunneling in terms of the Floquet Hamiltonian in the extended space which will help us understand the results of next section.

The time-averaged current going through the S-QD-S junction with a finite voltage bias is shown in Fig. 3.12. There exists sub-gap transport, for $V < 2\Delta$, that is characterized by peaks in the conductance at voltages $V_n = 2\Delta/n$ with integer odd n. This current-voltage relation has been understood in terms of Multiple Andreev Reflections (MAR).

An Andreev reflection is a process that appears at interfaces between normal and su-

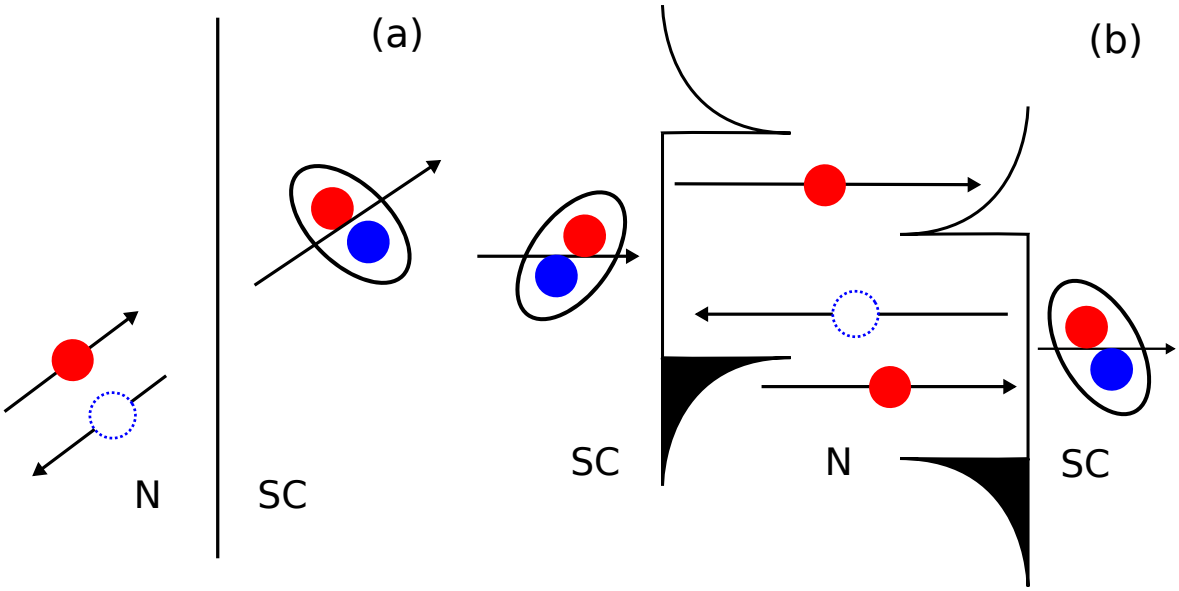

Figure 3.13: (a) Andreev reflection in an interface between normal and a superconductor. An electron with spin up (down) is reflected as a hole with spin down (up) and a Cooper pair is created in the superconductor. (b) Multiple Andreev reflections in a junction with a normal region between two superconductors with a voltage bias. An electron from the continuum of the left lead tunnels to the right lead, where it reflects back as a hole creating a Cooper pair in the right lead. The hole tunnels to the left lead and is reflected back as an electron, destroying a Cooper pair from the left lead and so on. The incident particle and the reflected one have opposite energy in the frame of reference of the superconductor.

perconducting materials. When an electron tunnels into the superconductor, a Cooper pair might be created on the superconductor and the electron is reflected back as a hole with opposite spin. This process transfers $2e$ charge to the superconductor.

MAR happens when the interface is between two superconductors with a voltage-bias. An electron from the continuum of the left superconductors can tunnel into the right superconductor, where a Cooper pair is created and the incident electron reflects back to the left superconductor as a hole. The hole destructs a Cooper pair in the left superconductor and is reflected back into the right superconductor as an electron and so on. The MAR process is only possible with even n reflections at voltages $2\Delta/(n+1) < V < 2\Delta/(n-1)$. Each point $V_n = 2\Delta/n$, for odd n, with a peak in the conductance reflects a transition from a MAR process with $n+1$ reflections to a MAR process with $n-1$ reflections.

In order to understand the MAR processes in terms of the Floquet formalism we are going to first study the effect of the voltage-bias in the infinite gap limit $\Delta \to \infty$. The Floquet self-energy in this limit reduces to

$$\Sigma^{r,a}_{\alpha,nm} = \begin{pmatrix} 0 & -\Gamma\delta_{n-m,2\frac{V_\alpha}{\omega}} \\ -\Gamma\delta_{n-m,-2\frac{V_\alpha}{\omega}} & 0 \end{pmatrix} \otimes \sigma_0, \tag{3.105}$$

where we dropped the superconducting phase ϕ_{sc} because it acts only as a shift in the time variable and we are only interested in time-averaged observables. With the

Floquet self-energy we can obtain the elements of the Floquet effective dot Hamiltonian, given by

$$H^F_{d,\text{eff},nm} = \sum_{\eta\eta'} \phi^\dagger_\eta [-\Gamma(\delta_{n-m,1} + \delta_{n-m,-1}) m^1]_{\eta\eta'} \phi_{\eta'} + n\omega\delta_{nm}. \tag{3.106}$$

The off-diagonal term in Nambu space related to the creation and annihilation of Cooper pairs in the dot is also off-diagonal in Floquet space. One of the main effects of the voltage bias is that the two electrons of a Cooper pair cannot tunnel to the same Floquet band anymore. Cooper pairs can only be created and destroyed in the quantum dot in different and neighboring Floquet bands.

If we apply the Bogoliubov transformation to the effective Hamiltonian we obtain

$$H^F_{d,\text{eff},nm} = \sum_{\eta\eta'} \gamma^\dagger_\eta [\Gamma(\delta_{n-m,1} + \delta_{n-m,-1}) m^3]_{\eta\eta'} \gamma_{\eta'}, \tag{3.107}$$

which is the Hamiltonian for a level being driven with an ac gate voltage. This explains the bound states that appear in the time-averaged density of states of the dot, showed in Fig. (3.14). The other feature observed in the time-averaged density of states arising from the voltage bias is the appearance of Floquet bands of the continuum states as well.

It is interesting to note that although we observe features associated with a drive with frequency $\omega = V$, the frequency of the current ends up being the well known Josephson frequency $\omega_J = 2V$, as can be seen in Fig. 3.14.

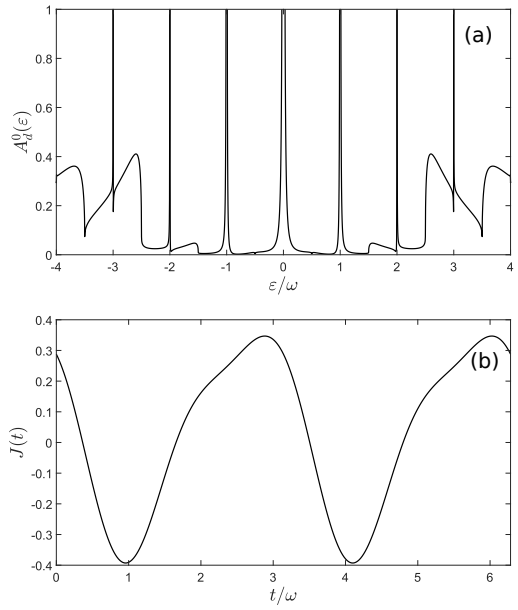

Figure 3.14: Time-averaged density of states of the dot and time-dependent current of a junction with a voltage-bias with parameters $\Gamma = \omega, \Delta = 3\omega, V = \omega = 1$. (a) Time-averaged density of states of the dot showing bound states at energies $n\omega$ and contributions from the continuum also inside the gap. (b) Time-dependent current showing that although in the time-averaged density of states we see Floquet features associated with a frequency ω the total current has frequency 2ω.

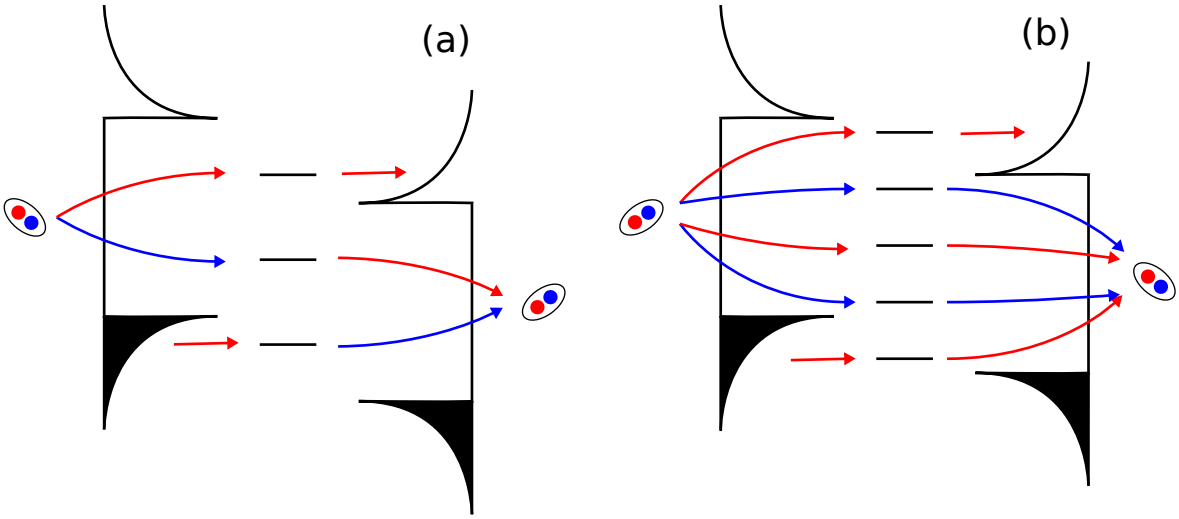

Figure 3.15: Multiple Andreev Reflection processes. Red (blue) lines represent tunneling of spin up (down) electrons. Electrons from a Cooper pair can only tunnel into two different and neighboring Floquet bands of the level. (a) Process with 2 reflections where one Cooper pair is transported from left to right lead with the help of the transport of one continuum electron. (b) Process with 4 reflections where two Cooper pairs are transported from left to right lead with the help of the transport of one continuum electron. Note that since the electrons in a Cooper pair have opposite energy in the reference frame of the superconductor, two of the electrons involved in the process must tunnel far from resonance.

With the Floquet formalism a MAR process can be understood as Cooper pairs tunneling through the different Floquet bands of the dot with the help of electrons from the continuum. A schematic of the MAR processes with 2 and 4 reflections is shown in Fig. 3.15. Lets take the case with 2 reflections. The Floquet state $|\sigma, 0\rangle\!\rangle$ of the dot is inside the gap of both superconductors, and the state $|\sigma, -1\rangle\!\rangle$ ($|\sigma, 1\rangle\!\rangle$) is inside the gap of the left (right) superconductor and the continuum of the right (left) superconductor. A Cooper pair can tunnel from the left lead to the states $|\sigma, 0\rangle\!\rangle$ and $|\sigma, 1\rangle\!\rangle$ while a electron from the continuum of the left lead tunnels to the state $|\sigma, -1\rangle\!\rangle$. Then, the electron that came from the continuum and the one in $|\sigma, 0\rangle\!\rangle$ tunnel into the right lead as a Cooper pair and the electron on $|\sigma, 1\rangle\!\rangle$ tunnels to the continuum of the right lead.

Therefore, the MAR process with n reflections is understood as the tunneling of $n/2$ Cooper pairs and one electron from the continuum, needed for energy conservation since the energy of the Cooper pairs is lowered when tunneling. Note that the MAR process with n reflections is only allowed when there are $n-1$ Floquet bands inside the gap of both superconductors.

3.5 Voltage-biased and phase-biased junction with a driven dot.

From what we learned last section, a natural extension of the problem of a S-QD-S junction with a voltage bias would be to consider what happens if we get rid of energy

conservation, allowing also tunneling of electrons between different Floquet bands in the dot by applying a harmonic drive. Systems with a similar behavior have been studied before, like a junction under microwave radiation [17], or a junction with a vibrating molecule [26].

The first difference we encounter arising from the dot drive is that by shifting the time in the Hamiltonian we see that the tunneling parameter has a phase $\phi_{sc} - 2\phi_d$ which cannot be neglected.

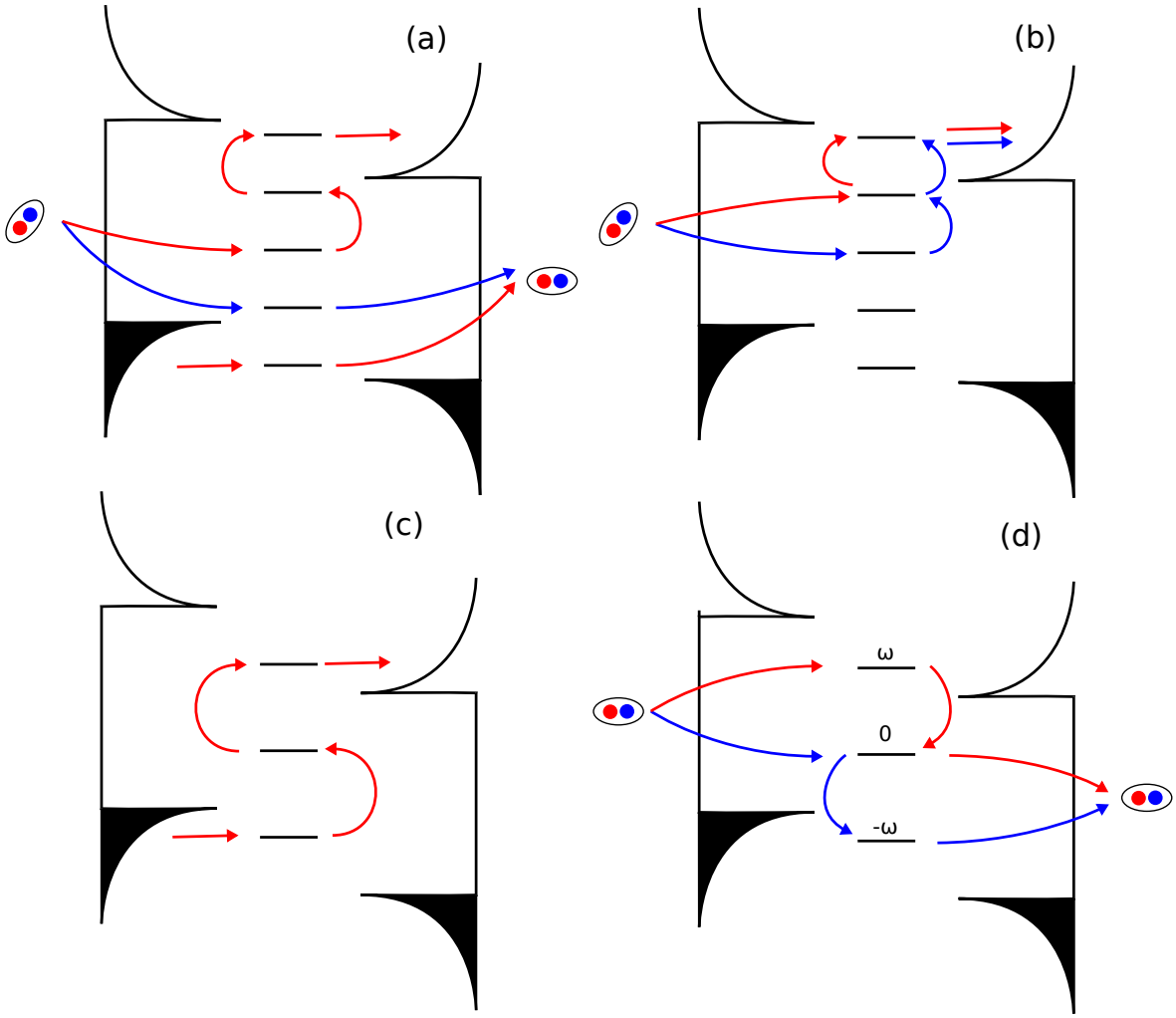

Figure 3.16: Example of two transport processes involving transport of Cooper pairs due to the voltage-bias and tunneling between Floquet bands due to the harmonic drive of the dot. Red (blue) lines represent electrons with spin up (down)(a) The 2 reflection MAR process is now allowed at any voltage due to the tunneling between Floquet bands of the dot. (b) New processes arise due to the drive where Cooper pairs can tunnel to the continuum. Note that the case where spin up and down are switched, the electron with spin down hopes only one Floquet band, and in the case of an applied ac magnetic field this results in an additional π phase and this process vanishes.

Some examples of the new processes arising from the dot drive are depicted in 3.16 and the time-averaged current for different parameters is shown in Fig. 3.17. By looking at the time-averaged current without a phase bias, $\phi_{sc} - 2\phi_d = 0$, the first thing

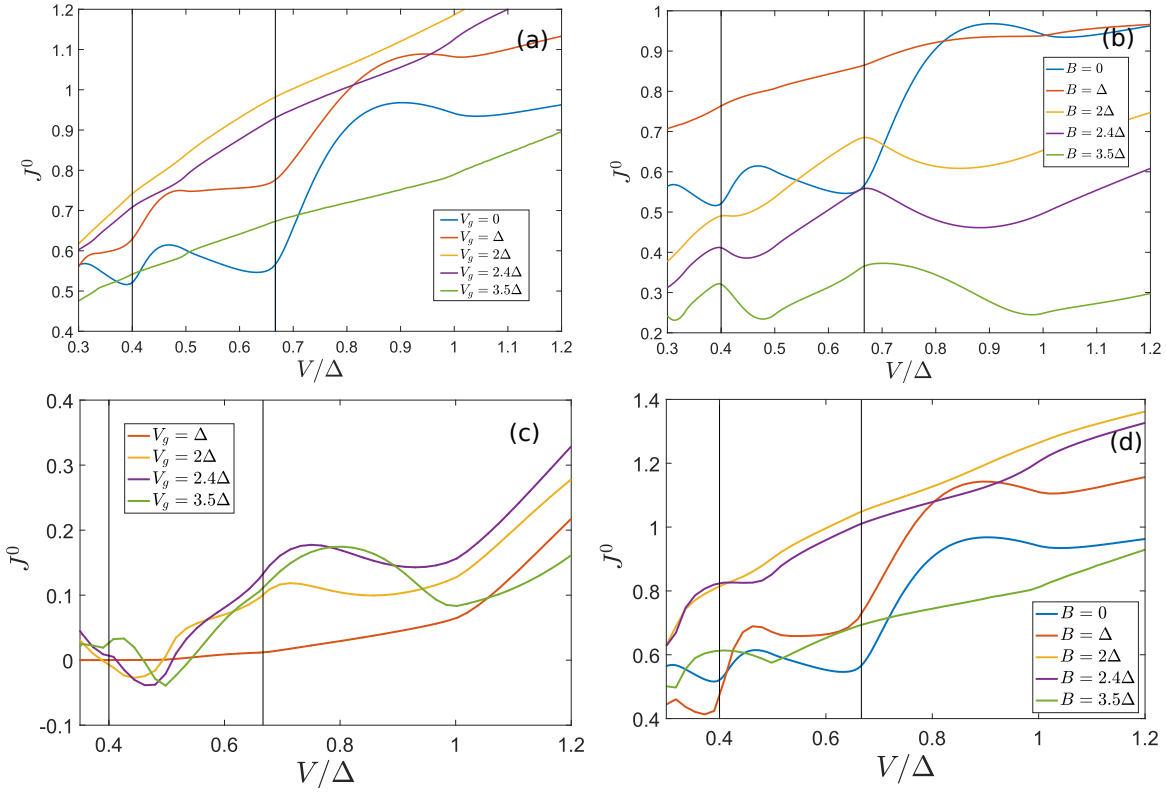

Figure 3.17: Voltage dependence of the time-averaged current for a junction with parameters $\phi_{sc} = 0, \Gamma = \Delta$ with a dot being driven with $\omega = V, \phi_d = 0$ for different drive amplitudes. Vertical lines have been added at $V_n = 2\Delta/n$, where the MAR conductance peaks appear without the drive. (a) Junction being driven with an ac gate voltage, $B = 0$. The conductance peaks arising from MAR are lost as we increase the drive amplitude. The current increases with the drive amplitude for small amplitude and starts decreasing at some point around $V_g = 2\Delta$, when electrons start tunneling also to the continuum of the left lead. (b) Junction being driven with an ac magnetic field, $V_g = 0$. Due to destructive interference the current starts decreasing more rapidly with the drive amplitude, at around $B = \Delta$. Peaks in the current appear at high drive amplitudes at voltages V_n, when the Floquet bands reach the peak in the DOS of the superconductors.

we notice for low amplitude of the drive is that the current increases and the MAR characteristics in the current disappear. This happens because the MAR process with n reflections that was only possible at voltages $2\Delta/(n+1) < V < 2\Delta/(n-1)$ without a dot drive now happens at any voltage. An example of this is shown in Fig. 3.16(a) .

The second feature we observe without a phase-bias is that when the amplitude of the drive is higher than the gap, Δ, and the coupling constant, Γ, peaks in the current appear at the voltages where we had the MAR conductance peaks, $V_n = 2\Delta/n$. This peaks appear very clear with an applied ac magnetic field. For the ac gate voltage, although one can discern this peaks, they are very broaden.

As we discussed last section, at the voltages V_n the Floquet bands are in resonance with the DOS peak of the superconductor, and this peaks in the current can be interpreted as resonant transport where electrons tunnel from continuum to continuum by tunneling between the Floquet bands of the dot, or tunneling of a Cooper pair to the

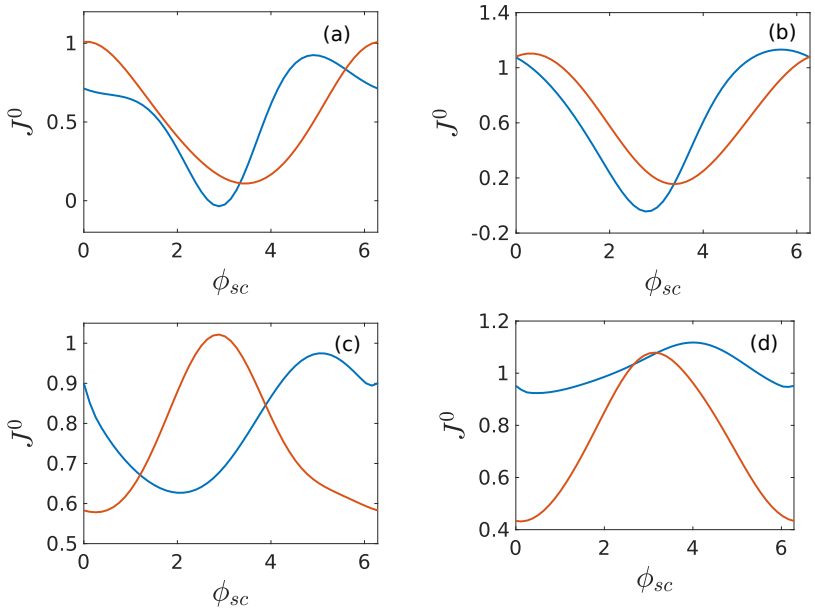

Figure 3.18: Phase-dependence of the time-averaged current for a junction with a voltage-bias with parameters $V, \Gamma = \Delta$ with a dot being harmonically drive with frequency $\omega = V$ and amplitude $A = \Delta$ for the blue curve and $A = 2.4\Delta$ for the red curve. There is a non-trivial phase dependence. (a) Junction harmonically driven with a gate-voltage, $B = 0$, with a voltage-bias of $V = 2\Delta/3$. (b) Junction harmonically driven with an ac gate-voltage, $B = 0$, with a voltage-bias of $V = 0.8\Delta$. (c) Junction harmonically driven with a ac magnetic field, $V_g = 0$, with a voltage-bias of $V = 2\Delta/3$. (d) Junction harmonically driven with an ac magnetic field, $V_g = 0$, with a voltage-bias of $V = 0.8\Delta$.

continuum, as shown in Fig. 3.16(b,c). The reason this peaks appear very broaden in the case of the ac gate voltage is not understood.

The phase dependence of the transport is very complex and not understood. The phase dependence of the time-averaged current for different parameters is shown in Fig. 3.18 and the time-averaged current for $\phi_{sc} - 2\phi_d = \pi$ is shown in Fig. 3.17(c,d). The overall behavior is that there is a destructive interference in the case of an ac gate voltage and a constructive interference with the ac magnetic field. Quite interestingly the result for the ac magnetic field resembles the result for the ac gate voltage with $\phi_{sc} - 2\phi_d = 0$. For the ac gate voltage the result seems more complex. The features at V_n are completely lost, and there is a suppression of the sub-gap current for low amplitude of the drive.

Another type of tunneling process arising from the dot is the one depicted in Fig.3.16(d), where a Cooper pair tunnels from one lead to the other without involving continuum electrons. This process resembles the transport happening at the junction in equilibrium with a phase bias, and we are going to see now that it is somewhat equivalent, which is going to land some interesting results.

Since this process is the only one happening where continuum electrons are not involved we can study it better in the infinite gap limit, $\Delta \to \infty$, where the dynamics of the system are given again by the Floquet effective dot Hamiltonian, given by the

elements

$$H^F_{d,\text{eff},nm} = \sum_{\eta\eta'} \phi^\dagger_\eta \Big[(V_g m^3 + B m^z)(e^{-i\phi_d}\delta_{n-m,1} + e^{e^{i\phi_d}}\delta_{n-m,-1}) \\ -\Gamma(e^{i\phi_{sc}}\delta_{n-m,1} + e^{-i\phi_{sc}}\delta_{n-m,-1}) m^1 \Big]_{\eta\eta'} \phi_{\eta'} + n\omega\delta_{nm}. \tag{3.108}$$

We can, again, apply the Bogoliubov transformation, and we obtain

$$H^F_{d,\text{eff},nm} = \sum_{\eta\eta'} \gamma^\dagger_\eta \Big[(V_g m^1 + B m^z)(e^{-i\phi_d}\delta_{n-m,1} + e^{e^{i\phi_d}}\delta_{n-m,-1}) \\ +\Gamma(e^{i\phi_{sc}}\delta_{n-m,1} + e^{-i\phi_{sc}}\delta_{n-m,-1}) m^3 \Big]_{\eta\eta'} \gamma_{\eta'} + n\omega\delta_{nm}. \tag{3.109}$$

Lets look first at what happens with an ac magnetic field, $V_g = 0$. The phase dependence of the density of states in this case with $\phi_d = 0$ is shown in Fig. 3.19. The DOS does not depend on the phase bias and therefore the current will vanish. By looking at the Floquet effective Hamiltonian in the ABS basis (3.109) we see that for $V_g = 0$ the Hamiltonian is diagonal in Nambu basis. As a result each ABS will be driven independently from the other one and we already know that the energies of the resulting FABS will be $\varepsilon_{\pm\sigma} = 0$ and independent of any parameter.

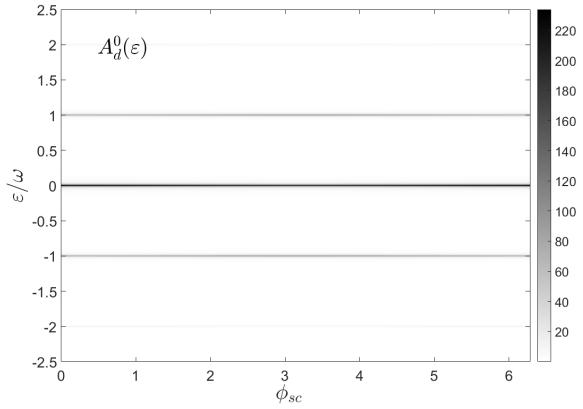

Figure 3.19: Phase dependence of the time-averaged density of states for a S-QD-S junction with a voltage bias $V = \Gamma$ and driven with an ac magnetic field with $B = \Gamma, \omega = \Gamma$. The two ABS do not interact with each other and as a result the energies of the FABS are phase-independent, which makes the current vanish.

There is another way we can understand why the current vanish. There are in fact two different processes competing, as shown in Fig. 3.20. The electrons from the Cooper pair have to tunnel to neighboring Floquet bands. After that, there are two possibilities. Either the electron in the higher band tunnels two times to be in the lower Floquet band or both electrons tunnel one Floquet band. For the case of the ac magnetic field the tunneling of a spin down electron between two Floquet bands has a π phase. As a result this two processes have an overall ϕ phase difference and therefore they cancel.

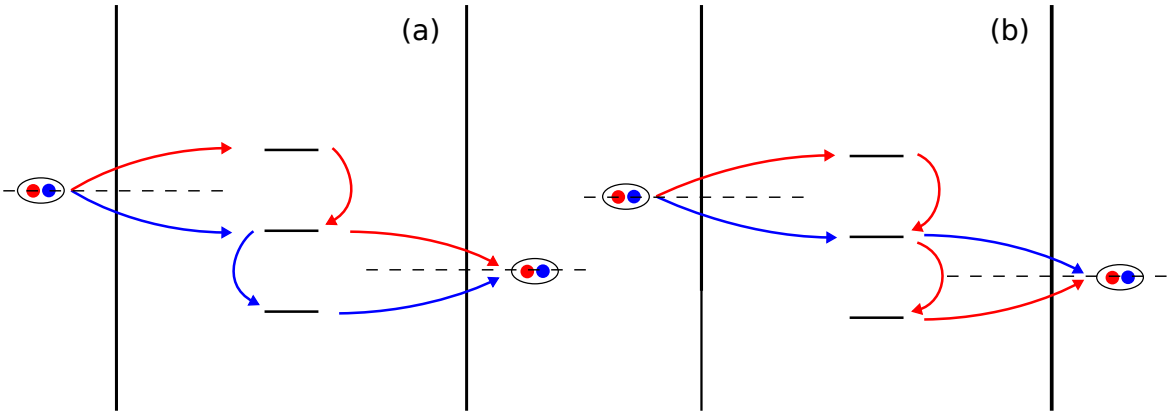

Figure 3.20: Transport processes happening in a S-QD-S junction with a voltage and phase bias and a harmonically driven dot in the infinite gap limit. Red (blue) lines represent electrons with spin up (down), and dotted lines indicate the chemical potential of the leads. The two process cancel in the case of an applied ac magnetic field because there is a π phase difference between them.

Lets look now at the case of an applied ac gate voltage. The Hamiltonian with $\Gamma = 0$ is the Hamiltonian of a level being driven, which we know can be diagonalized in Floquet space with unitary matrices with elements $\Lambda_{nm} = J_{n-m}(V_g m^3/\omega)$

$$\tilde{H}^F_{d,\text{eff},nm} = \sum_{n_1 n_2} \Lambda^\dagger_{nn_1} H^F_{d,\text{eff},n_1 n_2}(\Gamma = 0)\Lambda_{n_2 m} = n\omega\delta_{nm} \tag{3.110}$$

Performing the transformation on the off-diagonal term we obtain

$$\tilde{H}^F_{\Gamma,nm} = \sum_{n_1,n_2} J_{n_1-n}(Vm^3/\omega)\Gamma_{n_1 n_2} m^1 J_{n_1-m}(Vm^3/\omega), \tag{3.111}$$

where $\Gamma_{nm} = \Gamma(e^{i\phi_{sc}}\delta_{n-m,1} + e^{-i\phi_{sc}}\delta_{n-m,-1})$. We can rewrite the Nambu structure as

$$\tilde{H}^F_{nm} = \sum_{n_1,n_2} \begin{pmatrix} 0 & J_{n_1-n}(V/\omega)\Gamma_{n_1 n_2} J_{n_1-m}(-V/\omega) \\ J_{n_1-n}(-V/\omega)\Gamma_{n_1 n_2} J_{n_1-m}(V/\omega) & \end{pmatrix} \otimes \sigma^0. \tag{3.112}$$

Lets look at one of the terms,

$$\begin{aligned} &\sum_{n_1 n_2} J_{n_1-n}(V/\omega)\Gamma_{n_1 n_2} J_{n_1-m}(-V/\omega) \\ &= \Gamma\left(e^{i\phi_{sc}} \sum_{n_1} J_{n-n_1}(V) J_{n_1-m-1}(-V) + e^{-i\phi_{sc}} \sum_{n_1} J_{n-n_1}(V) J_{n_1-m+1}(-V)\right) \\ &= \tilde{\Gamma}^1_{nm} + \tilde{\Gamma}^{-1}_{nm}, \end{aligned} \tag{3.113}$$

where

$$\tilde{\Gamma}^\sigma_{nm} = \Gamma e^{i\sigma\phi_{sc}} \sum_{n_1} J_{n-n_1}(V) J_{n_1-m-\sigma}(-V) \tag{3.114}$$

is the coupling between different Floquet bands of the bound states obtained from harmonically driving the dot.

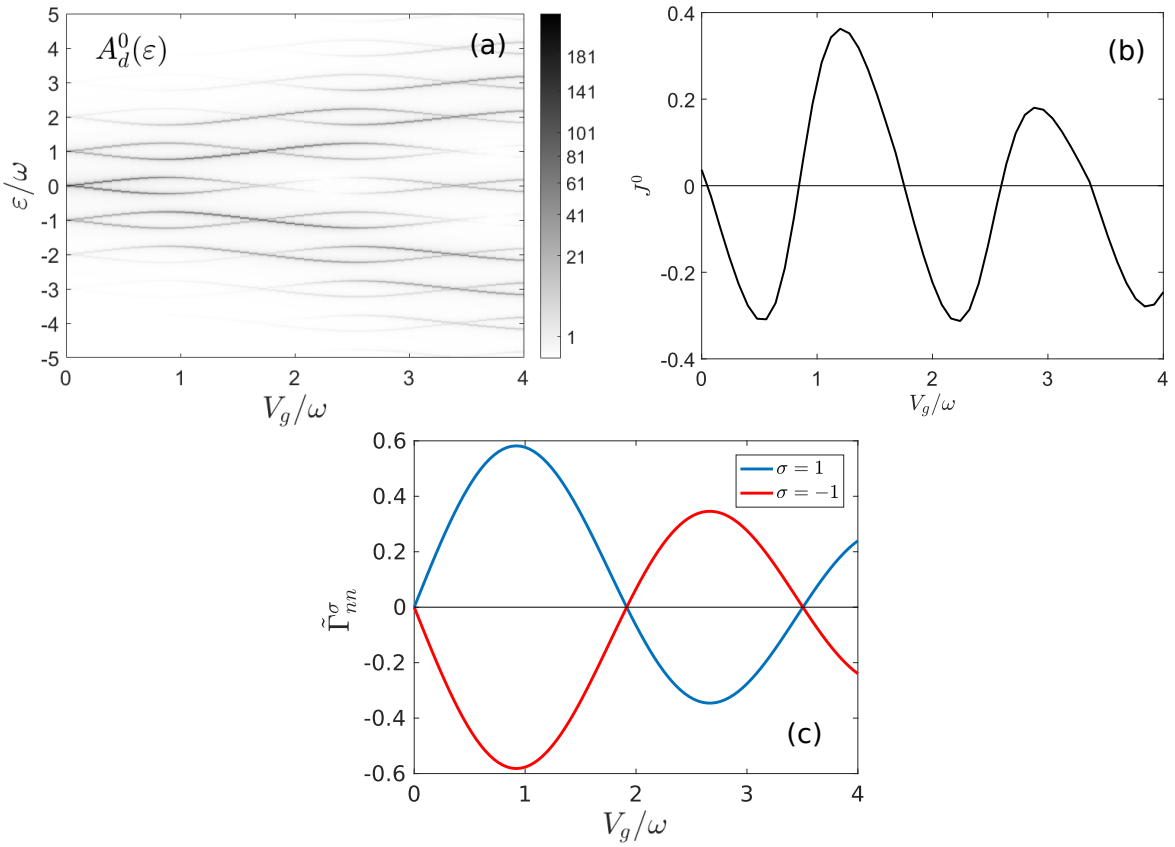

Figure 3.21: S-QD-S junction with a voltage bias $V = \omega$ and phase bias $\phi_{sc} = \pi/2$, with coupling $\Gamma = \omega$ and an ac gate voltage with frequency $\omega = 1$ and amplitude V_g. (a) Time-averaged DOS of the dot. The dot drive splits the bound states in an oscillatory manner. (b) Due to the oscillatory behavior of the bound state energies with the gate voltage the current oscillates around zero as well. (c) Coupling constant of the interaction between the same Floquet band of a bound state obtained for an isolated dot.

The dependence with the amplitude of the gate voltage of the time-averaged density of state and current are shown in Fig. 3.23. For the parameters we are interested in it seems that the most important interaction term is the one between the two states at the same Floquet band, $\tilde{\Gamma}^{\sigma}_{nn}$, which was also plotted there.

The interaction between the same Floquet band of different bound states oscillates around zero with the amplitude of the drive, and as a result the energies of the final FABS also oscillate with the amplitude of the drive, which results in also an oscillatory behavior of the current. The points where the gap between the same Floquet band of the two bound states closes follows the vanishing of the coupling term $\tilde{\Gamma}^{\sigma}_{nn}$, with a small discrepancy due to the interaction with the rest of the bands.

Since $\tilde{\Gamma}^{1}_{nn} = -\tilde{\Gamma}^{-1}_{nn}$, the coupling constant will depend sinusoidally with the phase bias. That dependence together with the fact that the zeroth Floquet band around zero energy is the most significant one results in a behavior which resembles quite a lot the junction at equilibrium with $\phi_{sc} = \pi$. We have obtained a π-junction. The fact that the current is not symmetric is due to the coupling with a metallic lead to artificially broaden the bound states in order to perform the numerical calculations.

If we increase the amplitude we reach a point where the most significant bound

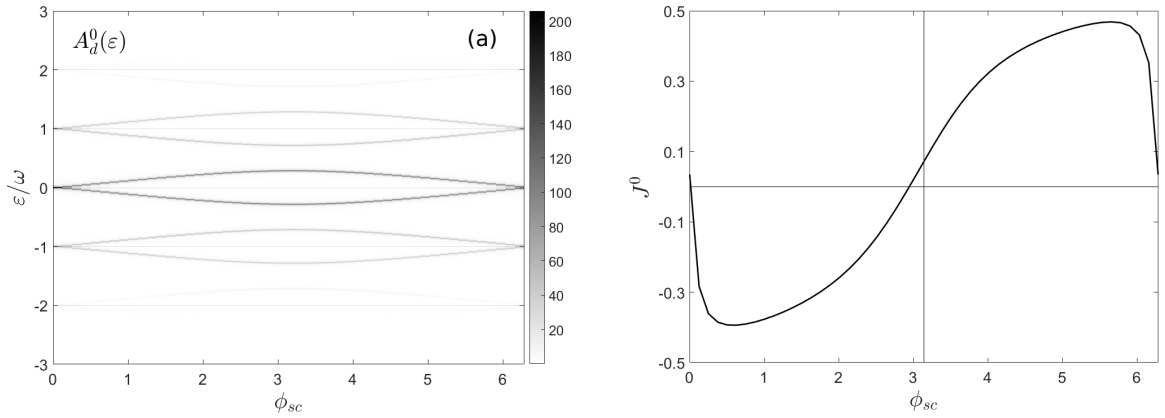

Figure 3.22: Phase dependence of the S-QD-S junction with coupling $\Gamma = \omega$, with voltage bias $V = \omega$ and phase bias ϕ_{sc}, with a dot being driven with an ac gate voltage with amplitude $V_g = \omega$ and frequency $\omega = 1$ and coupled to a metallic lead at $V_m = 0$ with coupling $\Gamma_m = 0.02\Gamma$ to broaden the bound states. (a) Time-averaged DOS of the dot. The bound states split sinusoidally with the phase bias. For low amplitude the zeroth Floquet band is the most significant. (b) Since the zeroth band dominates the transport, the current-phase relation is that of a junction in equilibrium with a π shift, a $\pi-$junction. There is a small asymmetry in the current because of the coupling to the metallic lead.

state is the First Floquet band of the state that gains energy in the avoided crossing. As a result we obtain a normal current-phase relation again. If we keep increasing the amplitude the most significant mode will be the First Floquet band of the state that lowers its energy in the avoided crossing, leading to a π-junction again, and so on.

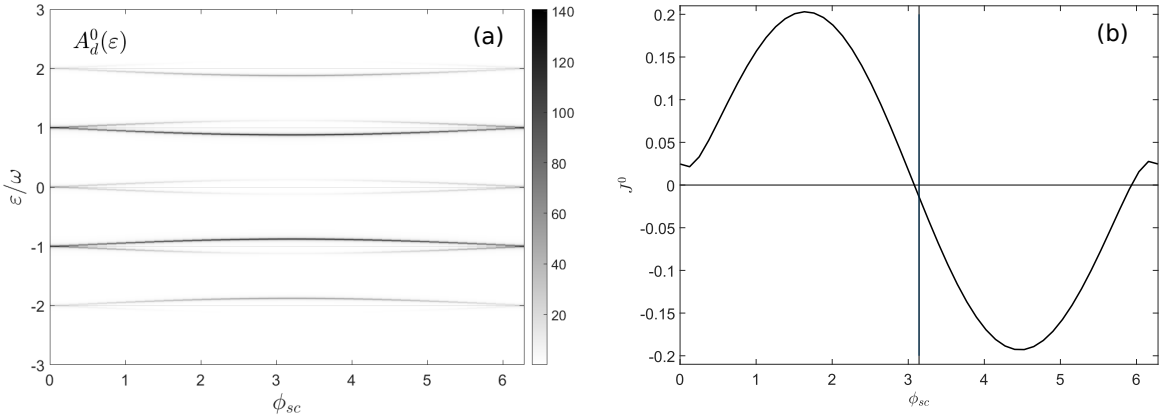

Figure 3.23: Phase dependence of the S-QD-S junction with coupling $\Gamma = \omega$, with voltage bias $V = \omega$ and phase bias ϕ_{sc}, with a dot being driven with an ac gate voltage with amplitude $V_g = 2\omega$ and frequency $\omega = 1$ and coupled to a metallic lead at $V_m = 0$ with coupling $\Gamma_m = 0.02\Gamma$ to broaden the bound states. (a) Time-averaged DOS of the dot. The bound states split sinusoidally with the phase bias. (b) Since the most significant Floquet band gains energy with the interaction we obtain a positive current for $\phi_{sc} \in [0, \pi)$. There is a small asymmetry in the current because of the coupling to the metallic lead.

Another way we can show the equivalence between the behavior observed for a low amplitude of the drive and that of a junction in equilibrium is by obtaining the time-

independent effective Hamiltonian using a high frequency approximation that describes the long-time dynamics of the system, as mentioned at the beginning of the chapter. A short derivation on how to obtain the first order can be found in Appendix C, and a extensive discussion on this can be found in [3–5, 29].

The zeroth order of the effective Hamiltonian is given by the time-average of the Hamiltonian, which for this case, vanishes. The first order in $1/\omega$ is given by

$$H^1_{d,\text{eff}} = \sum_{m>0} \left[H^m, H^{-m}\right], \tag{3.115}$$

where $H^m = \sum_{\eta_1\eta_2} \phi^\dagger_{\eta_1} h^m_{\eta_1\eta_2} \phi_{\eta_2}$ is the m'th Fourier component of the Hamiltonian. We can perform the commutator as

$$\begin{aligned}
[H^m, H^{-m}] &= \sum_{\eta_1\eta_2\eta_3\eta_4} [\phi^\dagger_{\eta_1} h^m_{\eta_1\eta_2}\phi_{\eta_2}, \phi^\dagger_{\eta_3} h^{-m}_{\eta_3\eta_4}\phi_{\eta_4}] \qquad (3.116)\\
&= \sum_{\eta_1\eta_2\eta_3\eta_4} h^m_{\eta_1\eta_2} h^{-m}_{\eta_3\eta_4} \left(\phi^\dagger_{\eta_1} \left\{\phi_{\eta_2}, \phi^\dagger_{\eta_3}\phi_{\eta_4}\right\} - \left\{\phi^\dagger_{\eta_1}, \phi^\dagger_{\eta_3}\phi_{\eta_4}\right\}\phi_{\eta_2}\right)\\
&= \sum_{\eta_1\eta_2\eta_3\eta_4} h^m_{\eta_1\eta_2} h^{-m}_{\eta_3\eta_4} \left(\phi^\dagger_{\eta_1}\phi_{\eta_4} m^0_{\eta_2,\eta_3} + \phi^\dagger_{\eta_1}\phi^\dagger_{\eta_3} m^4_{\eta_2\eta_4} - \phi^\dagger_{\eta_3}\phi_{\eta_2} m^0_{\eta_1\eta_4} - \phi_{\eta_4}\phi_{\eta_2} m^4_{\eta_1\eta_3}\right).
\end{aligned}$$

By using that the Nambu matrices h^m, m^0 and m^4 are symmetric, that $\phi^\dagger_\eta = \sum_{\eta_1} \phi_{\eta_1} m^4_{\eta\eta'}$, and that $m^4 m^i m^4 = -m^i$, we can write the commutator in terms of matrix products as

$$\begin{aligned}
[H^m, H^{-m}] =& \phi^\dagger h^m h^{-m}\phi + \phi^\dagger h^m m^4 h^{-m} m^4 \phi - \phi^\dagger h^{-m} m^0 h^m \phi - \phi^\dagger m^4 h^{-m} m^4 h^m \phi\\
=& -\phi^\dagger [h^m, h^{-m}]\phi \qquad (3.117)
\end{aligned}$$

For the case of a voltage-biased junction with a harmonically driven dot we only have $h^{\pm 1}$ and the effective Hamiltonian is given by

$$\begin{aligned}
H^1_{d,\text{eff}} =& -\frac{1}{4\omega}\sum_{\eta\eta'} \phi^\dagger_\eta [V_g e^{-i\phi_d} m^3 + B e^{-i\phi_d} m^z - \Gamma e^{i\phi_{sc}} m^1, V_g e^{i\phi_d} m^3 + B e^{i\phi_d} m^z - \Gamma e^{-i\phi_{sc}} m^1]_{\eta'}\phi_{\eta'}\\
=& \sum_{\eta\eta'} \phi^\dagger_\eta [-\frac{V_g\Gamma}{2\omega}\sin(\phi_{sc}/2 + \phi_d) m^2]_{\eta\eta'}\phi_{\eta'} \qquad (3.118)
\end{aligned}$$

The effective Hamiltonian is that of a junction in equilibrium with a coupling constant given by $\hat{\Gamma} = iV_g\Gamma/\omega\cos((\phi_{sc}+\pi)/2 - \phi_d)$. Even though it is only the first order approximation in $1/\omega$ this Hamiltonian reproduces the three most interesting features of the system. First, it shows that for $\phi_d = 0$ we have a $\pi-$junction. It also shows that we can obtain a $\varphi-$junction by tuning the phase of the drive. And finally, for the case of an ac magnetic field, with $V_g = 0$, the effective coupling constant vanishes, and therefore there is no current through the junction.

3.6 Discussion

In this chapter we have studied the main focus of this thesis, the S-QD-S junction out of equilibrium. First we have defined the Nambu spinors and the Nambu Green's functions and then we have used the non-equilibrium Floquet-Green's functions technique to solved the problem in the most general case.

The junction in equilibrium is characterized by the appearance of two Andreev Bound States below the gap which can carry current for a fixed phase bias and dominate the behavior of the current in the infinite gap limit.

When an ac magnetic field is applied on the dot the ABS are driven as isolated levels and the phase dependence of the energies of the FABS is the same as for the ABS in equilibrium. For $\omega > \Gamma$, when the first Floquet band of the positive FABS crosses zero, only the zeroth Floquet band contributes to the current and is proportional to the Bessel junction $|J_0(B/\omega)|^2$.

An applied ac gate voltage introduces interactions between Floquet bands of the two ABS and results in more complex behavior. For $\omega > \Gamma$, when the first Floquet band of the positive FABS is lower in energy than the zeroth Floquet band of the negative FABS a $0-\pi-$transition is obtained with the application of a constant magnetic field.

For the voltage-biased junction we described the MAR processes characterizing the sub-gap transport. We also found that in the voltage-biased junction electrons from a Cooper pair can only tunnel into the dot to different and neighboring Floquet bands.

Adding a harmonic drive to the voltage-biased junction resulted first in a loss of the MAR features due to the fact that they are not restricted to a voltage range anymore. In the case of an applied ac magnetic field with high amplitude of the drive, $B > 2\Delta$ we found peaks in the current associated to resonant tunneling, but it is not understood why they not appear for an ac gate voltage. We found that the current-voltage relation has a complex phase dependence. In particular for ϕ_π and an ac gate voltage there is suppression of the sub-gap transport.

In the infinite gap limit we found that the junction in the high frequency limit behaves like a junction in equilibrium, with an effective coupling constant that depends on the parameters of the drive, $\hat{\Gamma} = iV_g\Gamma/\omega\cos((\phi_{sc}+\pi)/2-\phi_d)$. The junction for $\phi_d = 0$ is a $\pi-$junction, and can be turned into a $\varphi-$junction by tuning the phase of the drive, ϕ_d. This last result is quite remarkable since all proposals to build $\varphi-$junctions with quantum dots rely to some extent in the magnetic properties of the system or spin-orbit coupling [30].

Chapter 4

Conclusions

In this thesis we have made a detailed and systematic study of the S-QD-S junction with a harmonically driven dot.

For a phase-biased junction we have found that the time-averaged current can be tuned with the parameters of the drive. In particular, for an applied ac magnetic field a current-phase relation can be obtained for the time-averaged current which is equal to the one in equilibrium, with a proportionality factor $|J(B/\omega)|^2$.

We have also found that we can modify the magnetic field dependence of the time-averaged current with the parameters of the drive, and found that is possible to obtain a $0-\pi$ transition for an applied ac gate voltage, and a non-trivial region of vanishing current for an ac magnetic field.

For a voltage-biased driven junction we have found peaks in the time-averaged current-voltage relation for an applied ac magnetic field due to resonant tunneling. In the case of an applied ac gate voltage, destructive interference leads to a suppression of the sub-gap current when a phase-bias is applied.

Finally we have found that in the infinite gap limit the voltage-biased junction with an ac gate voltage and a phase-bias has a non-vanishing current which oscillates around 0 with the amplitude of the drive. In the high frequency limit we have found that the junction behaves like a $\pi-$junction in equilibrium.

Quite remarkable the junction can be turned into a $\varphi-$junction by only tuning the phase of the bias, in contrast to all the existing proposals for $\varphi-$junctions using quantum dots, which involve spin-orbit and magnetic fields.

The work done in this thesis can be extended in different ways. First of all it would be interesting to study more in depth the phase dependence of the voltage-biased driven junction, to understand why the case with an ac gate voltage does not present resonant tunneling and why is the sub-gap current suppressed. More realistic models including more than one orbital on the dot and Coulomb interaction could be studied. It could also be interesting to add a drive on the leads and see if one can find similar behaviors to those of multiterminal Josephson junctions. One could also introduce new interactions in Floquet space by using different and more complex driving protocols that might lead to new physics. And finally, in a recent article a laser was built by placing a voltage-biased Josephson junction inside a cavity [30]. It would be interesting to study the interplay between the photons on the cavity and the drive.

Appendix A

Keldysh analytical continuation

Here we describe how to perform calculations in the Keldysh contour [13] following the derivations in [14]. Consider the expectation value of an operator O , defined as

$$\begin{aligned}\langle O(t)\rangle =&\frac{\mathrm{Tr}\left\{O\rho(t)\right\}}{\mathrm{Tr}\left\{\rho(t)\right\}}\\ =&\frac{1}{\mathrm{Tr}\left\{\rho(t)\right\}}\mathrm{Tr}\left\{(U)(-\infty,t)O\mathcal{U}(t,-\infty)\rho(-\infty)\right\},\end{aligned} \tag{A.1}$$

where we assume that we know the initial density matrix $\rho(-\infty)$. We have a time contour where we start at $t=-\infty$, where we know the density matrix, we evolve forward to t, where we calculate the operator O, and we go backwards to $t=-\infty$. Consider a system in equilibrium and at zero temperature. We use the fact that the states at $t=-\infty$ and $t=\infty$ have to the same up to a constant phase to write the expectation value

$$\langle O(t)\rangle = \langle 0|\,\mathcal{U}(\infty,t)O\mathcal{U}(t,-\infty)\,|0\rangle\,/e^{i\phi}, \tag{A.2}$$

and the curved contour reduces to the real axis with the downside that now we have to calculate the denominator, which accounts for the disconnected diagrams. In the non-equilibrium case we also consider the state at $t=-\infty$, and neglecting transient states in doing so, but we cannot make this transformation anymore since the states at $t=-\infty$ and $t=\infty$ no longer have to be related. The curved contour therefore can not be avoided, but it is still useful to extend the contour to $t=\infty$

$$\langle O(t)\rangle = \frac{1}{\mathrm{Tr}\left\{\rho(-\infty)\right\}}\mathrm{Tr}\left\{\mathcal{U}(-\infty,\infty)\mathcal{U}(\infty,t)O\mathcal{U}(t,-\infty)\rho(-\infty)\right\}, \tag{A.3}$$

The Keldysh contour therefore is composed of two branches, one goes forward in time from $t=-\infty$ to $t=\infty$, and the second one goes backwards again to $t=-\infty$. The contour-ordered Green's function is defined in this contour as

$$G^c_{\alpha,\beta}(t,t') = -i\left\langle \mathcal{T}_C\left[c_\alpha(t)c^\dagger_\beta(t')\right]\right\rangle \tag{A.4}$$

where the contour-ordering operator orders the operators according to a time contour. The contour-ordering operator reduces to the time-ordering operator when the contour considered is the real axis. The contour-ordered Green's function contains the four

types of Green's function considered at equilibrium depending on its times variables.

$$G^c_{\alpha,\beta}(t,t') = \begin{cases} G^t_{\alpha,\beta}(t,t') & \{t,t'\} \in C_\pm \\ G^<_{\alpha,\beta}(t,t') & t \in C_+\,,\; t' \in C_- \\ G^>_{\alpha,\beta}(t,t') & t \in C_-\,,\; t' \in C_+ \end{cases} \tag{A.5}$$

Consider a time-convolution on the Keldysh contour C of the form

$$C(t,t') = \int_C dt_1 A(t,t_1)B(t,t_1). \tag{A.6}$$

Consider the lesser part of $C(t,t')$, so that t is on the first branch of the Keldysh contour and t' on the second one. Deforming the contour by adding two more branches on the real axis as shown in (add figure) allows us to split the lesser function into two integrals in the two branches C_1 and C_1 as

$$C^<(t,t') = \int_{C_1} dt_1 A(t,t_1)B^<(t_1,t') + \int_{C_2} dt_1 A^<(t,t_1)B(t_1,t'). \tag{A.7}$$

The first integral can be obtained as

$$\begin{aligned} \int_{C_1} dt_1 A(t,t_1)B^<(t_1,t') &= \int_{-\infty}^{t} dt_1 A^>(t,t_1)B^<(t_1,t') + \int_{t}^{-\infty} dt_1 A^<(t,t_1)B^<(t_1,t') \\ &= \int_{-\infty}^{\infty} A^r(t,t_1)B^<(t_1,t'), \end{aligned} \tag{A.8}$$

where we used the definition of the retarded function as $G^r(t,t') = \theta(t-t')(G^>(t,t') - G^<(t,t'))$. The second term of the lesser function $C^<$ can be obtain in a similar manner as

$$\begin{aligned} \int_{C_2} dt_1\, A^<(t,t_1)B(t_1,t') &= \int_{-\infty}^{t'} dt_1\, A^<(t,t_1)B^<(t_1,t') + \int_{t'}^{-\infty} dt_1\, A^<(t,t_1)B^>(t_1,t') \\ &= \int_{-\infty}^{\infty} dt_1\, A^<(t,t_1)B^a(t_1,t'), \end{aligned} \tag{A.9}$$

where $G^a(t,t') = \theta(t'-t)(G^<(t,t') - G^>(t,t'))$ is the advanced function. Finally, we obtain an expression for the lesser function $C^<(t,t')$ known as the Langreth rule

$$C^<(t,t') = \int_{-\infty}^{\infty} dt_1\, \left[A^r(t,t_1)B^<(t_1,t') + A^<(t,t_1)B^a(t_1,t')\right], \tag{A.10}$$

which can be generalized easily to any number of time-convolutions by applying it recursively. As it is needed in the thesis, the lesser function of a two-time convolution is

$$\begin{aligned} D^<(t,t') = \int_{-\infty}^{\infty} dt_1 \int_{-\infty}^{\infty} dt_2\, [&A^r(t,t_1)B^r(t_1,t_2)C^<(t_2,t') + \\ &+A^r(t,t_1)B^<(t_1,t_2)C^a(t_2,t') + A^<(t,t_1)B^a(t_1,t_2)C^a(t_2,t')]\,. \end{aligned} \tag{A.11}$$

The same relations can be derived for the greater function $G^{>}(t,t')$ by changing $<$ to $>$ in the Langreth expression and with those results the retarded function $C^r(t,t')$ can be obtained as

$$\begin{aligned} C^r(t,t') =& \theta(t-t') \int_{-\infty}^{\infty} dt_1 \, [A^r(t,t_1)(B^{>}(t_1,t') - B^{<}(t_1,t')) \\ & + (A^{>}(t,t_1) - A^{<}(t,t_1))B^a(t_1,t')] \\ =& \theta(t-t') \int_{-\infty}^{t} dt_1 \, [(A^{>}(t,t_1) - A^{<}(t,t_1))(B^{>}(t_1,t') - B^{<}(t_1,t')) \\ & - (A^{>}(t,t_1) - A^{<}(t,t_1))(B^{<}(t_1,t') - B^{>}(t_1,t'))] \\ =& \int_{-\infty}^{\infty} dt_1 \, A^r(t,t_1)B^t(t_1,t'). \end{aligned} \tag{A.12}$$

A similar result is obtained for the advanced function,

$$C^a(t,t') = \int_{-\infty}^{\infty} dt_1 \, A^a(t,t_1)B^a(t_1,t'). \tag{A.13}$$

Appendix B

Proof of the Floquet theorem

Since the Hamiltonian is periodic in time with period T, it commutes with the time-evolution operator over one period $U(t+T,t)$. The eigenstates of the Hamiltonian are therefore also eigenstates of the time-evolution operator over one period. Since it is a unitary operator, its eigenvalues are of the form,

$$U(t+T,t)\left|\psi(t)\right\rangle = e^{iu(t,T)}\left|\psi(t)\right\rangle. \tag{B.1}$$

The eigensystem equation at a different time can be written as

$$U(t'+T,t')U(t',t)\left|\psi(t)\right\rangle = e^{iu(t',T)}U(t',t)\left|\psi(t)\right\rangle. \tag{B.2}$$

And we obtain that the factor $u(t,T)$ is in fact time-independent,

$$\begin{aligned} e^{iu(t,T)} =& \left\langle\psi(t)\right| U(t+T,t)\left|\psi(t)\right\rangle \\ =& \left\langle\psi(t)\right| U(t,t')U(t'+T,t')U(t',t)\left|\psi(t)\right\rangle \\ =& e^{iu(t',T)}. \end{aligned} \tag{B.3}$$

The time-evolution operator itself is periodic for time-translations in both variables,

$$\begin{aligned} U(t'+T,t+T) =& \mathcal{T}e^{-i\int_{t+T}^{t'+T}dt_1\,H(t_1)} \\ =& \mathcal{T}e^{-i\int_{t}^{t'}dt_1\,H(t_1-T)} \\ =& U(t',t). \end{aligned} \tag{B.4}$$

Now by exploiting the linearity of the time-evolution operator and its periodicity, $U(t'+T,t'+T)=U(t',t)$,

$$\begin{aligned} e^{iu(n_1T+n_2T)} &= \left\langle\psi(t)\right| U(t+n_1T+n_2T,t)\left|\psi(t)\right\rangle \\ &= \left\langle\psi(t)\right| U(t+n_1T+n_2T,t+n_1T)U(t+n_1T,t)\left|\psi(t)\right\rangle \\ &= \left\langle\psi(t)\right| U(t+n_2T,t)U(t+n_1T,t)\left|\psi(t)\right\rangle \\ &= e^{iu(n_1T)}e^{iu(n_2T)}, \end{aligned} \tag{B.5}$$

we find that $u(T)=\varepsilon_\psi T$, where we call ε_ψ the quasienergy of state $\left|\psi(t)\right\rangle$.

As a result, going back to the eigenvalue equation for the time-evolution operator over one period, we have

$$U(t+T,t)\left|\psi(t)\right\rangle = e^{i\varepsilon_\psi T}\left|\psi(t)\right\rangle \tag{B.6}$$

and the eigenstates of the Hamiltonian can be expressed as

$$\begin{aligned} |\psi(t)\rangle &= e^{-i\varepsilon_\psi t} e^{-i\varepsilon_\psi (T-t)} U(t+T,t) \, |\psi(t)\rangle \\ &= e^{-i\varepsilon_\psi t} \, |u_\psi(t)\rangle \, , \end{aligned} \tag{B.7}$$

where the state $|u_\psi(t)\rangle$ is periodic,

$$\begin{aligned} |u_\psi(t+nT)\rangle &= e^{-i\varepsilon_\psi (T-t-nT)} U(t+nT+T, t+nT) \, |\psi(t+nT)\rangle \\ &= e^{-i\varepsilon_\psi (T(1-n)-t)} U(t+T,t) e^{i\varepsilon_\psi nT} \, |\psi(t)\rangle \\ &= |u_\psi(t+nT)\rangle \, . \end{aligned} \tag{B.8}$$

Appendix C

High frequency approximation

The Floquet Hamiltonian acting on the extended space $\mathcal{H}_E = \mathcal{H} \otimes \mathcal{T}_\omega$ is given by

$$\hat{H}^F = \sum_{nm} H^{n-m} |n\rangle \langle m| - \hat{n}\omega. \tag{C.1}$$

The Floquet Hamiltonian can be diagonalized in Floquet space as

$$\hat{H}_D^F = e^{i\hat{G}} \hat{H}^F e^{-i\hat{G}}, \tag{C.2}$$

The diagonal Floquet Hamiltonian can be expressed as

$$\hat{H}_D^F = H_{FD}\hat{1} - \hat{n}\omega, \tag{C.3}$$

where The Floquet diagonal Hamiltonian, H_{FD}, is a time-independent Hamiltonian acting on $\mathcal{H}$.

The time-evolution operator in $\mathcal{H}$ can be expressed as

$$U(t, t') = U(t')e^{-iH_{FD}(t-t')}U^\dagger(t), \tag{C.4}$$

meaning that the long-time dynamics are given by the Floquet Diagonal Hamiltonian.

In general obtaining the Floquet diagonal Hamiltonian analytically is not possible and one can only aspire to obtain it perturbatively in $1/\omega$, i.e. by doing a high frequency approximation, where we expand the operators as $H = \sum_i H^i$, where H^i is of order $1/\omega^i$.

We can expand the Floquet diagonal Hamiltonian as

$$\hat{H}_D^F = \hat{H}^F + i[\hat{G}, \hat{H}^F] - \frac{1}{2}[\hat{G}, [\hat{G}, \hat{H}^F]] + ..., \tag{C.5}$$

and by expanding the operators we obtain

$$\begin{aligned} H_{FD}\hat{1} = &\sum_{nm} H^{n-m} |n\rangle \langle m| + i[\hat{G}^1, \hat{n}\omega] \\ &+ i[\hat{G}^1, \sum_{nm} H^{n-m} |n\rangle \langle m|] + i[\hat{G}^2, \hat{n}\omega] - \frac{1}{2}[\hat{G}^1, [\hat{G}^1, \hat{n\omega}]] \\ &+ \mathcal{O}(1/\omega^2), \end{aligned} \tag{C.6}$$

where the first line is the zeroth order and the second line is the first order in $1/\omega$. The zeroth order of the Floquet Diagonal Hamiltonian is then given by

$$H^0_{FD} = H^0. \tag{C.7}$$

And with this result we can calculate the commutator as

$$i[\hat{G}^1, \hat{n}\omega] = i\sum_{nm} G^{n-m,1}[|n\rangle\langle m|, \hat{n}] = -i\omega\sum_{nm} G^{n-m,i}(n-m)|n\rangle\langle m|. \tag{C.8}$$

and obtain $\hat{G}^i$ as

$$-i\omega\sum_{nm} G^{n-m,i}(n-m)|n\rangle\langle m| = -\sum_{n\neq m} H^{n-m}|n\rangle\langle m|, \tag{C.9}$$

and we identify

$$\hat{G}^1 = \sum_{n\neq m}\frac{1}{i(n-m)\omega}H^{n-m}|n\rangle\langle m|. \tag{C.10}$$

The first order of the Floquet Diagonal Hamiltonian is then

$$\begin{aligned}
H^1_{FD} &= \langle 0| i[\hat{G}^1, \sum_{nm} H^{n-m}|n\rangle\langle m|]|0\rangle \\
&= \langle 0| i\sum_{n\neq m,n'm'}\frac{1}{i(n-m)\omega}H^{n-m}H^{n'-m'}[|n\rangle\langle m|, |n'\rangle\langle m'|]|0\rangle \\
&= \langle 0| i\sum_{n\neq m,n'm'}\frac{1}{i(n-m)\omega}H^{n-m}H^{n'-m'}(|n\rangle\langle m'|\delta_{n'm} - |n'\rangle\langle m|\delta_{nm'})|0\rangle \\
&= i\sum_{n\neq m,n'm'}\frac{1}{i(n-m)\omega}H^{n-m}H^{n'-m'}(\delta_{n,0}\delta_{m'0}\delta_{n'm} - \delta_{n'0}\delta_{m0}\delta_{nm'}) \\
&= -\sum_{m\neq 0}\frac{1}{m\omega}H^{-m}H^m + \sum_{m\neq 0}\frac{1}{m\omega}H^mH^{-m} \\
&= \sum_{m>0}\frac{1}{m\omega}\left[H^m, H^{-m}\right]
\end{aligned} \tag{C.11}$$

Bibliography

[1] Jon H. Shirley. Solution of the Schrödinger equation with a hamiltonian periodic in time. *Physical Review*, 138(4B), 1965.

[2] Hideo Sambe. Steady states and quasienergies of a quantum-mechanical system in an oscillating field. *Physical Review A*, 7(6):2203–2213, 1973.

[3] André Eckardt and Egidijus Anisimovas. High-frequency approximation for periodically driven quantum systems from a Floquet-space perspective, 2015.

[4] Viktor Novičenko, Egidijus Anisimovas, and Gediminas Juzeliunas. Floquet analysis of a quantum system with modulated periodic driving. *Physical Review A*, 95(2), 2017.

[5] Takahiro Mikami, Sota Kitamura, Kenji Yasuda, Naoto Tsuji, Takashi Oka, and Hideo Aoki. Brillouin-Wigner theory for high-frequency expansion in periodically driven systems: Application to Floquet topological insulators. *Physical Review B*, 2016.

[6] Philipp Hauke, Olivier Tieleman, Alessio Celi, Christoph Ölschläger, Juliette Simonet, Julian Struck, Malte Weinberg, Patrick Windpassinger, Klaus Sengstock, Maciej Lewenstein, and André Eckardt. Non-Abelian Gauge Fields and Topological Insulators in Shaken Optical Lattices, 2012.

[7] J. Struck, M. Weinberg, C. Ölschläger, P. Windpassinger, J. Simonet, K. Sengstock, R. Höppner, P. Hauke, A. Eckardt, M. Lewenstein, and L. Mathey. Engineering Ising-XY spin-models in a triangular lattice using tunable artificial gauge fields. *Nature Physics*, 9(11):738–743, 2013.

[8] Jan Carl Budich, Ying Hu, and Peter Zoller. Helical Floquet Channels in 1D Lattices. *Physical Review Letters*, 118(10), 2017.

[9] M. Benito, A. Gómez-León, V. M. Bastidas, T. Brandes, and G. Platero. Floquet engineering of long-range p -wave superconductivity. *Physical Review B - Condensed Matter and Materials Physics*, 90(20), 2014.

[10] Xinyu Luo, Lingna Wu, Jiyao Chen, Qing Guan, Kuiyi Gao, Zhi-Fang Xu, L You, and Ruquan Wang. Tunable atomic spin-orbit coupling synthesized with a modulating gradient magnetic field. *Scientific reports*, 6(October 2015):18983, 2016.

[11] G. Wendin and V. S. Shumeiko. Quantum bits with Josephson junctions. In *Fizika Nizkikh Temperatur (Kharkov)*, 2007.

[12] Albert Verdeny, Andreas Mielke, and Florian Mintert. Accurate effective hamiltonians via unitary flow in floquet space. *Physical Review Letters*, 111(17), 2013.

[13] L. V. Keldysh. Diagram technique for nonequilibrium processes. *Jetp*, 20(5):1080, 1964.

[14] AP Jauho. Introduction to the Keldysh nonequilibrium Green function technique. *Lecture notes*, (5):17, 2006.

[15] B. H. Wu and J. C. Cao. Noise of Kondo dot with ac gate: Floquet-Green's function and noncrossing approximation approach. *Physical Review B - Condensed Matter and Materials Physics*, 81(8), 2010.

[16] B. H. Wu, J. C. Cao, and C. Timm. Polaron effects on the dc- and ac-tunneling characteristics of molecular Josephson junctions. *Physical Review B - Condensed Matter and Materials Physics*, 86(3), 2012.

[17] J C Cuevas, A Martin-Rodero, and A Levy Yeyati. Hamiltonian approach to the transport properties of superconducting quantum point contacts. *Phys. Rev. B*, 54:7366, 1996.

[18] T. Jonckheere, A. Zazunov, K. V. Bayandin, V. Shumeiko, and T. Martin. Nonequilibrium supercurrent through a quantum dot: Current harmonics and proximity effect due to a normal-metal lead. *Physical Review B - Condensed Matter and Materials Physics*, 80(18), 2009.

[19] Naoto Tsuji, Takashi Oka, and Hideo Aoki. Correlated electron systems periodically driven out of equilibrium: Floquet+DMFT formalism. *Physical Review B - Condensed Matter and Materials Physics*, 78(23), 2008.

[20] K J Pototzky and E K U Gross. How to interpret the spectral density of the Keldysh nonequilibrium Green's function. *arXiv*, cond-mat.m, 2014.

[21] A. Martín-Rodero and A. Levy Yeyati. Josephson and Andreev transport through quantum dots. *Advances in Physics*, 60(6):899–958, 2011.

[22] W. Chang, V. E. Manucharyan, T. S. Jespersen, J. Nygård, and C. M. Marcus. Tunneling spectroscopy of quasiparticle bound states in a spinful josephson junction. *Physical Review Letters*, 110(21), 2013.

[23] Y Zhu, W Li, T H Lin, and Q F Sun. Microwave-induced pi-junction transition in a superconductor/quantum dot/superconductor structure. *Physical Review B*, 2002.

[24] F. S. Bergeret, P. Virtanen, A. Ozaeta, T. T. Heikkilä, and J. C. Cuevas. Supercurrent and Andreev bound state dynamics in superconducting quantum point contacts under microwave irradiation. *Physical Review B*, 2011.

[25] J. F. Rentrop, S. G. Jakobs, and V. Meden. Nonequilibrium transport through a Josephson quantum dot. *Physical Review B - Condensed Matter and Materials Physics*, 89(23), 2014.

[26] A. Zazunov, R. Egger, C. Mora, and T. Martin. Superconducting transport through a vibrating molecule. *Physical Review B - Condensed Matter and Materials Physics*, 73(21), 2006.

[27] U. Zimmermann and K. Keck. Multiple Andreev-reflection in superconducting weak-links in the interaction with external microwave-fields. *Zeitschrift fer Physik B Condensed Matter*, 1996.

[28] Stephanie Droste, Sabine Andergassen, and Janine Splettstoesser. Josephson current through interacting double quantum dots with spinorbit coupling. *Journal of Physics: Condensed Matter*, 24(41):415301, 2012.

[29] N. Goldman and J. Dalibard. Periodically driven quantum systems: Effective Hamiltonians and engineered gauge fields, 2014.

[30] M. C. Cassidy, A. Bruno, S. Rubbert, M. Irfan, J. Kammhuber, R. N. Schouten, A. R. Akhmerov, and L. P. Kouwenhoven. Demonstration of an ac Josephson junction laser. *Science*, 355(6328):939–942, 2017.